NASA CONTRACTOR REPORT

TRANSATMOSPHERIC VEHICLE RESEARCH

Henry G. Adelman and Jean-Luc Cambier

Eloret Institute
1178 Maraschino Drive
Sunnyvale, CA 94087

Prepared for

Ames Research Center
under Cooperative Agreement NCC2-388

National Aeronautics and
Space Administration

Ames Research Center
Moffett Field, California 94035

NASA CONTRACTOR REPORT

TRANSATMOSPHERIC VEHICLE RESEARCH

Henry G. Adelman and Jean-Luc Cambier

CONTRACT NAS2–
NCC2-388

NASA

LIMITED REPRODUCIBILITY

MORE THAN 20% OF THIS DOCUMENT MAY BE AFFECTED BY:

- ☐ FAINT OR BROKEN TYPE
- ☑ COLOR PHOTOGRAPHS
- ☐ BLACK AND WHITE PHOTOGRAPHS
- ☐ FOLDOUTS
- ☐ DOT MATRIX PRINT
- ☐ CHARTS/GRAPHS with SCRIPT NOTATION
- ☐ NON-ROMAN ALPHABET
- ☐ OTHER (specify)_____

1. Report No.	2. Government Accession No.	3. Recipient's Catalog No.
4. Title and Subtitle TRANSATMOSPHERIC VEHICLE RESEARCH		5. Report Date 1 June 1990 6. Performing Organization Code
7. Author(s) Henry G. Adelman Jean-Luc Cambier		8. Performing Organization Report No. 10. Work Unit No.
9. Performing Organization Name and Address Eloret Institute 1178 Maraschino Drive Sunnyvale, CA 94087		11. Contract or Grant No. NCC2-388 13. Type of Report and Period Covered 12/1/85 - 05/31/90
12. Sponsoring Agency Name and Address National Aeronautics and Space Administration, Washington, D.C. 20456		14. Sponsoring Agency Code

15. Supplementary Notes

Point of Contact: Gene P. Menees, c/o 230-2 NASA Ames Res. Ctr. Moffett Field, CA 94035

16. Abstract

Research was conducted into the alternatives to the supersonic combustion ramjet ("scramjet") engine for hypersonic flight. A new engine concept, the Oblique Detonation Wave Engine (ODWE) was proposed and explored analytically and experimentally. Codes were developed which can couple the fluid dynamics of supersonic flow with strong shock waves , with the finite rate chemistry necessary to model the detonation process. An additional study was conducted which compared the performance of a hypersonic vehicle powered by a scramjet or an ODWE. This work included engineering models of the overall performances of the two engines. This information was fed into a trajectory program which optimized the flight path to orbit. A third code calculated the vehicle size, weight, and aerodynamic characteristics.

The experimental work was carried out in the Ames 20MW arc-jet wind tunnel, focusing on mixing and combustion of fuel injected into a supersonic airstream. Several injector designs were evaluated by sampling the stream behind the injectors and analyzing the mixture with an on-line mass spectrometer. In addition, an attempt was made to create a standing oblique detonation wave in the wind tunnel using hydrogen fuel. It appeared that the conditions in the test chamber were marginal for the generation of oblique detonation waves.

17. Key Words (Suggested by Author(s))	18. Distribution Statement
National Aerospace Plane Transatmospheric Vehicles Pathfinder Program Hypersonic Flight	Unclassified, Unlimited

19. Security Classif. (of this report)	20. Security Classif. (of this page)	21. No. of Pages	22. Price*
Unclassified	Unclassified		

*For sale by the National Technical Information Service, Springfield, Virginia 22161

TRANSATMOSPHERIC VEHICLE RESEARCH

Final Technical Report

for the program period
December 1, 1985 - May 31, 1990

Submitted to

National Aeronautics and Space Administration
Ames Research Center
Moffett Field, California 94035

Aerothermodynamics Branch
George S. Deiwert, Chief and Technical Monitor

NASA-Cooperative Agreement NCC2-388

Prepared by

ELORET INSTITUTE
1178 Maraschino Drive
Sunnyvale, CA 94087
Phone: 408 730-8422 and 415 493-4710
Fax: 408 730-1441
K. Heinemann, President and Grant Administrator
Henry G. Adelman, Principal Investigator
Jean-Luc Cambier, Co-Principal Investigator

1 June 1990

Final Reporting on the research efforts under Cooperative Agreement NCC2-388 is in two parts. Part 1 includes primarily the work performed by Dr. Henry Adelman during the period 12/1/85 through 5/31/90, focusing on the experimental aspects of the Oblique Detonation Wave Engine (ODWE) project. Part 2 emphasises the numerical simulations of the ODWE experiment and related analytical work, performed by Dr. Jean-Luc Cambier who joined the team during 1 January to 31 December, 1989.

PART 1

OVERVIEW AND EXPERIMENTAL WORK

by Dr. Henry G. Adelman

During the period from December 1, 1985 to May 31, 1990, Dr. Adelman worked on several tasks related to the National Aerospace Plane(NASP), Transatmospheric Vehicles(TAV), and the Pathfinder program for planetary exploration. This work has resulted in the publication of many papers and several journal article.

OBLIQUE DETONATION WAVE ENGINE STUDIES

Abstract:

Dr. Adelman's research on the propulsion system for hypersonic flight focused on alternatives to the supersonic combustion ramjet (scramjet) engine. A comprehensive literature search showed that very little test data or analytical modeling existed for a scramjet or for a vehicle powered by a this type of engine. In addition, this data and our own analytical predictions showed that the scramjet powered vehicle may not provide the performance necessary for orbital missions. Therefore, Dr. Adelman proposed a new engine concept, the Oblique Detonation Wave Engine (ODWE).

The study of this new engine required both analytical and experimental research. The analytical work was done in cojunction with others at Ames and Eloret Institute. The cooperative effort with Jean-Luc Cambier was to develop codes which can couple the fluid dynamics of supersonic flow with strong

shock waves with the finite rate chemistry necessary to model the detonation process.

An additional study was conducted which compared the performance of a hypersonic vehicle powered by a scramjet or an ODWE. This work included engineering models of the overall performances of the two engines. This information was fed into a trajectory program which optimized the flight path to orbit. A third code calculated the vehicle size, weight, and aerodynamic characteristics. Results of this study were presented by Dr. Adelman at the 9th International Symposium on Airbreathing Engines in Athens, Greece in September, 1989.

The experimental work was carried out in the Ames 20 MW arc-jet wind tunnel. Dr. Adelman coordinated this work with personnel from Aerojet TechSystems and the Facilities branch of NASA-Ames RT Division. Experimental studies were begun in September, 1988 and continued through August, 1989. These studies focused on mixing and combustion of fuel injected into a supersonic airstream. Several injector designs were evaluated by sampling the stream behind the injectors and analyzing the mixture with an on-line mass spectrometer. Preliminary results were reported at the AIAA Joint Propulsion Conference in Monterey in July, 1989.

In addition to the injection studies, an attempt was made to create a standing oblique detonation wave in the wind tunnel using hydrogen fuel. The results of these tests were reported

for the first time at an Agard Hypersonic Propulsion Meeting in Madrid. It appeared that the conditions in the test chamber were marginal for the generation of oblique detonation waves.

Fuel Injection Experimental Studies:

Several fuel injection designs were tested for air-fuel mixing. Since the oblique detonation wave experiment requires good air fuel mixing, the extent of mixing had to be determined. This was accomplished by an in-stream probe which passed gas samples to an on-line mass spectrometer. The probe assembly was supported on a 3-D traverse table which could span the entire flow field of interest. Results of the fuel-air sampling showed a narrow fuel jet which takes considerable distance to spread. Several methods of increasing the extent of mixing were tested including a blunt trailing edge strut. Unfortunately, this blunt design allowed premature burning of the fuel in the wake of the strut. Another design incorporated a bifurcated trailing edge strut. However, this design was not tested due to the lack of time.

Detonation Wave Experimental Studies:

Several attempts were made to create a standing oblique detonation wave. Before this was attempted, it was necessary to detremine the state of the air in the arc-jet wind tunnel, which required a water cooled calorimeter mounted in the stream. After the free stream conditions were determined by the calorimeter, a wedge was placed

behind the fuel injection struts to create an oblique shock wave that would become an oblique detonation wave.

Flow diagnostics were used to determine the wave state including shadowgraph and schlieren optics to allow comparisons of the wave shapes with and without fuel injection. The results of these experiments showed that fuel injection caused the wave to move away from the wedge and become more normal. However, the cause of this wave movement could not be attributed to combustion since both hydrogen and helium created the same effects.

During one test run, a pressure rise was noted behind the oblique wave indicating combustion. On other occassions, no pressure rise was observed. Some difficulties were due to the erratic operation of the steam vacuum system which could not maintain a constant test chamber vacuum. The cause of this problem was later discovered to be a faulty isolation valve on another arc-jet wind tunnel. However, due to the extended period required to repair the leaking isolation valve and the tight scheduling of the 20 MW arc-jet tunnel, no further mixing or detonation wave tests could be carried out during this period.

The wave displacement observed with inert gases was due to their low molecular weights which create higher speeds of sound and, therefore, lower Mach numbers. Decreasing the Mach number of the flow causes an increase in the oblique wave angle.

Analytical Studies:

From the beginning of this program on wave combustion, it was realized that predictions of fuel injection, mixing and combustion phenomena would help to design the experiment and intrepret the results. Various calculations and numerical simulations were used for this purpose.

Fuel Injection Simulations:

The extent of fuel-air mixing was initially predicted by a correlation developed from other studies found in the literature. In order to verify this correlation and design the best injector, simulations of fuel injection were begun using a 2-D code. While this code modeled the injector as a slot, the actual injectors consisted of 19 individual holes. These circular holes create 3-D effects which cannot be modeled by a 2-D simultion. Therefore, the 2-D models underestimated the extent of mixing by a large degree. The 2-D simulations were, however, usefull for predicting the necessary conditions for combustion and detonation. They also predicte the effects of light injected gases on the oblique wave shape and angl This was illustrated when an unmixed jet of hydrogen encountered an oblique wave and distorted the shape due to the low molecular weight and low Mach number.

Detonation Wave Simulations:

Initial predictions of the existence of detonation waves at the expected test conditions were carried out with a staedy flow, 1-D code. While this code predicted ignition delays and combustion behind an oblique shock wave, it could not simulate

the coupling between the flame front and the wave which has been observed with detonation waves. An attempt was made to determine this coupling by the method of characteristics. These calculations indicated that coupling would occur for certain test conditions depending on the wind tunnel free stream temperature and pressure.

Since a more accurate method of predicting detonations was needed, the 2-D code which had been developed for the injection simulations was extended to model combustion behind a detonation wave. Several calculations were made which verified the trends predicted by the 1-D model. Detonations were shown to couple the heat release and pressure rise to the oblique wave front and cause the wave to become less oblique. Since it was possible that the fuel would not be completely mixed with air before encountering the oblique wave, a simulation was carried out with relatively unmixed fuel and air. The results showed a distorted, bowed forward, "oblique" wave which appeared almost identical to the case without combustion discussed in the injection section. The most obvious difference was the appearance of small areas where normal detonations occured. The predicted wave shape distortion was remarkably similar to the shap observed in the experiments.

Mission Studies:

In order to asses the performance potential of an Oblique Detonation Wave Engine installed in a single-stage-to-orbit Transatmospheric Vehicle, a mission analysis study was

performed. First, it was necessary to develop a 1-D engineering code which could predict the performance of both an ODWE and a scramjet engine. This code calculated specific impulses and thrust coefficients for both engines at various flight paths corresponding to different dynamic pressures. Engine cooling requirements were assumed to be satisfied by heat absorption into the liquid hydrogen fuel. If the heat loads exceeded the heat capacities of a stoichiometric amount of fuel, then excess fuel was used for cooling. Injecting this excess fuel into the supersonic airstream inside the engine created lower specific impulses and, therefore, lower engine performance. Since the ODWE combustion zone is much smaller than that of the scramjet, the ODWE needed less cooling and had less performance degradation than the scramjet due to excess fuel injection. This effect was seen in the performance data. The specific impulse degradation of the ODWE occured at a higher Mach number than for the scramjet. At lower Mach numbers, the scramjet had higher performance than the ODWE due to lower losses in the four shock inlet system compared to the ODWE two shock inlet. However, the results of a comprehensive mission analysis study showed that high Mach number performance is more important than low Mach number performance, so the ODWE was more efficient overall.

TRANS-ATMOSPHERIC VEHICLE HEATING LOADS STUDIES

One problem which faces airbreathing single-stage-to-orbit

vehicles is the tremendous heating loads imposed on the airframe and engines. Several studies were conducted of the expected heating loads on a typical TAV mission. A chemical equilibrium program was modified for this purpose in order to predict the composition of the air at the high temperatures seen at the stagnation points on the nose and the wing leading edges. Heating loads on the body were determined for laminar and turbulent boundary layer conditions. The determination of the transition from laminar to turbulent flow was made using previously derived criteria.

Peak heating rates and integrated heating loads were calculated for various missions with different trajectories of altitude-speed histories. These results were presented in several AIAA conferences and in archival AIAA journals.

INTERPLANETARY EXPLORATION STUDIES

The exploration of Mars was studied for different scenarios of approach trajectories and earth return trajectories. A manned mission was examined with landings and take-offs from the Martian surface. Vehicle sizes, weights and shapes were considered along with aerodynamic characteristics. The ability to explore large portions of the Martian surface was noted for certain configurations.

References:

M.E. Tauber, G.P. Menees and H.G. Adelman, "Aerothermodynamics

of Transatmospheric Vehicles", AIAA 4th Thermophysics and Heat Transfer Conference, Boston, June, 1986.

G.P. Menees, M.E. Tauber, J.T. Wilson and H.G. Adelman, "Ascent Aeromaneuvering Capabilities of Transatmopheric Vehicles", AIAA 25th Aerospace Sciences Meeting, Reno, January, 1987.

M.E. Tauber and H.G. Adelman, "The Thermal Environment of Transatmospheric Vehicles", AIAA 5th Joint Thermophysics and Heat Transfer Conference, Honolulu, June, 1987.

J.L. Cambier, H.G. Adelman and G.P. Menees, "Detonation Processes in Supersonic Combustion", 8th International Symposium on Airbreathing Propulsion, Cincinnati, June, 1987.

H.G. Adelman et. al., "Analytical and Experimental Validation of the Oblique Detonation Wave Engine", AIAA Paper 88-0097, 26th Aerospace Sciences Meeting, Reno, January, 1988.

J.L. Cambier, H.G. Adelman and G.P. Menees, "Numerical Simulations of an Oblique Detonation Wave Engine", AIAA Paper 88-0063, 26th Aerospace Sciences Meeting, Reno, January, 1988.

M.E. Tauber and H.G. Adelman, "Thermal Environments of Trans-Atmospheric Vehicles", AIAA Journal of Aircraft, Vol.25, No.4, April, 1988, pp 355-363.

J.L. Cambier and H.G. Adelman, "Numerical Simulations of a Pulsed Detonation Wave Engine", AIAA Joint Propulsion Conference, Boston, July, 1988.

G.P. Menees, J.F. Wilson and H.G. Adelman, "Comparative Flight Strategies for Ascent from Martian Surface to Orbiter Rendezvous", Paper 89-0634, 27th Aerospace Sciences Meeting, Reno, Jan. 1989.

H.G. Adelman et. al., "Experimental and Analytical Investigations of Wave Enhanced Combustors", AIAA Joint Propulsion Conference, Monterey, July, 1989, Paper 89-2787.

G.P. Menees, J.F. Wilson and H.G. Adelman, "Comparative Strategies for Ascent from Martian Surface to Orbiter Rendezvous", Paper 89-0634, 27th Aerospace Sciences Meeting, Reno, Jan. 1989.

J.L. Cambier, H.G. Adelman and G.P. Menees, "Numerical Simulations of Oblique Detonations in Supersonic Combustion Combustion Chambers", AIAA Journal of Propulsion, Vol.5, No.4, July-August, 1989.

G.P. Menees, H.G. Adelman, J.L. Cambier and J.V. Bowles, "Wave Combustors for Trans-Atmosdpheric Vehicles", Paper 11-5, 9th International Symposium on Airbreathing Engines", Athens, Greece, September, 1989.

J.L. Cambier, H.G. Adelman and G.P. Menees, "Numerical Simulations of an Oblique Detonation Wave Engine", AIAA Journal of Propulsion and Power, Vol.6, No.3, May-June, 1990, pp 315-323.

G.P. Menees, H.G. Adelman and J.L. Cambier, "Analytical and Experimental Investigations of the Oblique Detonation Wave Engine", AGARD PEP 75th Symposium on Hypersonic Combined Cycle Propulsion, Madrid, Spain, May 28-June 1, 1990, (Preprint attached).

Note: Copies and/or preprints of the above papers were included in earlier progress reports.

PART 2

NUMERICAL SIMULATIONS

by Dr. Jean-Luc Cambier

Report to Contract NCC2-388 : Jan.-Dec 1989

Part I: Numerical Simulations of ODWE Experiment and Related Analytical Work

Jean-Luc Cambier, Research Scientist
Eloret Institute, Sunnyvale ,CA.

I: Introduction

The computational work for the ODWE research program and for the year 1989 was divided in three parts:

- continued code development and enhancement of numerical capability
- application of TVD code (re: 'MOZART') to simulation of fuel injection process and comparison with experimental data.
- continued validation of the code MOZART by simulation of shock induced combustion and comparison with ballistic experimental data.

In addition, some computational work was performed on another code, originally provided by D. Bogdanoff, and extensively modified, for the 1-dimensional analysis of generic scramjet engine designs.

Complementary to this computational and analytical work, some conceptual research was done for the creation and submission of research proposals to NASA Headquarters for two different programs.

II: Code Development

II-A: Introduction

The code MOZART was further developed in 1989 from a 2D to a 3D capability. The algorithm for chemical kinetics was modified to fully use the conservation of elements, and thereby reducing the chances of error. The code MOZART is now a well-rounded

capability and few further modifications are projected. Some numerical experiments on an implicit version have been carried out, but the development of a fully implicit version of the code is not planned for the immediate future. The most immediate area of concern is the enhancement of the grid-patching capability, to accomodate grid sliding (steady/unsteady) and grid embedding when nodal points from different grid systems are not on the same locations. This problem occurs for highly complex geometries; the algorithms required for the solution of this problem have been written and will be tested in 1990. This increased capability will be similar to the 'chimera' capability in development in the RF division.

Most of the new code development was focused on a series of TVD codes for the simulation of non-equilibrium, multi-temperature gas and plasma codes. Three types of codes were originally written:

- a 3-Temperature and a N_v-temperature code for neutral, non-equilibrium gas. The 3-T version was tested and compared to experimental data on shock layers and with the 2-T code by Candler.
- a one-fluid, multi-T code for neutral and/or strongly ionized flows.
- a multi-fluid code for ionized flows.

The multi-fluid description is obtained by solving a full set of Euler equations of the heavy component (both neutrals and heavy ions), and one for the electron component. The various exchange terms for mass, momentum and energy between all fluid components are explicitely solved on the right- hand side. The time scales are very small, and the code is therefore applicable for plasma flows in highly non-equilibrium, with potential charge separation. This is the case near electrodes in arc-heated flows, for example.

The one-fluid description assumes no charge separation, and only the mass and energy transfers are explicitely computed. This approximation is valid for most flows, such as high temperature shock layers. The results of both one-fluid and two-fluid versions were observed to be consistent with one another.

The algorithms for chemical and ionization kinetics in the case of multi-T plasmas were decisively more complex, due to several translational temperatures and the effect on the correct computation of the energy balance. The case of strong ionizing shock was computed and compared to an analytic solution. The case of a shock in a pre-ionized plasma, and the dramatic effect of electron heat conduction as a precursor was also computed and compared with known analytic solutions. It was observed that the essential physics were well reproduced by the code.

The one-fluid code was then extended to include radiation emission/absorption and radiative transfer. The physics of emission and absorption have been currently modelled, and are expected to be tested in the first half of 1990. These major developments in computational capability are expected to be useful in various areas of flow modelling for Ames, in the very near future. The simulation of strongly ionized shock layers, arc-jet flows, laser-heated flows and plasma ignition of combustible mixtures will hopefully be attempted with these codes in the future.

The plasma at low and medium temperatures is composed of three components, i.e. the neutral particles, ions, and free electrons. Each component satisfies its own system of conservation equations with additional coupling terms responsible for the exchange of momentum, energy, as well as chemical and ionization/recombination reactions. Some of the multi-fluid effects can be modelled by multiple translational temperatures, there-

fore by separately convecting the translational energies of each component. If electromagnetic effects are important or very small spatial scales must be resolved, one must also separately solve for the momentum equation of each component. In the following, we designate a multi-fluid description by the number of separate momentum equations that are being solved; thus, a one-fluid description can have different ion and electron temperatures, but only the global momentum equation is solved. The mass and momentum conservation equations for a plasma component α (=n, i or e), in the absence of chemical reactions, take the form:

$$\frac{\partial \rho_s}{\partial t} + \vec{\nabla} \cdot (\vec{u_\alpha} \rho_s) = 0 \qquad \forall s \in \alpha \tag{1}$$

$$\frac{\partial \rho_\alpha \vec{u}_\alpha}{\partial t} + \vec{\nabla}(P_\alpha + \rho_\alpha u_\alpha^2) = Z_\alpha e n_\alpha \vec{\mathcal{E}} + \vec{R}_\alpha \tag{2}$$

where Z_α is the charge of the plasma component, $\vec{\mathcal{E}}$ is the electric field. The force of friction $\vec{R}$ accounts for the exchange of momentum through collisions with other components of the plasma. The total energy density is transported according to:

$$\frac{\partial E_\alpha}{\partial t} + \vec{\nabla}(\vec{u}_\alpha(E_\alpha + P_\alpha)) = Z_\alpha e n_\alpha \vec{u}_\alpha \vec{\mathcal{E}} + \vec{R}_\alpha \vec{u}_\alpha + \sum_\beta \dot{Q}_{\alpha\beta} \tag{3}$$

while internal energies follow a linear convection rule:

$$\frac{\partial E_{v,\alpha}}{\partial t} + \vec{\nabla}(\vec{u}_\alpha E_{v,\alpha}) = \dot{Q}_{v,tr} + \dot{Q}_{v,*} \tag{4}$$

The exchange terms $\dot{Q}_{v,tr}, \dot{Q}_{v,*}$ are the coupling terms between vibration and translational/electronic modes; similar terms exist for the relaxation of the internal electronic excitation energy[1]. The conservation equations must also be supplemented on the right hand side by the viscous terms, which are not explicitely written here. The translational and rotational degrees of freedom are combined, since they are at the same temperature. The electrons having no internal structure, the system of conservation equations for the

[1]The electronic excitation energies and temperatures are indicated here by the * suffix, to distinguish it from free electronic quantities with a traditional e suffix.

electron gas takes the very simple form of an ideal gas with $\gamma_e \equiv 5/3$.

Since the pressure is governed by the translational degrees of freedom only, the equation of state, for a given component only, is:

$$P_\alpha = n_\alpha \hat{R} T_{tr,\alpha} = (\gamma_{tr,\alpha} - 1) E_{tr,\alpha} = (\gamma_{tr,\alpha} - 1)(E_\alpha - \frac{1}{2}\rho_\alpha u_\alpha^2 - E_{v,\alpha} - E_{*,\alpha} - E^o_{f,\alpha}) \quad (5)$$

where $\gamma_{tr,\alpha}$ is the ratio of specific heats, but taking into account the translational and rotational degrees of freedom only. $E^o_f = \sum_s \rho_s h^o_s$ is the heat of formation at $T = 0$, and $\hat{R}$ is the Boltzmann constant.

The exhange terms on the right-hand-side operate at frequencies that are characteristic of the respective collision frequencies. For example, if ν_{ei} is the average collision frequency between electrons and ions, the rate at which momentum is exchanged between these two components is given by the friction force density:

$$\vec{R}_{u,ei} = \rho_e \nu_{ei} (\vec{u_i} - \vec{u_e})$$

This term represents the momentum gained by the electrons per unit of time, through collisions with ions. A more general and systematic description of the coupling terms can be found in Ref. [2]. Similar terms exist for collisions between heavy particles.

If the gas is substantially ionized, the coulomb collisions between charged particles are very frequent, and lead to a more rapid relaxation of the velocity difference between ions and electrons. In addition, such a velocity difference would induce a charge separation; the rapidly rising electric field would then restore neutrality within a time scale

characteristic of the inverse of the plasma frequency[2]:

$$\omega_p = \left(\frac{n_e e^2}{m_e \epsilon_o}\right)^{1/2} \tag{6}$$

A steady-state can be realized by balancing the electric force with the pressure and thermal gradients: this leads to the characteristic polarization effect at the shock discontinuity in a plasma. The momentum equation for the electrons in quasi steady state leads to:

$$\frac{\partial \rho_e \vec{u}_e}{\partial t} \simeq -\vec{\nabla} P_e + \vec{R}_T + \vec{R}_u - e n_e \vec{\mathcal{E}} \simeq 0 \tag{7}$$

where the inertial contribution has been neglected. $\vec{R}_u$ is the friction force due to collisions, and $\vec{R}_T$ is the thermal friction [**2,3**]:

$$\vec{R}_T = -0.71 n_e \hat{R} \vec{\nabla} T_e \tag{8}$$

Assuming that a steady state is achieved, the electric field can be estimated from equation (7) above, and the charge separation by solving the Poisson equation:

$$\vec{\nabla} \cdot \vec{\mathcal{E}} = \frac{e}{\epsilon_o}(n_i - n_e) \tag{9}$$

This method will be used in the one-fluid model to estimate the electric field and charge separation.

By summing the momentum equations for ions and electrons, it is clear that there is no electric or friction force appearing in the resulting equations of motion. Since the solution of the momentum equation for the electrons may require a time resolution comparable to the natural oscillation period of the plasma ($1/\omega_p$), significant savings in computational work can be obtained. However the method described above to estimate the steady electric properties of the plasma will, in this one-fluid model, lead

[2]We use here the MKSA system of units.

to inaccurate results. The one-fluid model can be used therefore in cases where these electro-magnetic effects are expected to play only a minor role.

There are however no restrictions on the number of translational temperatures, since all energies are separately convected. Let us also mention that the algorithm used to compute the energy exchange terms must be able to provide the correct asymptotic limit when the exchange time scales are not resolved. This can be very easily implemented.

Let us consider a one-fluid description of a fully ionized plasma, i.e. only ions and electrons. During the summation of the momentum equations, the body forces and friction forces cancel out after assuming no charge separation ($n_i \simeq n_e$) and no current density ($u_i \simeq u_e$). An equation for the total energy of the plasma can be obtained in a similar fashion. The energy for the electron gas is convected separately, therefore allowing two distinct translational temperatures. When incorporated into a one-fluid algorithm, this energy equation for electrons is a non-linear convection equation which would require to compute the generalized Riemann invariants along the three characteristic paths ($u_e, u_e \pm c_e$). The stability and/or accuracy becomes then severely constrained from the large values of c_e. However by using the conservation of mass and momentum for electrons, it is possible to reduce the left-hand side of this equation to a linear convection problem:

$$\frac{\partial E_{e,tr}}{\partial t} + \vec{\nabla} \cdot (\vec{u}_e E_{e,tr}) = -P_e \vec{\nabla} \cdot \vec{u}_e + \dot{Q}_{ei} \tag{10}$$

where only the *translational* energy $E_{e,tr} = \frac{3}{2} n_e \hat{R} T_e$ is convected. The fast time scales due to the electrostatic forces have been removed, and the transport equation can be easily incorporated into a multiple temperature TVD algorithm. We however pay the price of a source term on the r.h.s. written in a non-conservative form. This term will

present difficulties at a shock, where the gradients are not resolved.

II-B: One-Fluid Model

Let us consider a fully-ionized plasma, composed of n species of ions and electrons only. The hyperbolic system we intend to solve, written in a conservative form, is:

$$\frac{\partial Q}{\partial t}+\frac{\partial F}{\partial x}=\frac{\partial}{\partial t}\begin{pmatrix}\rho_1\\ \vdots\\ \rho_n\\ \rho_e\\ m\\ E\\ E_v\\ E_*\\ E_{e,tr}\end{pmatrix}+\frac{\partial}{\partial x}\begin{pmatrix}u\rho_1\\ \vdots\\ u\rho_n\\ u\rho_e\\ P+\rho u^2\\ uH\\ uE_v\\ uE_*\\ uE_{e,tr}\end{pmatrix}=RHS$$

where $m=\rho u$ is the momentum density, and $H=E+P$ is the enthalpy per unit volume. The mass density of the electron gas can be convected as another specie, or can be obtained at each time step by using the fact that there is no charge separation. The pressure is the sum of individual plasma components:

$$P=(\bar{\gamma}_{i,tr}-1)(E-\frac{1}{2}\rho u^2-E_v-E_*-E_{e,tr}-E_f^o)+(\gamma_e-1)E_{e,tr} \qquad (12)$$

The derivatives of the pressure are computed with respect to the conserved variables, i.e. $\rho_s, m, E, E_v, E_*, E_{e,tr}$. Using the notation $P_q=\frac{\partial P}{\partial q})_{q'\neq q}\forall q=\rho_s, m, E..$, and using the definitions of the mass fractions $\hat{c}_s=\rho_s/\rho$, and of the internal energies per unit mass $e_v=E_v/\rho$, $e_*=E_*/\rho$ and $e_{e,tr}=E_{e,tr}/\rho$, we compute these derivatives as (compare with [4,7]):

$$P_E=-P_{E_v}=-P_{E_*}=\bar{\gamma}_{i,tr}-1\ , \qquad P_m=-uP_E\ , \qquad P_{E_{e,tr}}=\gamma_e-1-P_E \quad (13)$$

$$P_{\rho_s}=(\bar{\gamma}_{i,tr}-1)(\frac{u^2}{2}-C_{v,s}T_{tr,s}-h_s^o)+\frac{\hat{R}}{m_s}T_{tr,s}\ \ \forall s\neq e\ , \qquad P_{\rho_e}=(\bar{\gamma}_{i,tr}-1)\frac{u^2}{2} \quad (14)$$

With these definitions, one can compute the determinant of the jacobian; the speed of sound is then obtained in the form ($\hat{c}_s = \rho_s/\rho$):

$$c^2 = \sum_s \hat{c}_s P_{\rho_s} + (h - u^2 - e_v - e_*)P_E + P_{E_{e,tr}} e_{e,tr} \simeq \hat{R}\, \frac{\bar{\gamma}_{i,tr} T_{i,tr} + \gamma_e T_e}{m_i} \qquad (15)$$

where one recognizes the expression for the ion-acoustic speed of sound. The TVD scheme requires the projection of our non-linear system of equations onto the characteristic eigenspace, through transformation matrices $\mathbf{T}, \mathbf{T}^{-1}$. Let $\alpha^k_{i+1/2} = \mathbf{T}^{-1}_{i+1/2} \Delta_{i+1/2} Q$ be the component of ΔQ in the k^{th} characteristic direction. The jumps in characteristic variables $\alpha^k_{i+1/2}$ and the transformation matrix $\mathbf{T}$ satisfy:

$$\begin{aligned} \Delta Q &= \mathbf{T}\alpha \\ \Delta F &= \mathbf{T}\mathbf{\Lambda}\alpha \end{aligned} \qquad (16)$$

where $\mathbf{\Lambda}$ is the diagonal matrix whose elements are the eigenvalues of the hyperbolic system of equations. After some algebra, we find:

$$\alpha = \begin{pmatrix} \Delta\rho_1 - \hat{c}_1 \frac{\Delta P}{c^2} \\ \vdots \\ \Delta\rho_n - \hat{c}_n \frac{\Delta P}{c^2} \\ \Delta\rho_e - \hat{c}_e \frac{\Delta P}{c^2} \\ \frac{(\Delta P + c\Delta m - uc\Delta\rho)}{2c^2} \\ \frac{(\Delta P - c\Delta m + uc\Delta\rho)}{2c^2} \\ \Delta E_v - e_v \frac{\Delta P}{c^2} \\ \Delta E_* - e_* \frac{\Delta P}{c^2} \\ \Delta E_{e,tr} - e_{e,tr} \frac{\Delta P}{c^2} \end{pmatrix}$$

$$\mathbf{T} = \begin{pmatrix} 1 & \dots & 0 & \hat{c}_1 & \hat{c}_1 & 0 & 0 & 0 \\ \vdots & \ddots & \vdots & \vdots & \vdots & \vdots & \vdots & \vdots \\ 0 & \dots & 1 & \hat{c}_n & \hat{c}_n & 0 & 0 & 0 \\ u & \dots & u & u+c & u-c & 0 & 0 & 0 \\ u^2 - \frac{P_{\rho_1}}{P_E} & \dots & u^2 - \frac{P_{\rho_n}}{P_E} & h+uc & h-uc & -\frac{P_{E_v}}{P_E} & -\frac{P_{E_*}}{P_E} & -\frac{P_{E_{e,tr}}}{P_E} \\ 0 & \dots & 0 & e_v & e_v & 1 & 0 & 0 \\ 0 & \dots & 0 & e_* & e_* & 0 & 1 & 0 \\ 0 & \dots & 0 & e_{e,tr} & e_{e,tr} & 0 & 0 & 1 \end{pmatrix} \qquad (17)$$

The rest of the numerical method follows closely the usual procedure for computing the fluxes, according to the original scheme by A. Harten [5]. The energy exchange terms are of the following form:

$$\dot{Q}_{ei} = \nu'_{ei}(E_{i,tr} - E_{e,tr}) \tag{18}$$

where ν'_{ei} is related to the collision frequency: $\nu'_{ei} = (2m_e/m_i)\nu_{ei}$. This equation has an exact exponential solution. We choose therefore to express this term as:

$$\delta E_{e,tr} \simeq \frac{1}{2}(E_{i,tr} - E_{e,tr})(1 - e^{-2\nu'_{ei}\Delta t}) \tag{19}$$

Notice that when the time scale of coupling is resolved ($\nu'_{ei}\Delta t \ll 1$) we obtain in this limit the correct exchange term:

$$\delta E_{e,tr} \simeq \nu'_{ei}\Delta t(E_{i,tr} - E_{e,tr}) \tag{20}$$

while if a large time step is used:

$$\delta E_{e,tr} \simeq \frac{1}{2}(E_{i,tr} - E_{e,tr}) \tag{21}$$

which also the correct asymptotic limit (both $T_{i,tr}$ and $T_{e,tr} \rightarrow T_{eq} = \frac{T_i+T_e}{2}$). This numerical scheme provides both accuracy and stability for large time steps. The same method is used for other modes of relaxation (T-V, V-*, T-* couplings). When a shock is propagating into a plasma, the heat conduction of electrons becomes an important process which acts on very small time scales. The electron heat conduction is (in the absence of magnetic field):

$$\kappa_e = 3.1616\frac{n_e k^2 T_e}{m_e \nu_{ei}} \simeq \kappa' T_e^{5/2} \tag{22}$$

where we have isolated the temperature dependence. The heat conduction flux then takes the form:

$$\vec{F}_{hc} \simeq \frac{2}{7}\kappa'\vec{\nabla}T_e^{7/2}$$

The jacobian term $(\partial F/\partial T_e)$ will have a $T_e^{5/2}$ dependence. A simple implicit algorithm can be written for this heat conduction problem, and solved in Δ-form for the electron temperature. The time step used can then be much larger: this implicit algorithm has been compared with an explicit one. Accuracy can be maintained if the relative change in temperature induced by the heat conduction process alone is kept to a reasonable value ($< 5\%$). This still allows us great savings (about 50-fold) in computational costs.

A test of the numerical method was performed by simulating the propagation of a shock in a one-dimensional system. The plasma neutral was composed only of singly ionized atomic nitrogen N^+ and electrons. The free stream density was $\rho_\infty = 10^{-6}\text{kg/m}^3$, or a number density[3] $N_\infty \simeq 7.143\ 10^{-5}$ moles/m^3. The free stream velocity and temperature were respectively $U_\infty = 7$ km/s and $T_\infty = 275^\circ K$. Grids of various resolution were used for this test case, depending whether the one-fluid or two-fluid models were used. The free stream velocity and temperatures are too small for this test to be representative of laboratory conditions; however we are only interested at this stage in checking the numerical method and the reproduction of the essential physics.

Figure 1 shows the temperature profiles obtained for this shock reflecting from the closed end on the right-hand side. The dashed lines indicate the ion and electron temperatures obtained when the electron heat conduction is artificially suppressed. The ion viscous shock is very well defined; the relaxing zone behind the shock, due to the ion-electron energy exchange through collisons, is also well reproduced. The electron temperature jumps to a post-shock value $T_{e2} \simeq 1050^\circ K$, then increases due to the energy exchange. The density is shown in Figure 2 (dashed curve); the post-shock value is $N_{e2} \simeq 2.83\ 10^{-4}$. The solid curves for both Figures 1 & 2 indicate the temperature and

[3]Number densities with a capital letter are expressed in moles/m^3 throughout the text.

density profiles obtained when the electron heat conduction is included. Because the latter process is considerably faster than the ion-electron energy exchange, the shocked electron gas is essentially isothermal. The heating of electrons prior to the ion shock extends to considerable distances, and through energy exchange, is also responsible for a slight heating and compression of the ionic component, as can be observed in Figures 1 & 2.

These results qualitatively the correct features expected in strong shocks in completely ionized plasmas. However, even in the absence of heat conduction (& neglecting the electron viscosity), the electron heating should be adiabatic. This implies that the post-shock electron temperature should be given by:

$$T_{e2} = T_{e1} \left(\frac{n_{e2}}{n_{e1}} \right)^{\gamma - 1} \simeq 690^{o} K \tag{23}$$

We see therefore that in the absence of resolution of the shock structure, the non-conservative term $-P_e \vec{\nabla} \vec{u}$ over-estimates the heating of the electron gas. When heat conduction is allowed, the problem may be less serious, and the error will translate into an error in the distance through which pre-shock heating will occur. Nevertheless, there are situations in which this over-estimate of the electron heating may lead to significant errors: such is the case of magnetized plasma in a transverse field, and possibly for ionizing shocks.

Another uncertainty arises when the electric field is computed: assuming a steady-state for the electron momentum equation, the (time) asymptotic field can be expressed as a combination of the gradient of pressure and thermal and friction forces. However, because the shock structure is not completely resolved, the length scale that must be used for the electron pressure gradient in the vicinity of the viscous shock must be based

on the shock thickness for the electrons. We have therefore two methods for computing the electric field in this approximation. The first method uses the grid scale, and is assumed valid in the regions of smooth variations. The second method uses the Debye length scale [4]

$$\lambda_D = \left(\frac{\epsilon_o k T_e}{n_e e^2} \right)^{1/2} \tag{24}$$

as an estimate of the width of the compression region for electrons, and is expected to yield better estimates at the shock, i.e. for the peak electric field. The results are shown in Figure 3. It is apparent that the two methods gives very different answers, in particular for the peak values ($\simeq$ 2000 and $\simeq$ 7500 V/cm respectively). In order to gain better knowledge of the shock structure, and associated phenomena, it is necessary to turn to the two-fluid model.

II-C: Two-Fluid Model

As explained in the previous sections, the multi-fluid description of the plasma amounts in solving simultaneously the momentum equations for each component. Since the electrons are very mobile, we expect large variations in the electron velocity, which must be correctly reproduced for an accurate answer. This imposes small time steps, such that $\omega_p \Delta t \ll 1$. Because the electron gas is always subsonic, it is not necessary to use a shock-capturing method to model this component. The scheme we use is a simple 1^{st}-order accurate scheme, i.e. a donor-cell method based on the linearized system of equations [**6**]:

$$\frac{\partial \rho_e}{\partial t} + \vec{\nabla}(\vec{u}_e \rho_e) = 0 \tag{25}$$

$$\frac{\partial \rho_e u_{e,i}}{\partial t} + \vec{\nabla}(\vec{u}_e \rho_e u_{e,i}) = -\nabla_i P_e - e n_e \mathcal{E}_i + R_{T,i} + R_{u,i} \tag{26}$$

[4] This expression is the one-dimensional Debye length. The Debye radius, i.e. in 3-dimensions, should include a factor 4π.

$$\frac{\partial E_{e,tr}}{\partial t} + \vec{\nabla}(\vec{u}_e E_{e,tr}) \;=\; -P_e \vec{\nabla}\vec{u}_e - (\vec{R}_T + \vec{R}_u)\vec{u}_e \qquad (27)$$

The electron heat conduction is not considered here. In addition, we artificially set $\dot{Q}_{ei} \equiv 0$, for clarity: this does not affect the validity of the numerical methods.

The electric field is computed at each time step by solving the Poisson equation (eq. 9). The thermal and pressure forces on the r.h.s. of the momentum equation are assumed constant during the time step. After developing the friction term, this equation integrates to:

$$(\rho_e u_e)^{(n+1)} = (\rho_e u_e)^{(n)} e^{-\nu_{ei}\Delta t} + \left[-\nabla(P_e + \rho_e u_e^2) - e n_e \mathcal{E} + R_T\right]^{(n)} e^{-\nu_{ei}\Delta t} + \rho_e^{(n)} u_i^{(n)} (1 - e^{-\nu_{ei}\Delta t}) \qquad (28)$$

where the convective term has been brought into the r.h.s. Essentially, the ion-electrons collisions force the velocity to relax towards the ion velocity with the characteristic ion-electron collision frequency $\nu_{ei} \simeq 0.51\nu_{ee}$. This relaxation provides the damping of plasma oscillations over large time scales. An explicit integration of the equations of motion is performed for the same test case, over a refined grid. The time step is sufficiently small that plasma oscillations are resolved. Figure 4 shows the density profiles for both ion and electron components. Oscillations are clearly visible for most quantities of the electron gas (including the temperature, if shown on a linear scale). These oscillations can be artificially suppressed however by enhancing the damping through collisions. This can be easily done in equation (29) by using larger values of the collision frequency. Setting for example $\nu'_{ei} \simeq 5\nu_{ei}$ in eq. (29) leads to a strong damping of the velocity fluctuations, as can be seen in Figure 5. This is sufficient to completely damp all fluctuations in density, temperature, and other variables. In Figure 6 we show the electric field, for both cases of naturally and artificially damped oscillations, while Figure 7 shows the relative charge density $\delta n/n$. Similar results are obtained if the

artificial increase of the damping is 10 or 20-fold.

It is clear that the artificial damping smoothes out the fluctuations, without affecting the mean or peak values of any physical variable. This is possible because the dynamics of the plasma depend only upon the electron gas *averaged over many plasma oscillations.* Therefore the artificial enhancement of collision damping will not generate inaccuracies, but will only filter out the time scales of plasma oscillation. This is also apparent during the computation, as the time step allowed for stability is found to increase by one order of magnitude when damping is used. The density profiles are then shown in Figure 8. The post-shock electron temperature (the relaxation is not considered here) is found to be 700^0K, matching closely the adiabatic value. It was found that suppressing the joule heating of the electrons would give the exact adiabatic value, as expected.

Other simple checks can be performed. The wavelength of oscillations, as seen for example in Figure 5, is $\simeq 0.7\mu$, which is also the computed Debye length scale. By using the relation:

$$\lambda_D = \left(\frac{\epsilon_o k T_e}{n_e e^2}\right)^{\frac{1}{2}} = \left(\frac{kT_e}{m_e}\right)^{\frac{1}{2}} \left(\frac{n_e e^2}{\epsilon_o m_e}\right)^{-\frac{1}{2}} \simeq v_e/\omega_p$$

it is easy to observe that these are indeed the natural plasma oscillations. Similarly, the electric potential jump over the shock profile $\Delta\Phi$ can be estimated (using the width at half the peak value) as: $\Delta\Phi \simeq (3\ 10^4 V/m) \times (2\ 10^{-6} m) \simeq 0.06V$. According to the Debye criterion $e\Phi \simeq kT$, this corresponds to a temperature jump $\Delta T \simeq 696^o K$, as measured.

II-D: Chemical/Ionization Kinetics

As mentioned previously, we have slightly modified the algorithm for chemical kinetics

in MOZART to enforce the conservation of elements. This same modification is also being used here. Let us consider an elementary reaction and its reverse $f(r)$ and $b(r)$:

$$\nu_A^r A + \nu_B^r B \leftrightarrow \nu_C^r C + \nu_D^r D$$

with the elementary conservation law:

$$\frac{1}{\nu_A}\frac{dn_A}{dt} = \frac{1}{\nu_B}\frac{dn_B}{dt} = -\frac{1}{\nu_C}\frac{dn_C}{dt} = -\frac{1}{\nu_D}\frac{dn_D}{dt}$$

for a given (one-way) reaction. Listing all reactions involving specie A in that form, the total change in density is:

$$\Delta^{(r)} n_A = \sum_{b(r)} \nu_A^r n_C^{\nu_C^r} n_D^{\nu_D^r} k_b \Delta t - \sum_{f(r)} \nu_A^r n_A^{\nu_A^r} n_B^{\nu_B^r} k_f \Delta t = \mathcal{P}_A - \mathcal{L}_A n_A$$

The last for is conveniently used for numerical integration:

$$\Delta n_A = (\frac{\mathcal{P}_A}{\mathcal{L}_A} - n_A)(1 - e^{-\mathcal{L}_A \Delta t})$$

which is stable for large time steps. The integration form is not linear however, and does not exactly conserve the elements. This would be possible only if an explicit time integration was used, which is not desirable for its unstability. The remedy is to stabilize by the exact exponential integration each pair (forward/reverse) of elementary reactions. We write therefore the change due to each reaction as:

$$\frac{dn_A}{dt} = \nu_A^r \{ n_C^{\nu_C^r} n_D^{\nu_D^r} k_b - n_A^{\nu_A^r} n_B^{\nu_B^r} k_f \} = \nu_A^r \{ \Pi_A^r - \Gamma_A^r n_A \}$$

and the integration leads to:

$$\Delta^{(r)} n_A = \nu_A^r (\frac{\Pi_A^r}{\Gamma_A^r} - n_A)(1 - e^{-\Gamma_A^r \Delta t})$$

Here after numerical integration, one can still write:

$$\frac{\Delta^{(r)} n_A}{\nu_A^r} = \frac{\Delta^{(r)} n_B}{\nu_B^r} = -\frac{\Delta^{(r)} n_C}{\nu_C^r} \cdots$$

and the overall scheme conserve the elements while being stable at large time steps. The formulation differs in details between dissociation/recombination reactions and bi-molecular reactions, but the essential features are described above.

For ionization reactions due to electron impact, special care must be taken for the energy balance. In the scheme used here, heavy ions have a (large) positive enthalpy of formation, and the free electron has no zero-point energy. In the one fluid formulation, the total energy convected is:

$$E = E_{tr} + E_v + E_* + E_k + E_o + E_e$$

which is broken down respectively into the translational/rotational, vibrational, electronic energies of heavy particles, kinetic energy, zero-point energy and free electron energy. Considering a reaction involving heavy particles only, here atoms in the ground state:

$$A + B \leftrightarrow A^+ + B + e$$

the conservation of total energy allows us to directly translate the change in total formation energy into temperature changes for the heavy particles. If excited atoms are considered:

$$A^* + B \leftrightarrow A^+ + B + e$$

there is also a net change of total electronic energy, and therefore electronic temperature which must be accounted for. The same is true for impact ionization:

$$A + e \leftrightarrow A^+ + e + e$$

$$A^* + e \leftrightarrow A^+ + e + e$$

Consider for example the impact ionization from ground state: the positive change in zero-point energy from the forward reaction (ionization) would lead to a decrease in

heavy ion translational temperature if it was not compensated. Indeed, the change in electron energy in that case is exactly given by the change in zero point energy, s.t.:

$$\delta E_e + \delta E_o = 0$$

and this indicates that energy is removed from the thermal modes of the free electron gas component. The complete kinetics algorithm then computes the changes in energies due to various reaction mechanisms: $\Delta E_v, \Delta E_*, \Delta E_e$. Note that the conservation of total energy implies:

$$\Delta E_v + \Delta E_* + \Delta E_e + \Delta E_o = 0$$

The separately convected energies E_v, E_*, E_e are then modified accordingly. Note also that if different gas components are considered at different velocities, the change in kinetic energies ΔE_k must also be considered. This will be used in the future when the kinetics algorithm is implemented in the two-fluid formulation.

Figure 9 shows the profile of a one-dimensional strong ionizing shock in Argon. The relaxation zone is shown in detail for the temperatures, (ion and electron), ionization fraction, and density ratio. The insert is taken from a calculation by Biberman & Yakubov [8], and shows fairly good agreement. This calculation was done for ionization from ground state only. Other tests including effect of precursor excitation are being conducted.

III: Simulation of ODWE Experiment

The focus of this work was the simulation of the flow field in the strut region. This was done first with an Euler (inviscid) computation to obtain the position of the reflected shocks. The computations were done for a free stream Mach numbers of 4.5 and

5.4. Two values of the vertical separation between the struts were considered: 2/3" and 3/4". It was apparent from the results that multiple shock interactions occured between the struts, as well as shock impingement on the struts flat plate. It was clear then that in the case of high stagnation enthalpy, extreme care should be taken in avoiding locally high temperatures. However, the experiment proceeded nevertheless and the struts melted.

Another series of computations were made with greater refinement, including the blunt leading edge of the struts, and with high gridding density. The full Navier-Stokes were solved, for an assumed laminar case. The conditions were $M_\infty = 5.4$, $T_\infty = 42.2K$, $P_\infty = 0.0128$ atm, $Rey_\infty \simeq 210^5/in$. The total length of the strut is approximately 5", and one should expect transition to turbulence somewhere at the end of the strut. However because of the leading compressive ramp (7°) and of the porous (i.e. rough) plate in the first half of the flat plate section, one could expect transition sooner. There is however no definite way to predict the transition with precision and there were no measurements intended to measure the properties of the boundary layer on the strut. We decided to ignore these effects for the moment. In addition, when fuel injection takes place, the flow becomes obviously turbulent: the algebraic (Baldwin-Lomax) model is then unable to model the correct physics, and ideally one should use a 2-equation model at this point. The development and validation of a $k-\epsilon$ model is one of the high priority development for 1990.

Figure 10 shows the computed density contours in logarithmic scale for the strut flow field prior to fuel injection. Of special significance is the boundary layer detachment on the top and bottom surfaces, at the start of the trailing ramp section. The detachment and development of the shear layer are also clearly visible on the schlieren. In addition,

weak recompression shocks are seen to originate from the trailing edge itself. This can also be observed in the computed density field, although the pattern is more complex: it appears that weak shocks are thrown off from the pairs of vortices on opposite sides of the strut. The flow between the struts shows a regular diamond pattern from the multiple shock intersections. There is also a recirculation region on the flat plate in front of the first shock impingement. Because of the good resolution of bot grid systems and numerical scheme, one can observe in detail the pattern of shocks and expansion waves, especially near the recirculation region. Figures 11 through 19 show the development of the flow field during injection by a time accurate simulation. This series of computations was done to provide the camera crew of the NOVA series with data for a future PBS presentation. Notice at the end of the run (near 200 μsec) that there is a flickering instability (better shown in the movie version) of the mixing layer at the trailing edge, upper section of the strut. We assume that this transient dissipates at later times; this may also happen only within the laminar flow assumption, where dissipation through viscous effects is a slow mechanism.

Another calculation (done previous to the time-accurate one) was done for steady state. The difference lies in the fact that the flow in each region is computed individually (or by small groups) until steadiness is achieved, using extrapolation boundary conditions instead of grid overlaps. There is therefore a local time variable for each grid. In this calculation, initial values and initial boundary conditions differ from the time-accurate version. The results are identical, except for the absence of this 'whipping' layer at the trailing edge (Figure 20). In Figures 21 through 23, we show the temperature, Mach number and stagnation pressure. It can be seen that the fuel injection and its associated shock lead to large drops in stagnation pressure.

The corresponding schlieren is shown in Figure 24: in this picture, the flow between the two strut surfaces is very complex, and there seems to be larger areas of flow separation and recirculation on the surfaces. It is however difficult to obtain a clear experimental picture of the flow. Most of the features of the flow however are reproduced by the simulations, especially the strong bow shocks in front of the injectors, and the diamond pattern of shock interactions. The mixing obtained by a strictly 2-dimensional simulation is very poor, and is below the measured mixing. This can be easily explained by the importance of three-dimensional effects, especially longitudinal vortices. In addition, it is not clear what are the turbulence levels in the experimental flow: a more detailed comparison could be obtained only if three dimensional computations are performed. Although this task was planned, upcoming funding difficulties for this project make the realization of these computations in the near future doubtful.

IV: Simulation of Ballistic Experiment

The series of ballistic experiments performed in the 1970's at the Institute of Saint-Louis provides us with a clean database for code validation. These experiments involved the shooting of a projectile of simple geometry (sphere-cylinder or cone) into a pre-mixed hydrogen-air or hydrogen-oxygen gas mixture. The problems of injection and mixing are therefore alleviated, and one can concentrate on the validation of the chemical kinetics and the coupling between the flow dynamics and chemical kinetics. One of the most difficult cases to reproduce is the intermediate case between detonative regime and uncoupled shock-flame regime. In the first case, the heat release occurs immediately behind the shock front, and it is impossible to distinguish the shock from the flame, even looking at the experimental schlieren. The simulation of this case is easy, because the finite size of the grid elements provides a spurious coupling between the shock and

flame. Indeed, if shock and flame are located within the same computational cell, or are in neigboring cells, the inherent numerical diffusion of the algorithm will automatically combine the two. In fact, the situation is much worse, because of the sensitivity of the width of the reaction zone to the chemical kinetics. Previous attempts at reproducing the experimental results had partly failed because the numerical diffusion was too large: the radical species diffusion into the pre-ignition zone accelerated the chemistry, and the point where the shock and flame decoupled was not properly located. By appropriately slowing the chemistry (by $\simeq 30-50\%$), one could compensate for this numerical effect, bu at the expense of loosing predicting value.

Since these first attempts, we have continued the simulations, but with a much higher grid resolution, and the results have been spectacularly good. Here, we simulate the hydrogen-air case at $M_\infty = 6.46$, for a sphere-cylinder model. The experimental schlieren is shown in Figure 25. The decoupling of the flame and shock is clearly shown. The corresponding numerical result (Temperature contours) is shown in Figure 26. The point of decoupling occurs relatively at the same position (angle estimation), and this constitutes an excellent validation of the code. In the course of this calculation, we have revised some of the reaction rates, although the most important for flame propagation ($H + O_2 \rightarrow OH + O$) or ignition delay ($H_2 \rightarrow H + H$) did not change by much. We also incorporated the effects of various 3^{rd}-body efficiency into the kinetics algorithm, an additional development that was long overdue. These calculations used 44 one-way reaction steps, and 9 species (N_2 inert), including HO_2, H_2O_2. We would like to pursue these validations for other cases, and plan to attempt the case of oscillating combustion, pictured in Figure 27. This case is extremely difficult, and requires the modelling of the interaction between chemical kinetics and sound pressure waves. We believe however that the code has the required capabilities to reproduce this flow, with minor changes

and enhancements. This task will be pursued in 1990.

V: One-dimensional Engineering Analysis of ODWE

In addition to strict CFD, we have worked on an engineering code and provided the engine data base for the analysis and comparison of the ODWE performance, versus conventional scramjet. The engine data was supplied to another code for structural and mission analysis, and the overall results were presentd at the ISABE conference in Athens, Greece. The original code was provided to us by D. Bogdanoff, and extensively modified by ourselves. First runs were made for a scramjet engine. After succesful tests of the modifications, a second code version was made to model the ODWE. Both analysis were made in one dimension, and involved many simplifying assumptions which are common in these types of analyses. The resulting codes, as the original one, are very specialized, and there was no time available to attempt to make these codes more user-friendly for future purposes. Rather than describe the work here, we refer to the paper presented at the ISABE conference, a copy of which is provided in the Appendix.

VI: Proposal Research

During the year 1989, we have also made serious efforts in attempting to obtain funding for the project and related projects from NASA Headquarters. The first series of attempts was made concerning the Generic Hypersonics program. Several of our proposals (ODWE, Bifurcated Spiralling Strut, Shock Impingement in Combustors) were well received by F. Moore, who acted as technical consultant to NASA Headquarters, and were to be funded for a total of nearly $900,000. Unfortunately, after the recommendations of F. Moore, the budget went into a state of flux, and intense competition

from NASA-Lewis killed most of this funding. It is not known what final arrangements were made concerning this program, between Ames and Lewis, and Headquarters.

Another (starting) program was the High Speed Civilian Transport (HSCT): several proposals were written and some were accepted for initial funding (plasma ignition, reacting fluid element model, new combustor concepts for low NO emission) of $150,000. This funding was attributed to the RT branch.

VII: Conclusions

The code development has focused principally in 1989 on non-equilibrium flows, at high temperature. This development was originally intended to provide a numerical capability for the simulation of arc-jet flows, in which the ODWE experiment was taking place. However several spin-off applications can be derived from such a capability, and we feel that it may be used in the future to considerably extend the scope of the overall numerical capability of ELORET and Ames RTA division.

Continued validation of the MOZART code was succesful in reproducing a shock-flame interaction. This work will continue in 1990, on more difficult cases yet.

The simulation of the strut flow field in the ODWE experiment provided great detail on the shock-shock interactions and shock-boundary layer interactions. Notably, the flow structure near the injector is particularly detailed (barrel shock, mach disk, etc..). The results agree reasonably well with the experimental schlieren, despite the uncertainty in turbulence levels.

The work completed in 1989 shows the excellent capabilities of the code MOZART, but also its limitations, namely in the area of turbulence modelling. For this reason the development of $k - \epsilon$ and multi scale capabilities will be an essential focal point for 1990. This is especially important since, due to enormous funding, other centers such as Lewis, have finally developed capabilities of the same type and same accuracy. It is crucial that the lead in code development must be kept intact, otherwise Ames will loose another area of dominance, and therefore area of funding. For that reason, we intend to focus on new developments in several areas of flow physics.

References

[1] J.L. Cambier & G.P. Menees, 'A Multi-Temperature TVD Algorithm for Relaxing Hypersonic Flows', AIAA 89-1971. Presented at the 9^{th} AIAA Conf. on Comp. Fluid Dynamics, Buffalo, New-York, 1989.

[2] J.M. Burgers, *Flow equations for Composite Gases*, Academic Press, 1969.

[3] S.I. Bragiinski, in *Reviews of Plasma Physics*, vol. **1**, Consultants Bureau, 1965.

[4] S. Eberhardt & K. Brown, 'A Shock-Capturing Technique for Hypersonic, Chem. Relaxing Flows', AIAA 86-0231.

[5] A. Harten, *J. Comp. Phys.*, vol **49** (1983), pp. 357-393.

[6] A. Kauffman, in *Plasma Physics in Theory and Application*, W.B. Kunkel ed., Mc Graw-Hill, 1966.

[7] P.A. Gnoffo, R.N. Gupta & J.L. Shinn, 'Conservation Equations and Physical Models for Hypersonic Air Flows in Thermal and Chemical Nonequilibrium', NASA TP-2867, 1989.

[8] L.M. Biberman & I.T. Yakubov, 'Approach to Ionization Equilibrium behind the Front of a Shock Wave in an Atomic Gas', *Sov. Phys. - Techn. Phys.* (engl. transl.), **8**, 1001 (1964).

Figure 1: Temperature profiles for 1-fluid model. Solid line includes electron heat conduction, dashed line is without conduction.

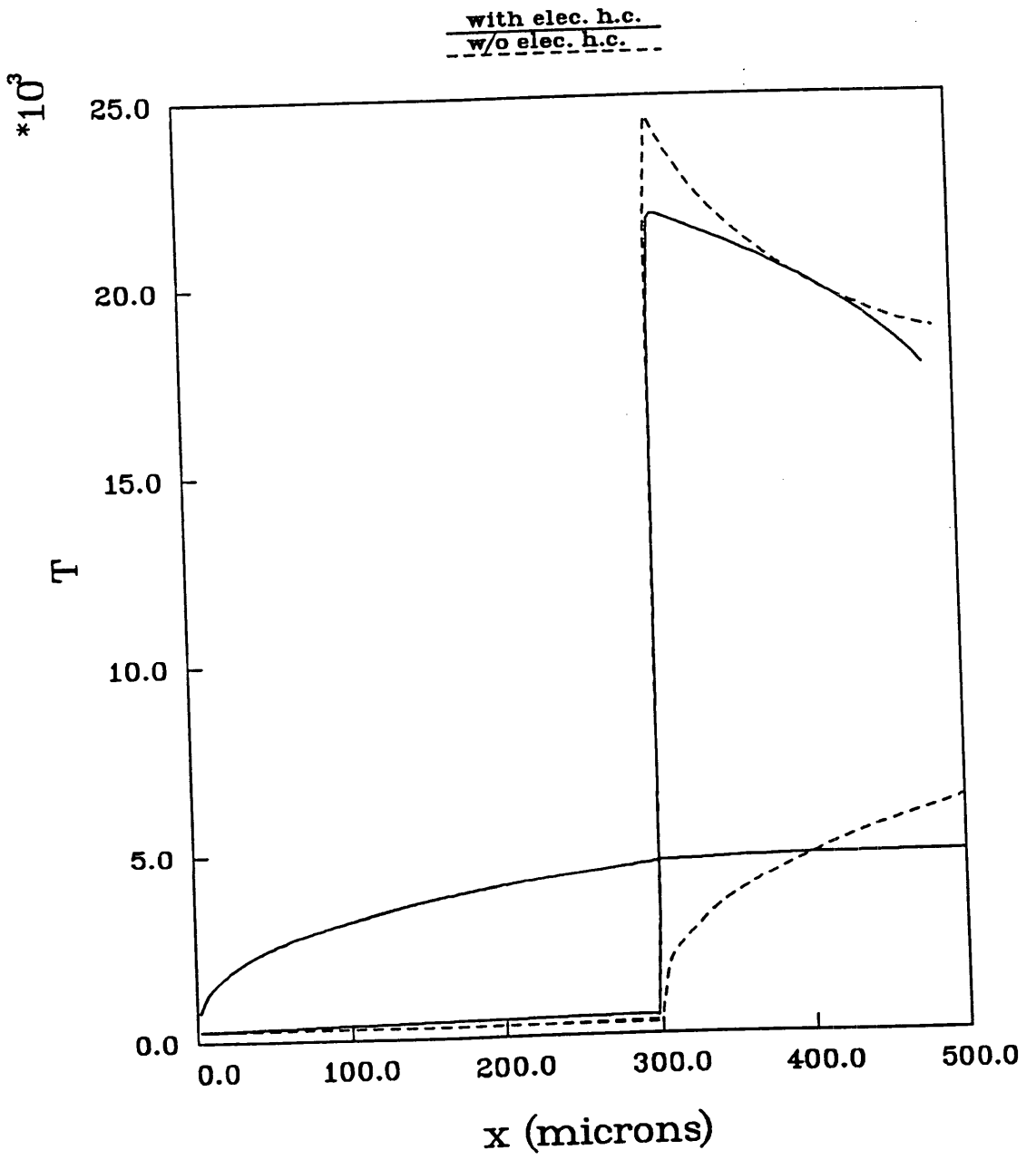

Figure 2: Density profile for 1-fluid model. Solid (dashed) line is with (without) conduction.

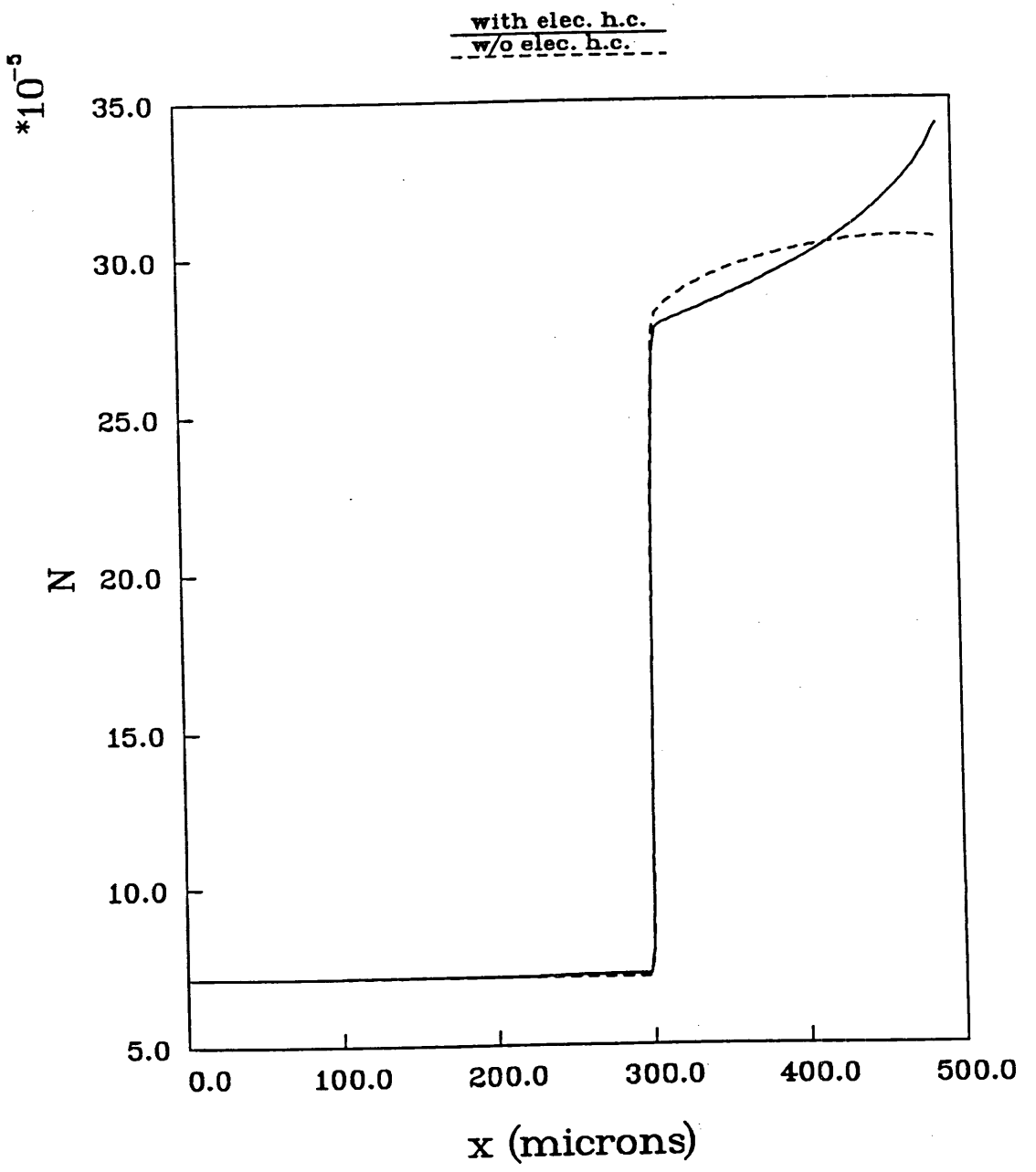

Figure 3: Electric field for 1-fluid model. Estimates use grid-scale (dashed) or Debye scale (solid) in computation of gradients.

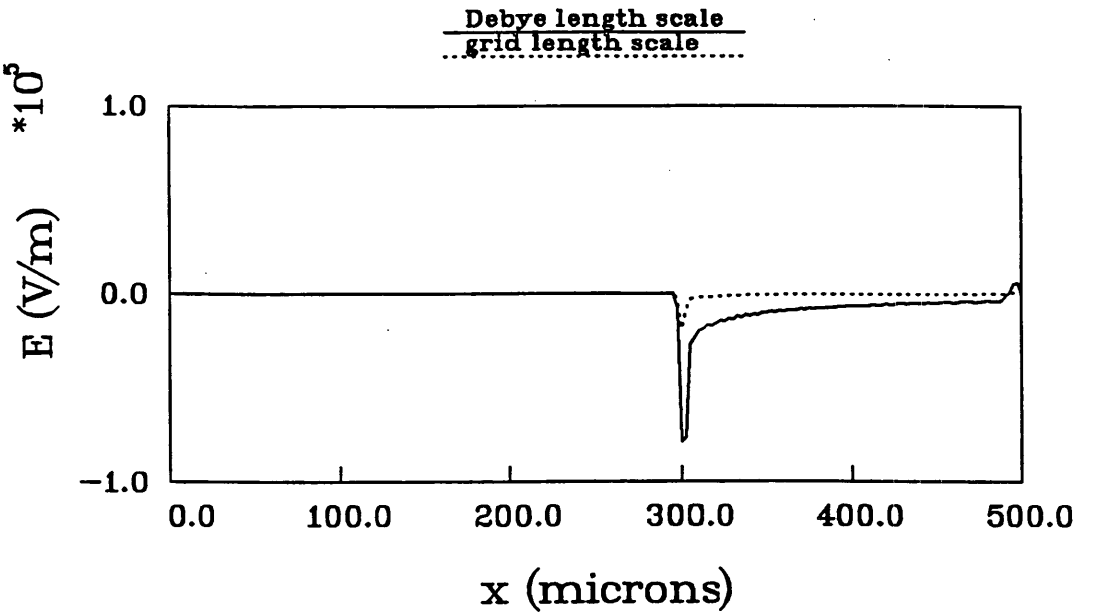

Figure 4: Density profiles for 2-fluid model, no artificial damping. Distance in microns.

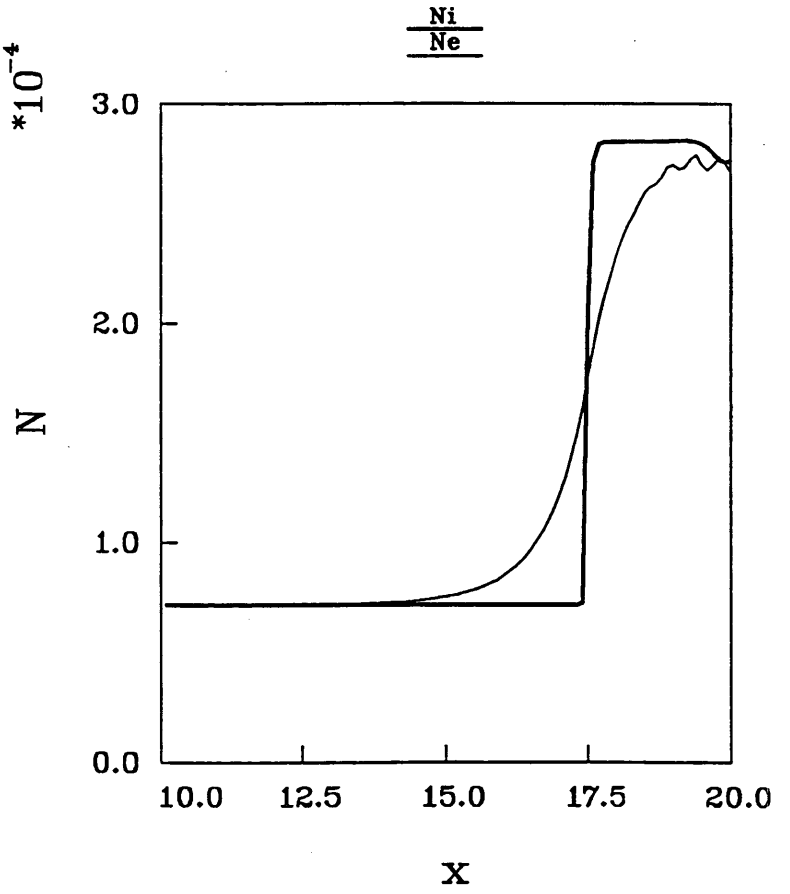

Figure 5: Electron velocity. Solid line without artificial damping. Dashed line obtained for $\nu'_{ei} = 5 \times \nu_{ei}$.

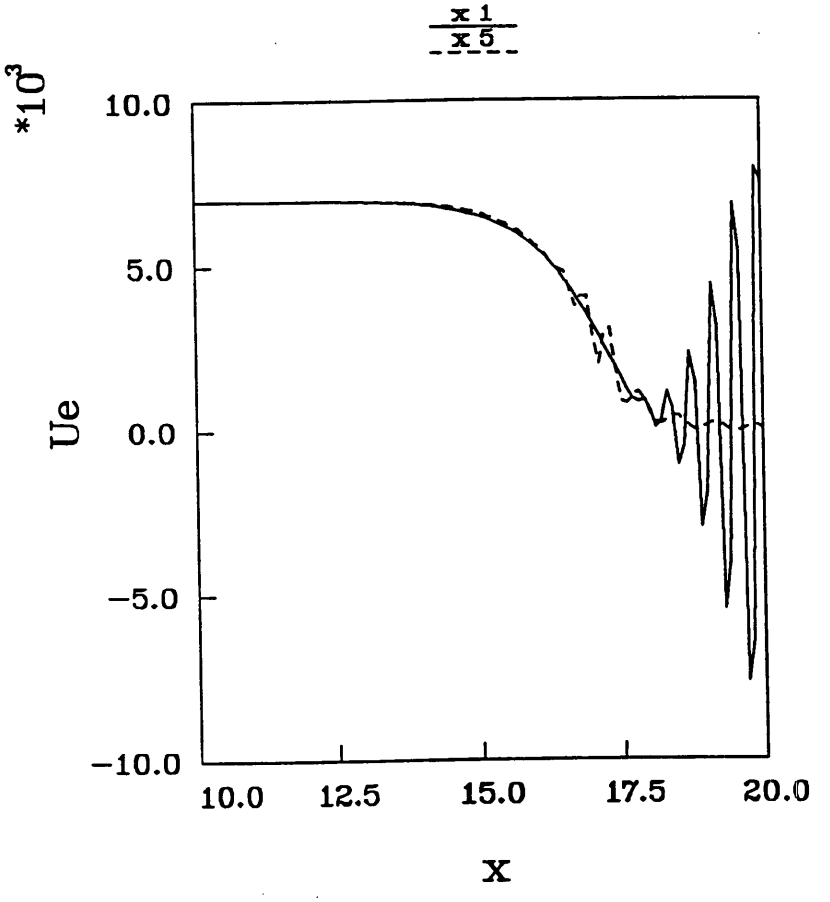

Figure 6: Electric field obtained for 2-fluid model. Dashed line is for artificially damped solution ($\times 5$).

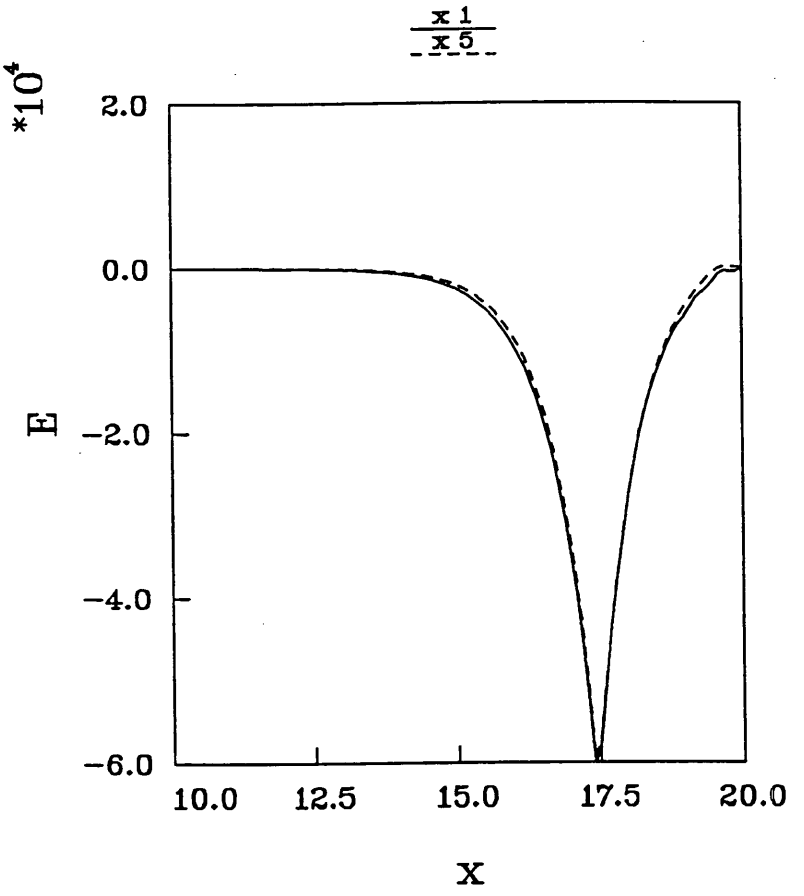

Figure 7: Relative charge density, 2-fluid model. Naturally and artificially damped solutions.

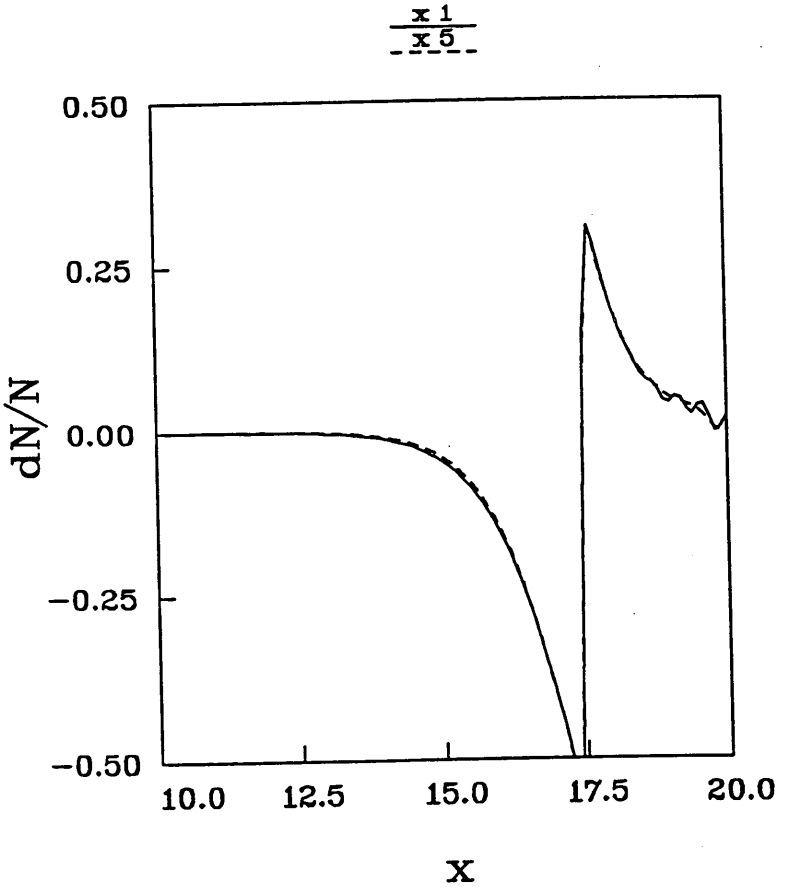

Figure 8: Density profiles for damped ($\times 5$) solution. Smoothing of oscillations does not affect the plasma dynamics.

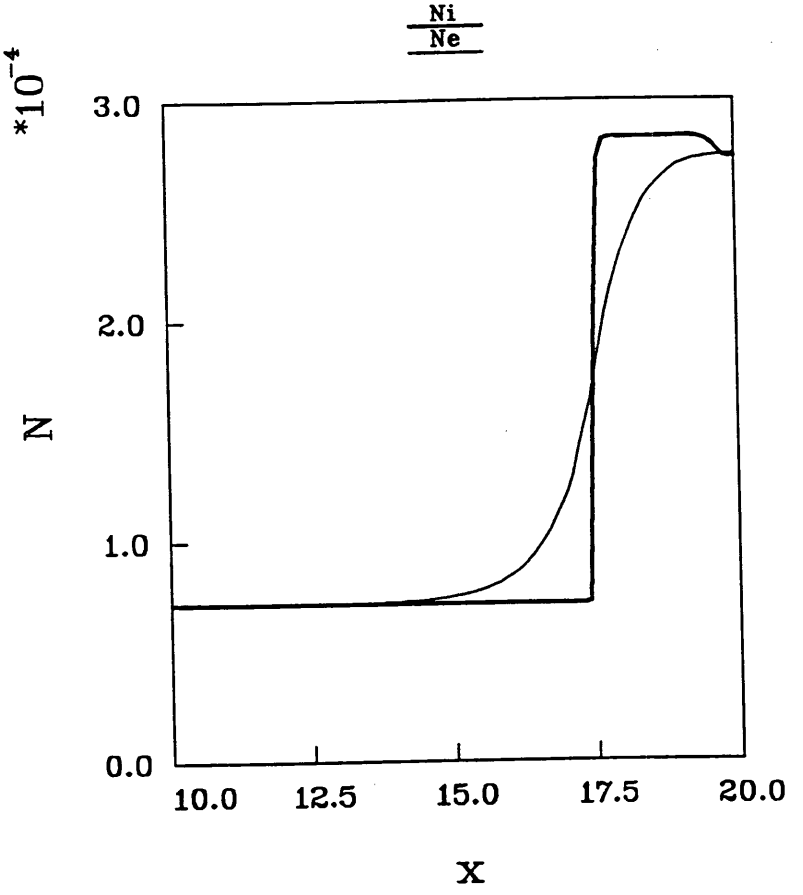

Figure 9: $T_i, T_e, \alpha, N_2/N_1$ for strong ionizaing shock in Argon. Insert is copied from ref. [8]. Ionization from ground state only, no precursor.

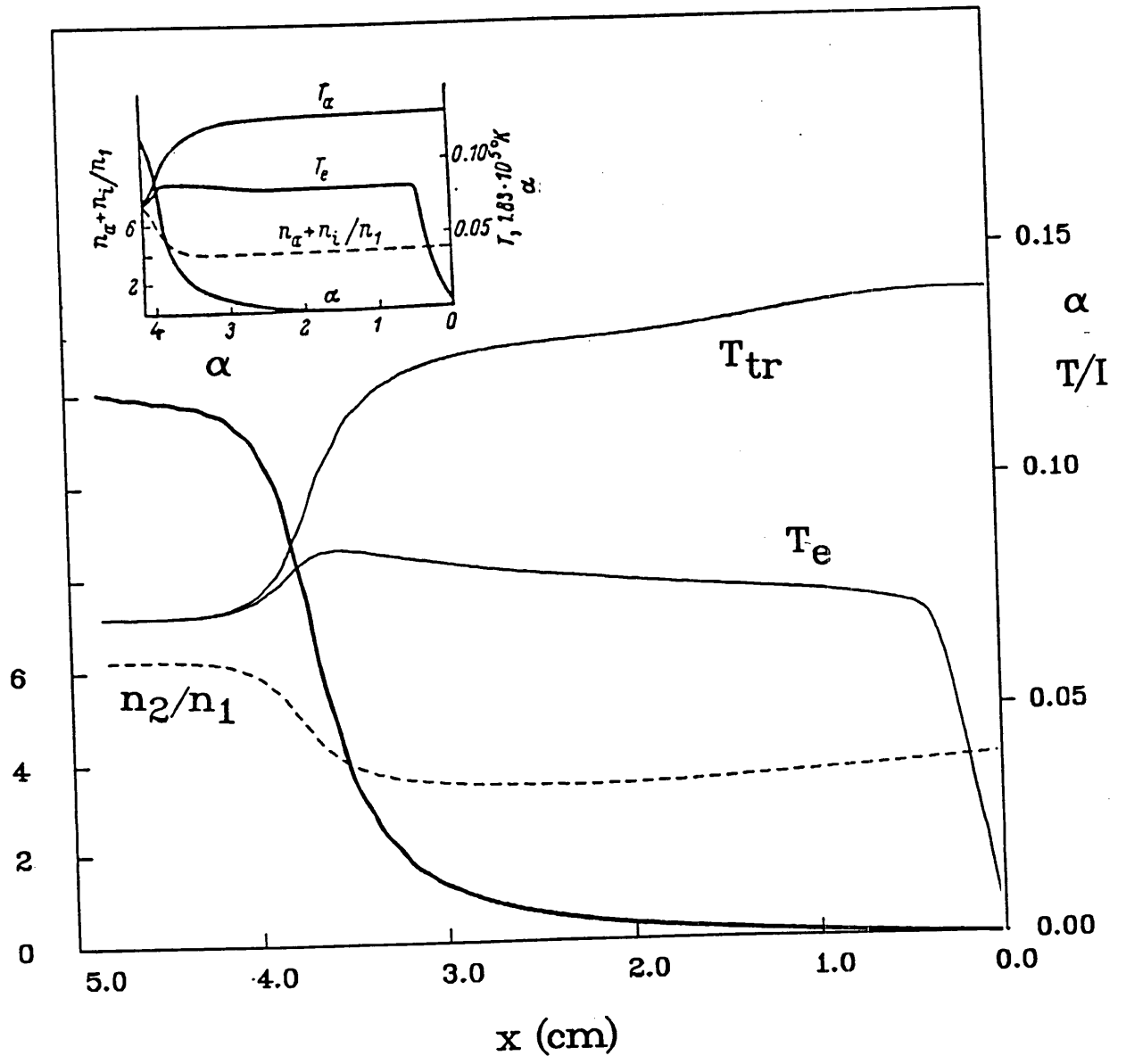

Figure 10: Density contours ($\log_{10}$ scale) for cold flow prior to ionization (t=0).

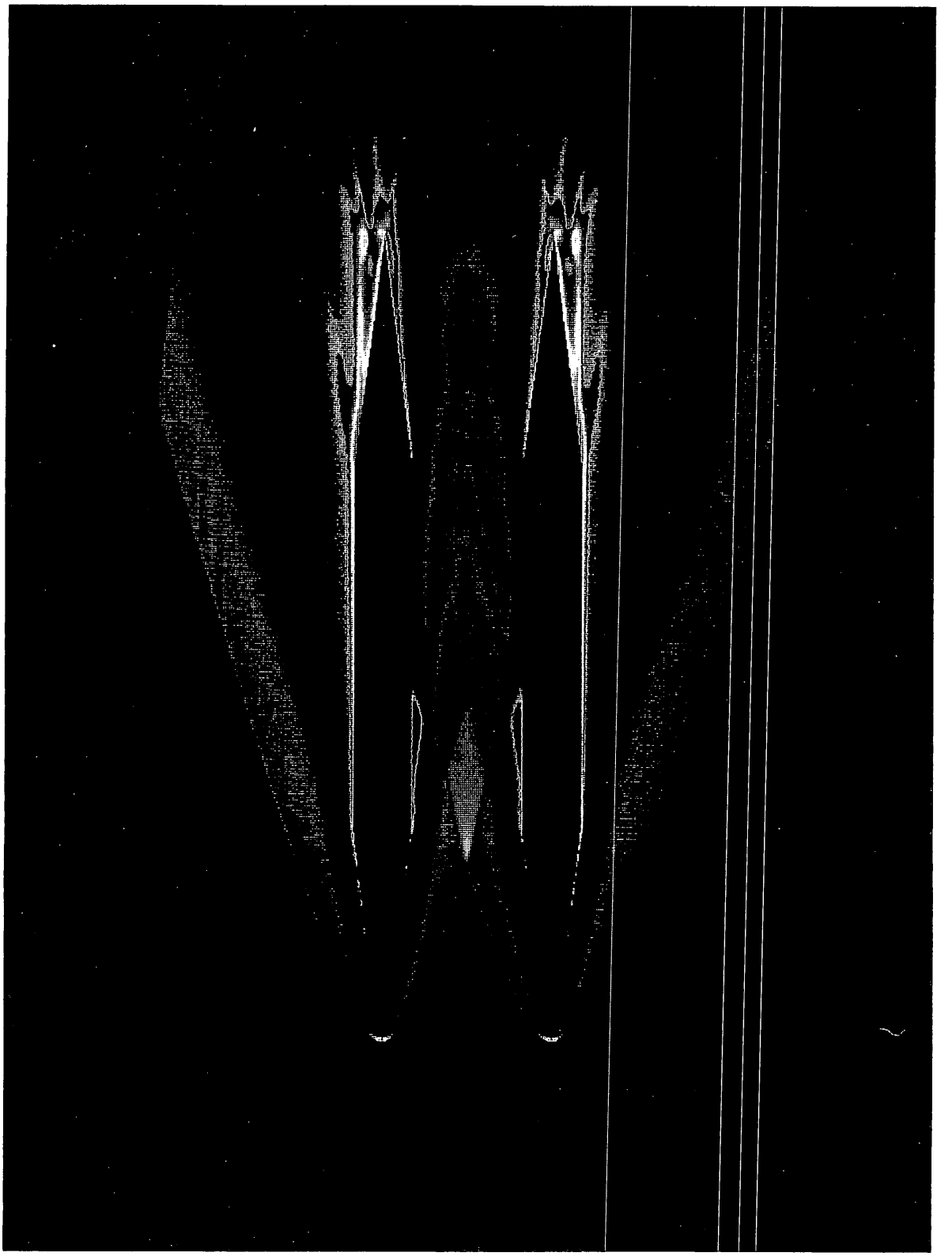

Figure 11: Density contours during injection. t=25 μsec.

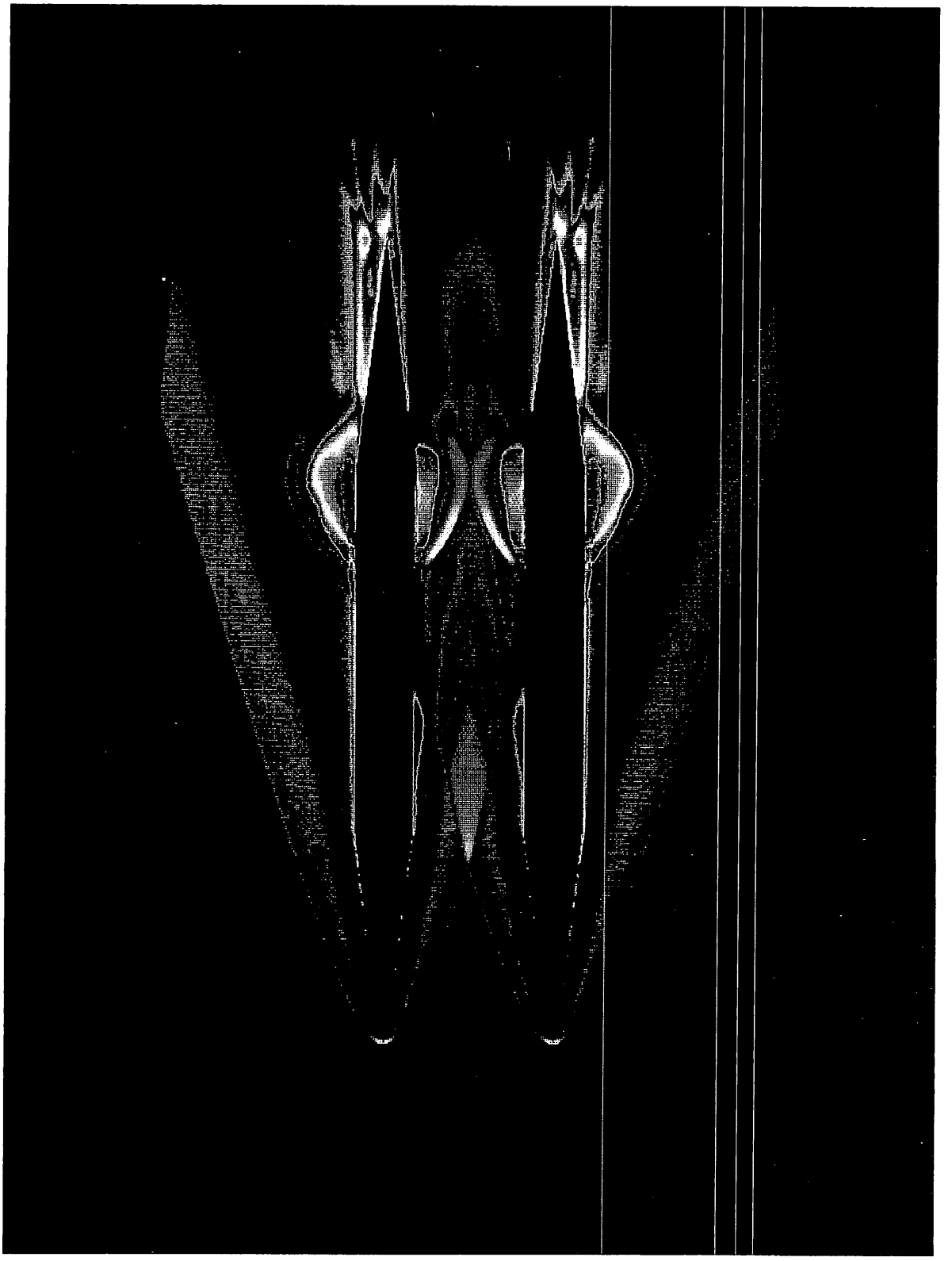

Figure 12: Density contours at t=50 μsec.

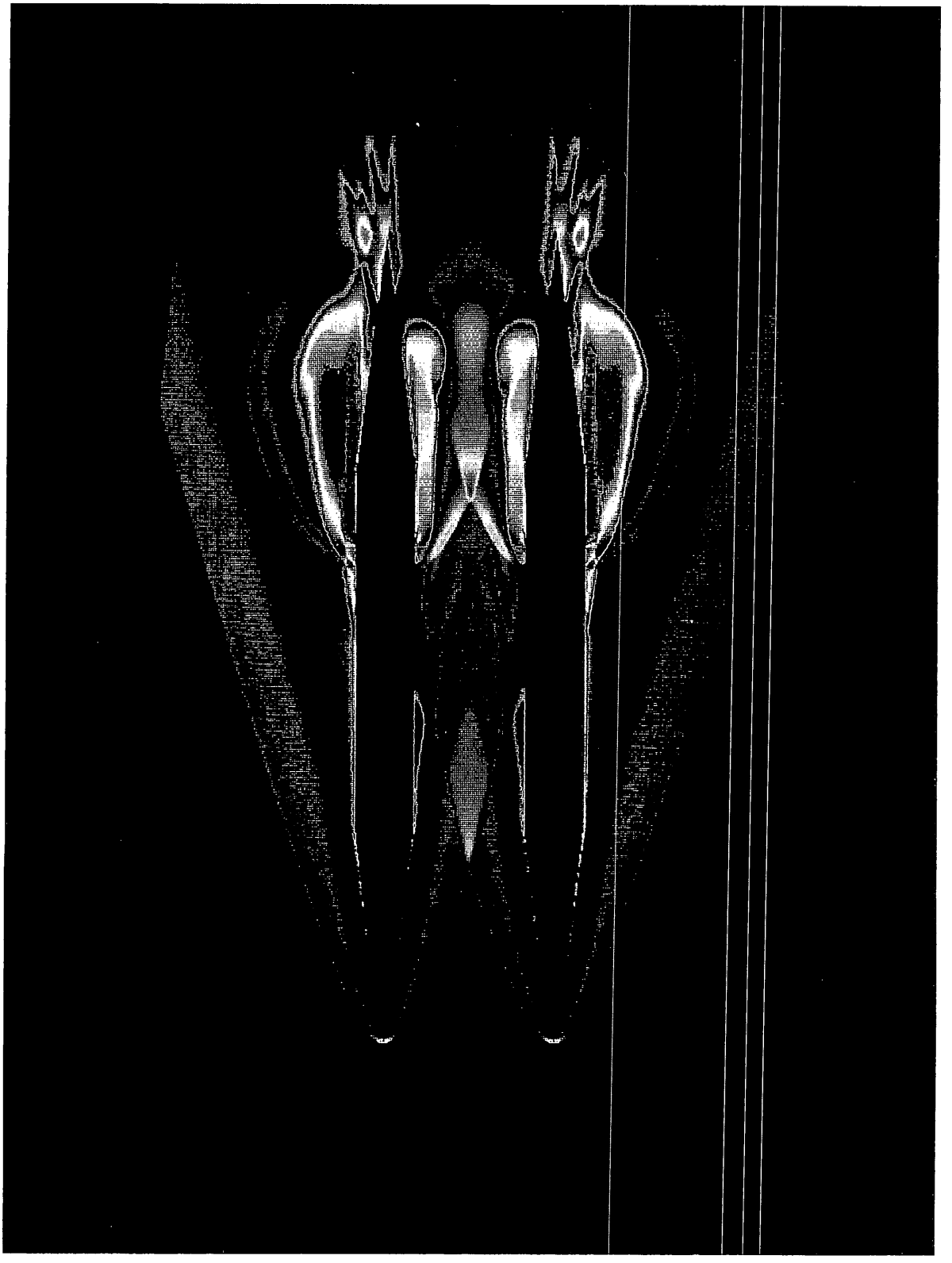

Figure 13: Density contours at t=75 μsec.

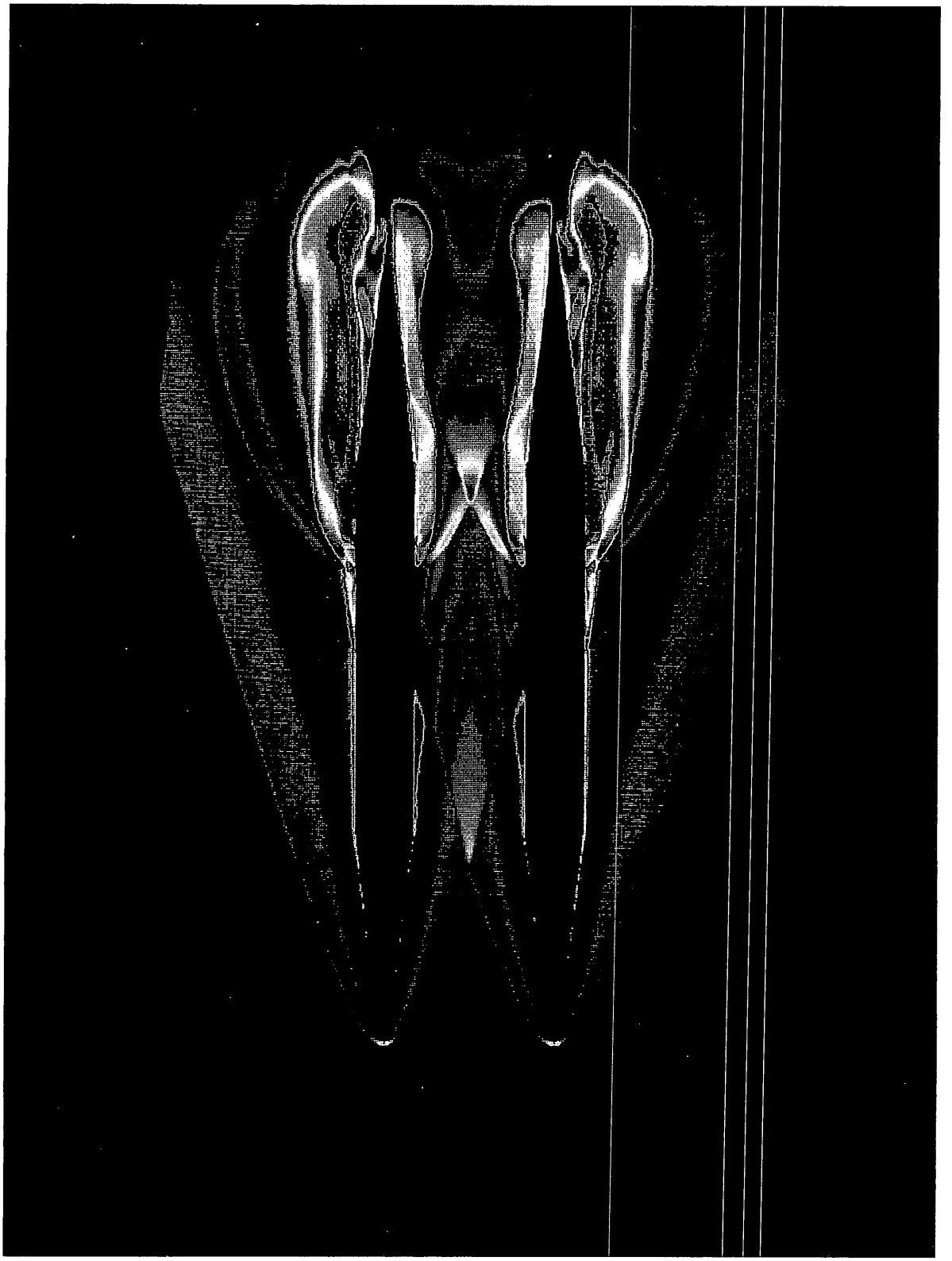

Figure 14: Density contours at t=100 μsec.

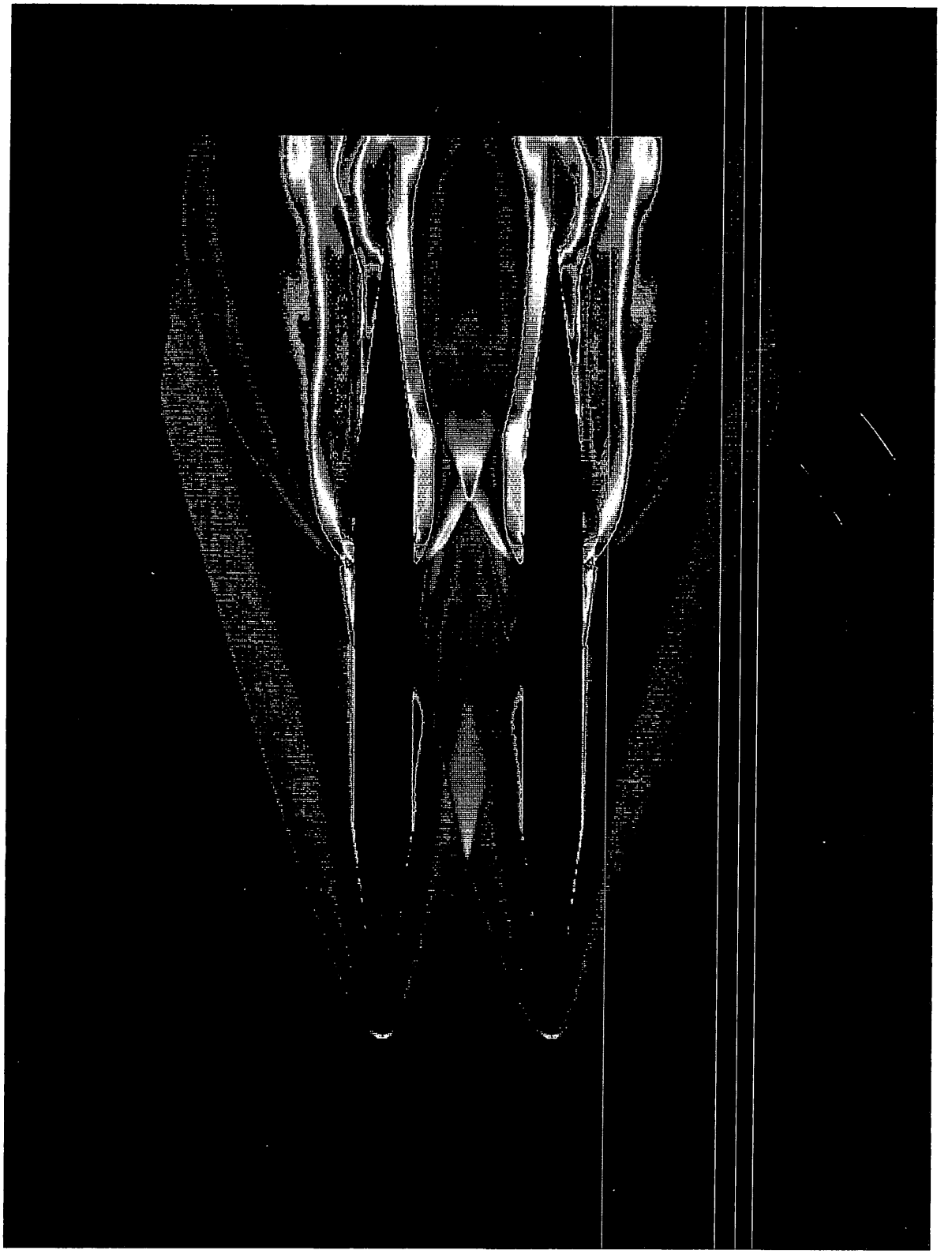

Figure 15: Density contours at t=125 μsec.

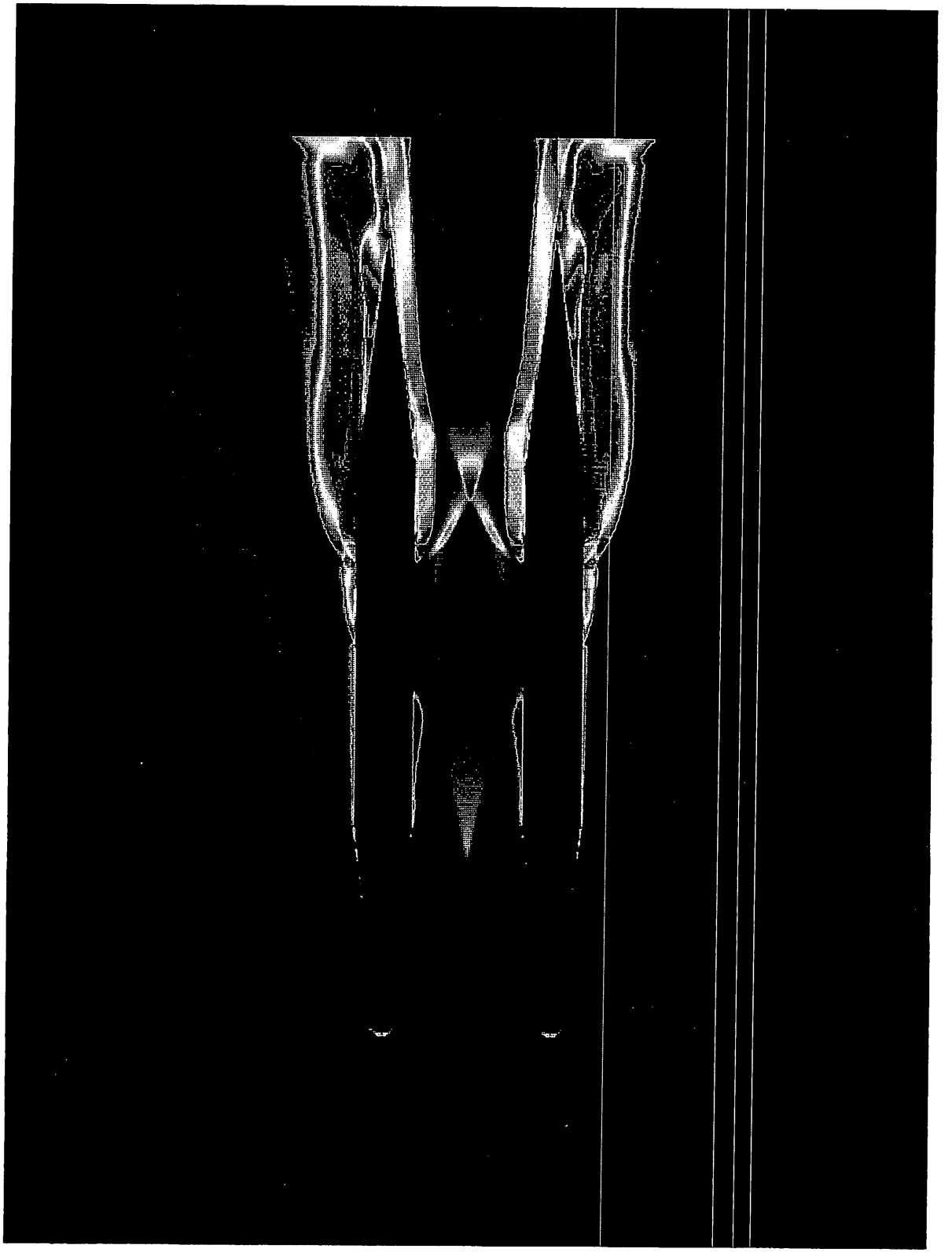

Figure 16: Density contours at t=150 μsec.

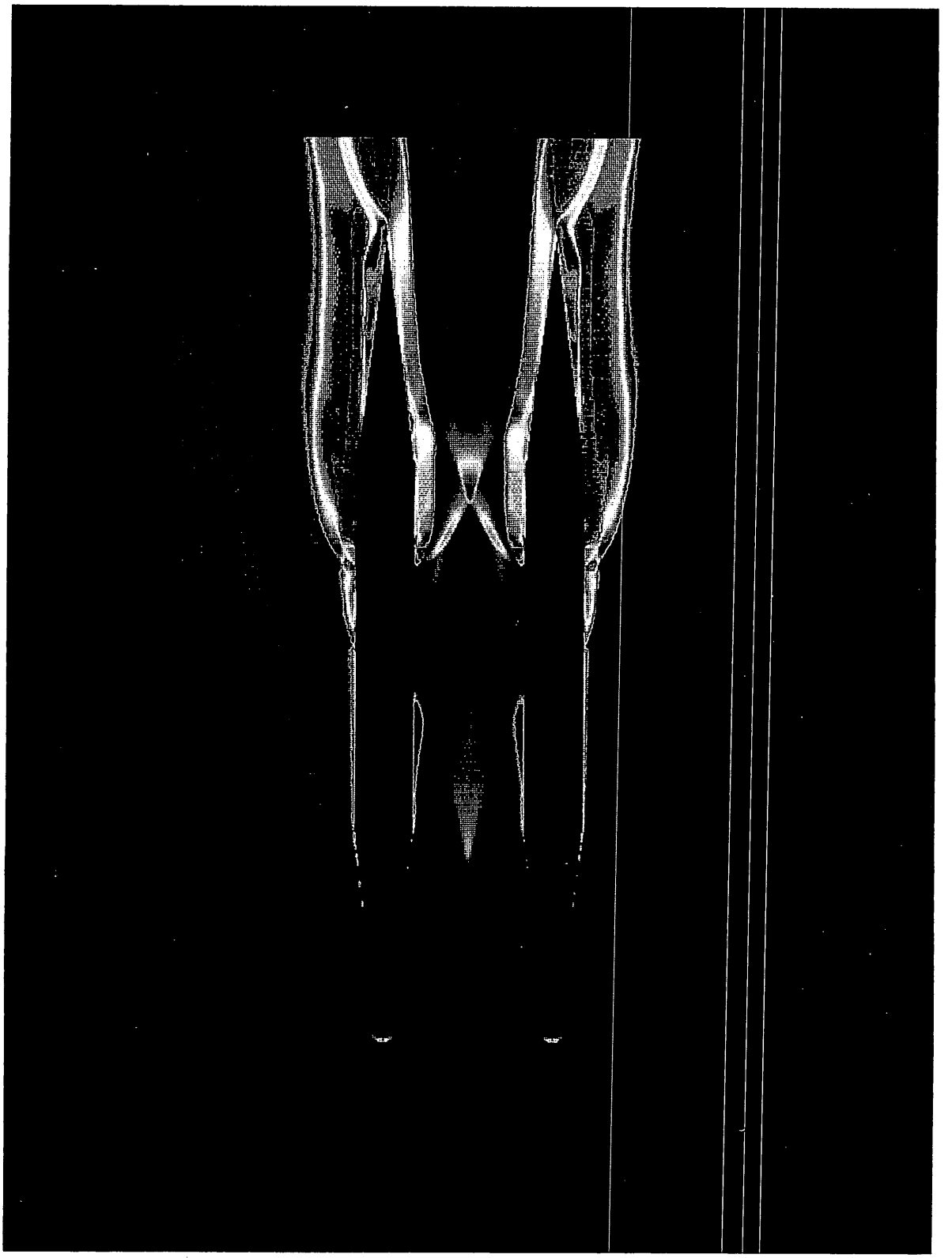

t=175

Figure 17: Density contours at t=175 μsec.

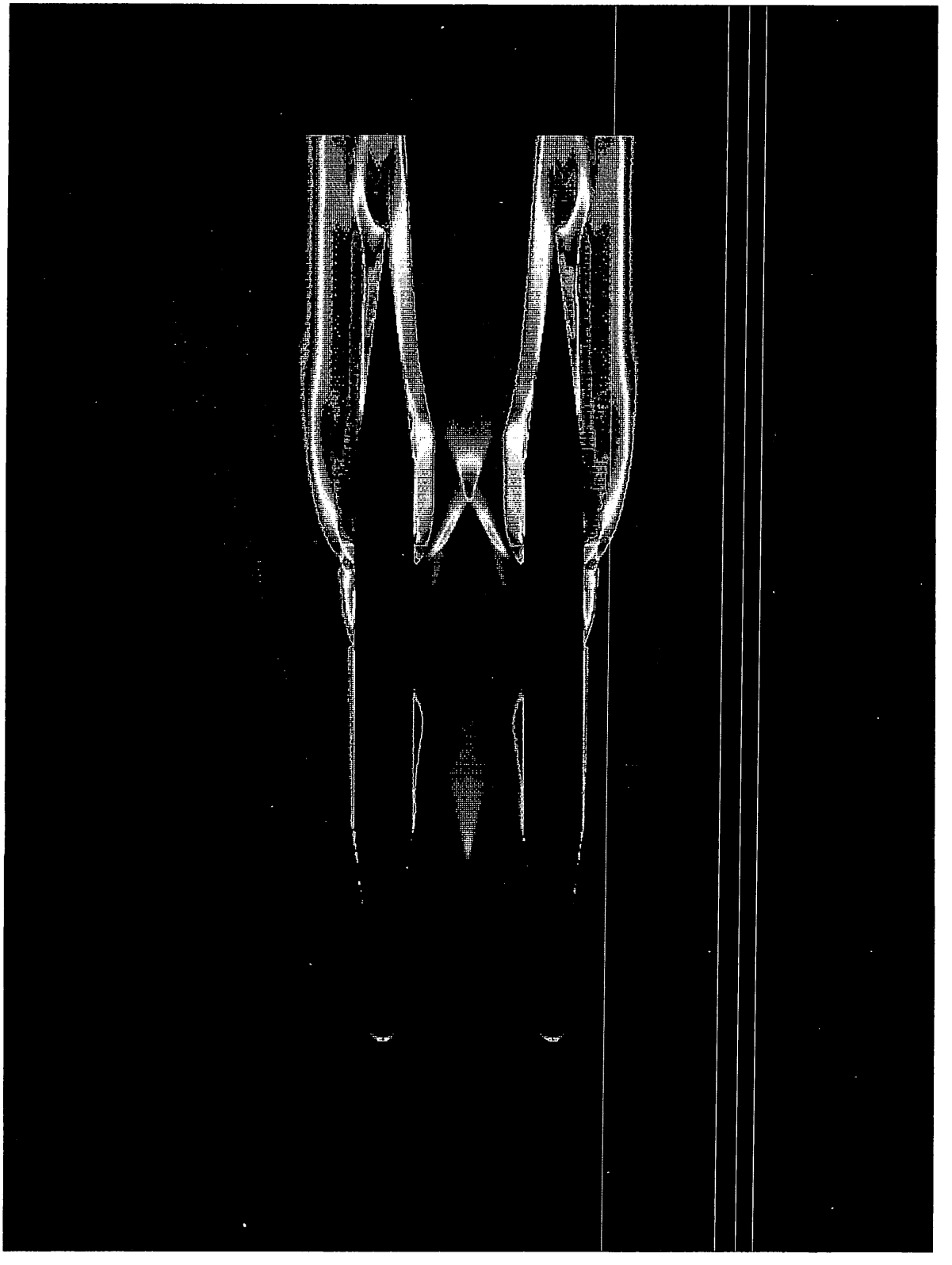

t= 200

Figure 18: Density contours at t=200 μsec.

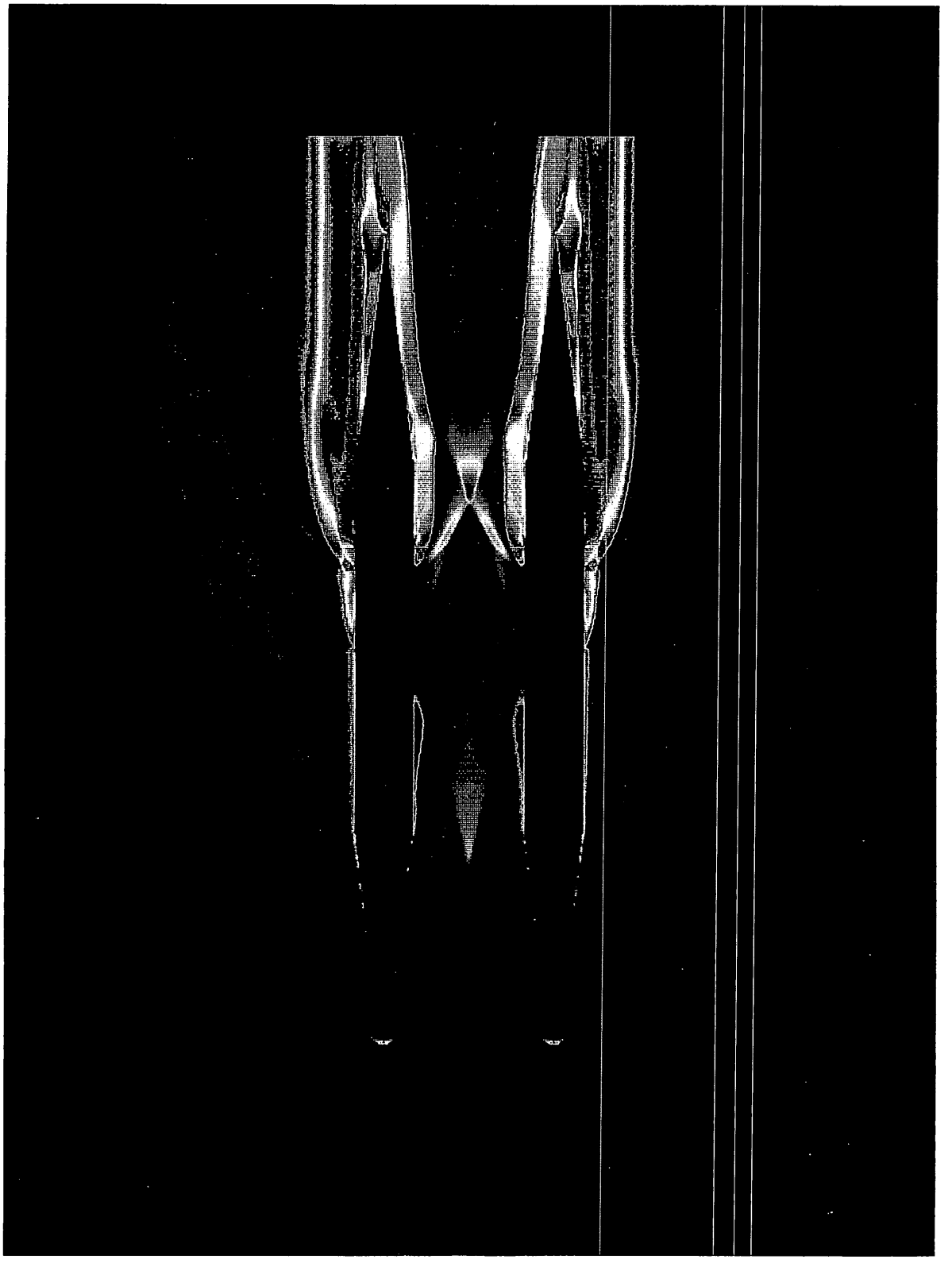

t= 225

Figure 29: Density contours at t=225 μsec.

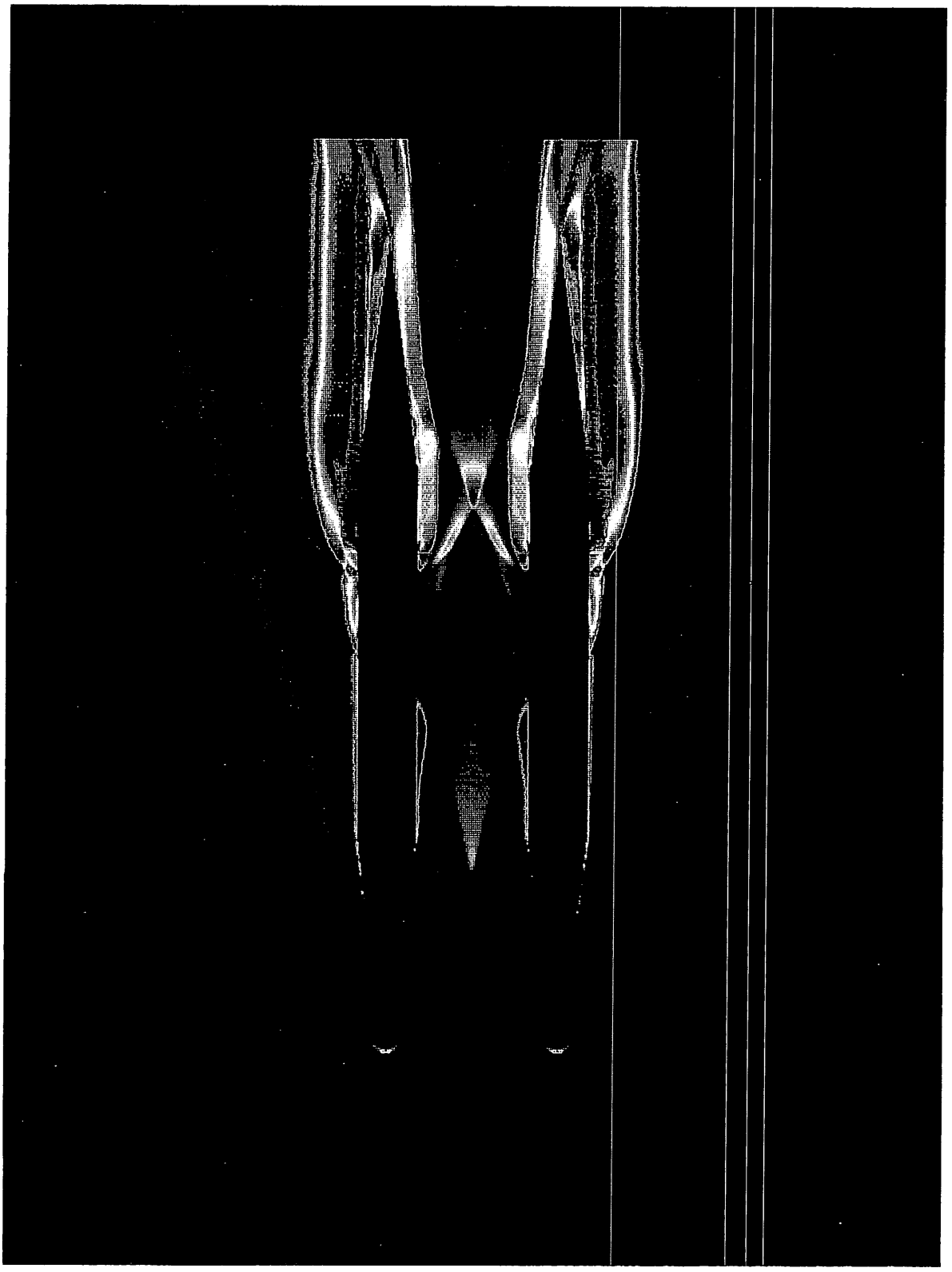

Figure 20: Density contours for steady-state calculation.

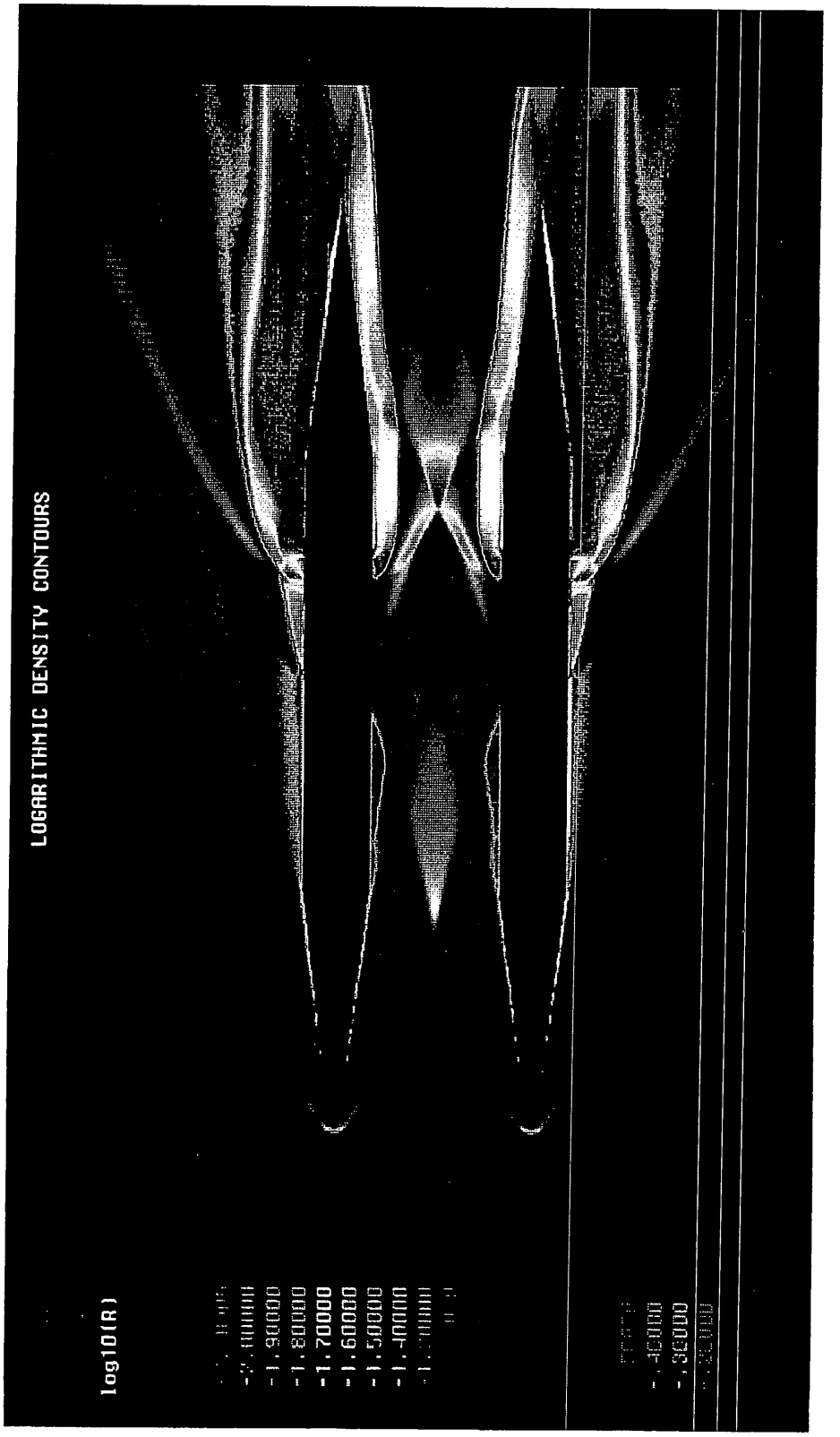

Figure 21: Temperature contours for steady-state calculation.

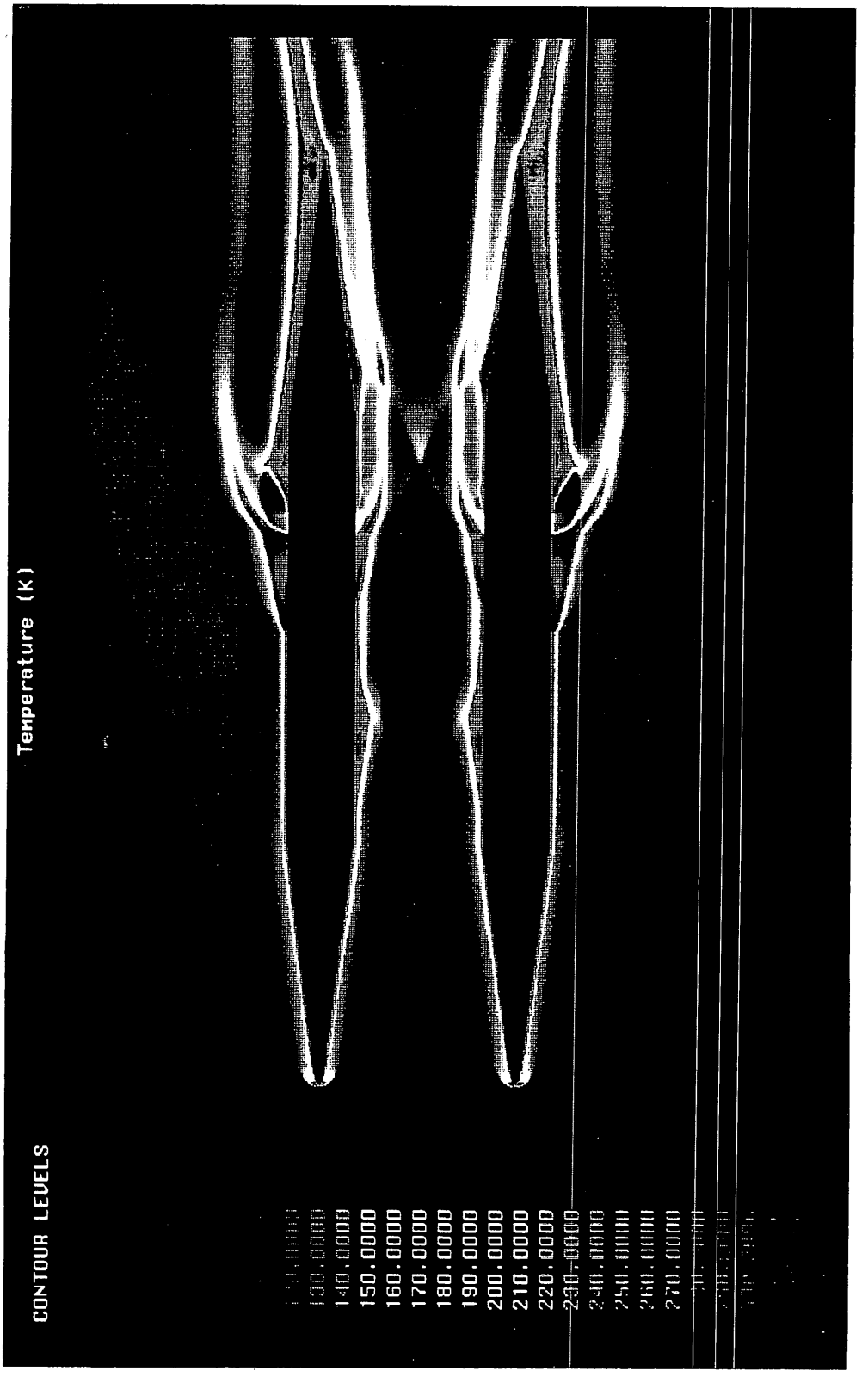

Figure 22: Mach number contours for steady-state calculation.

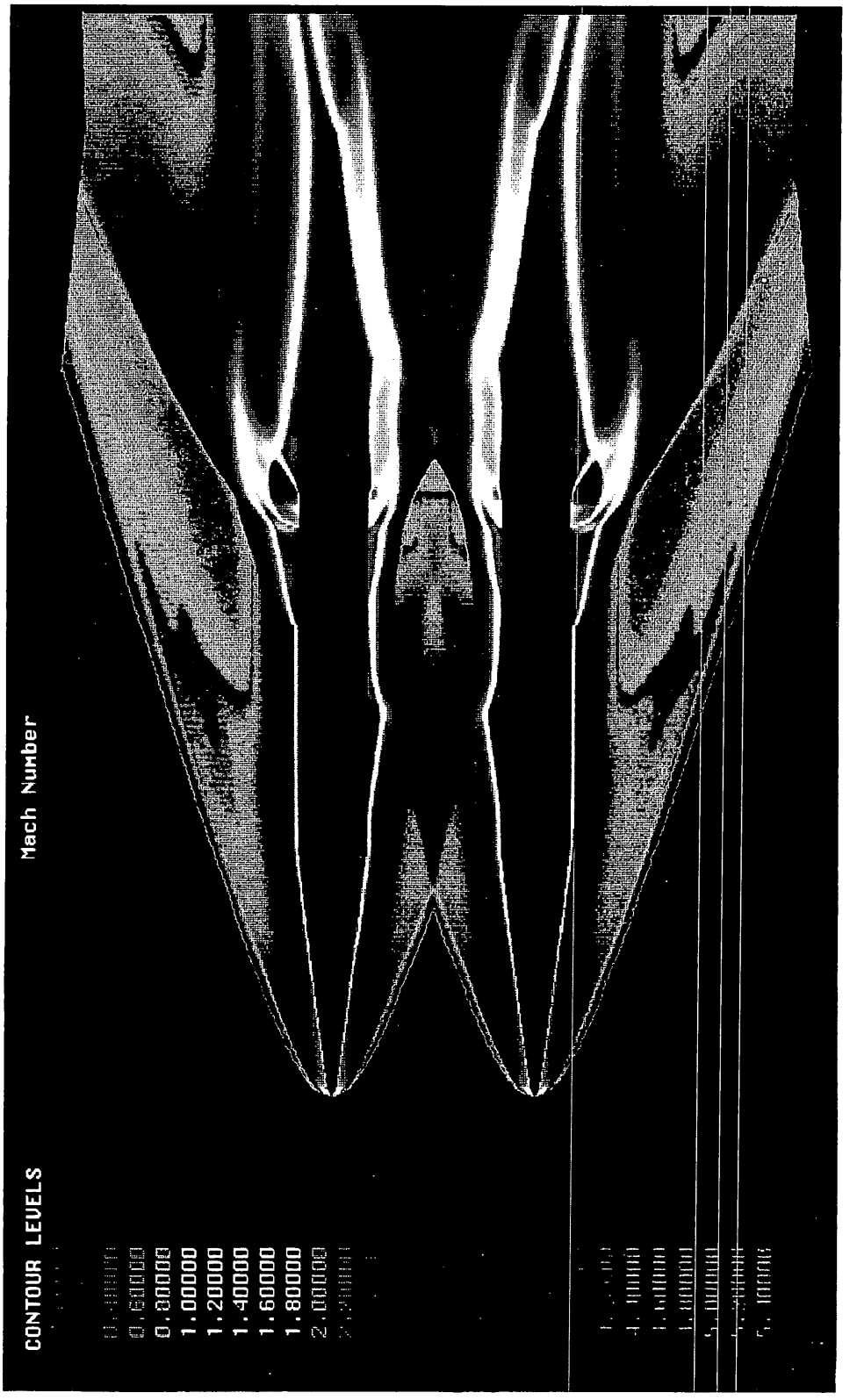

Figure 23: Stagnation pressure (atm) steady-state.

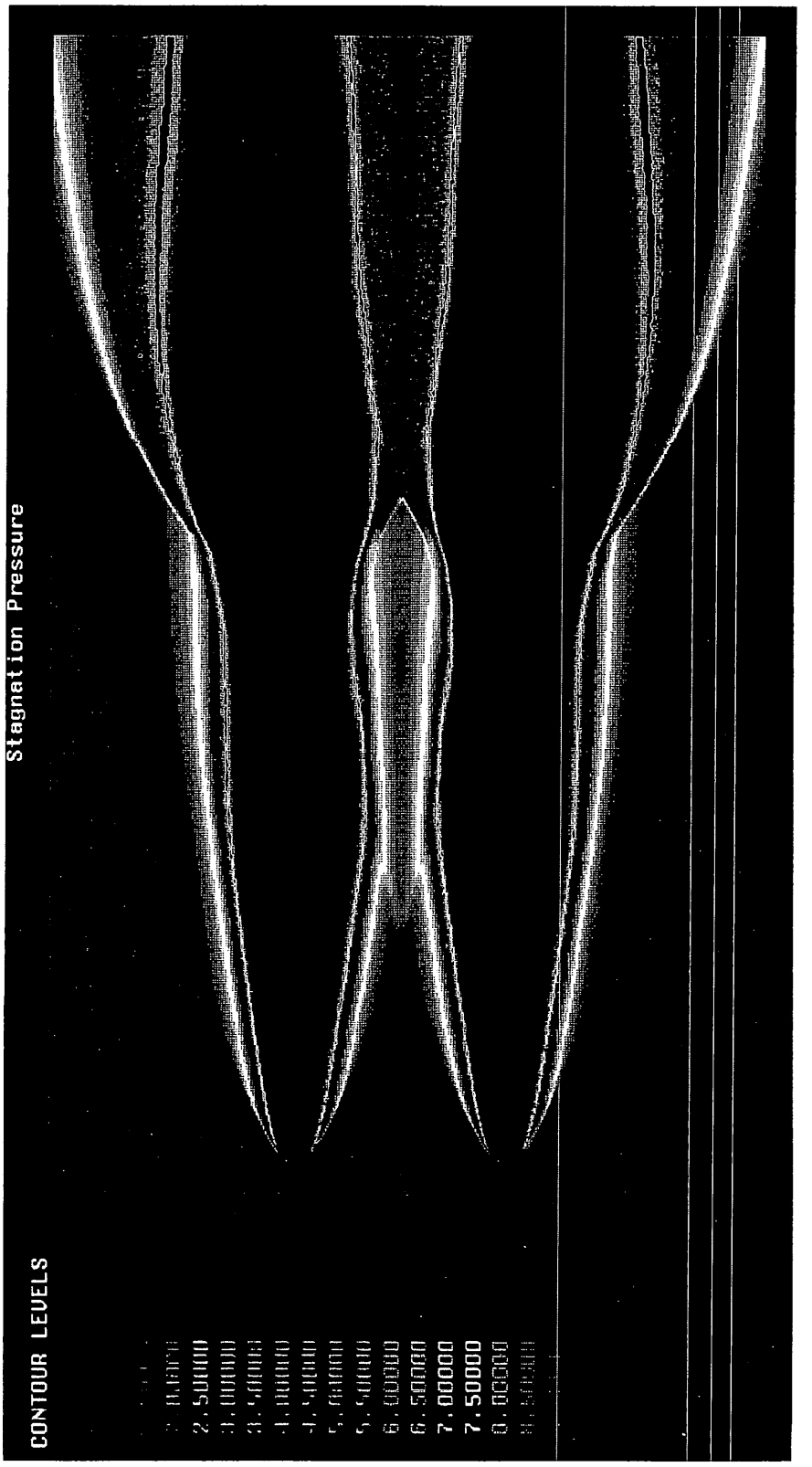

Figure 24: Schlieren for hot flow, fuel injection.

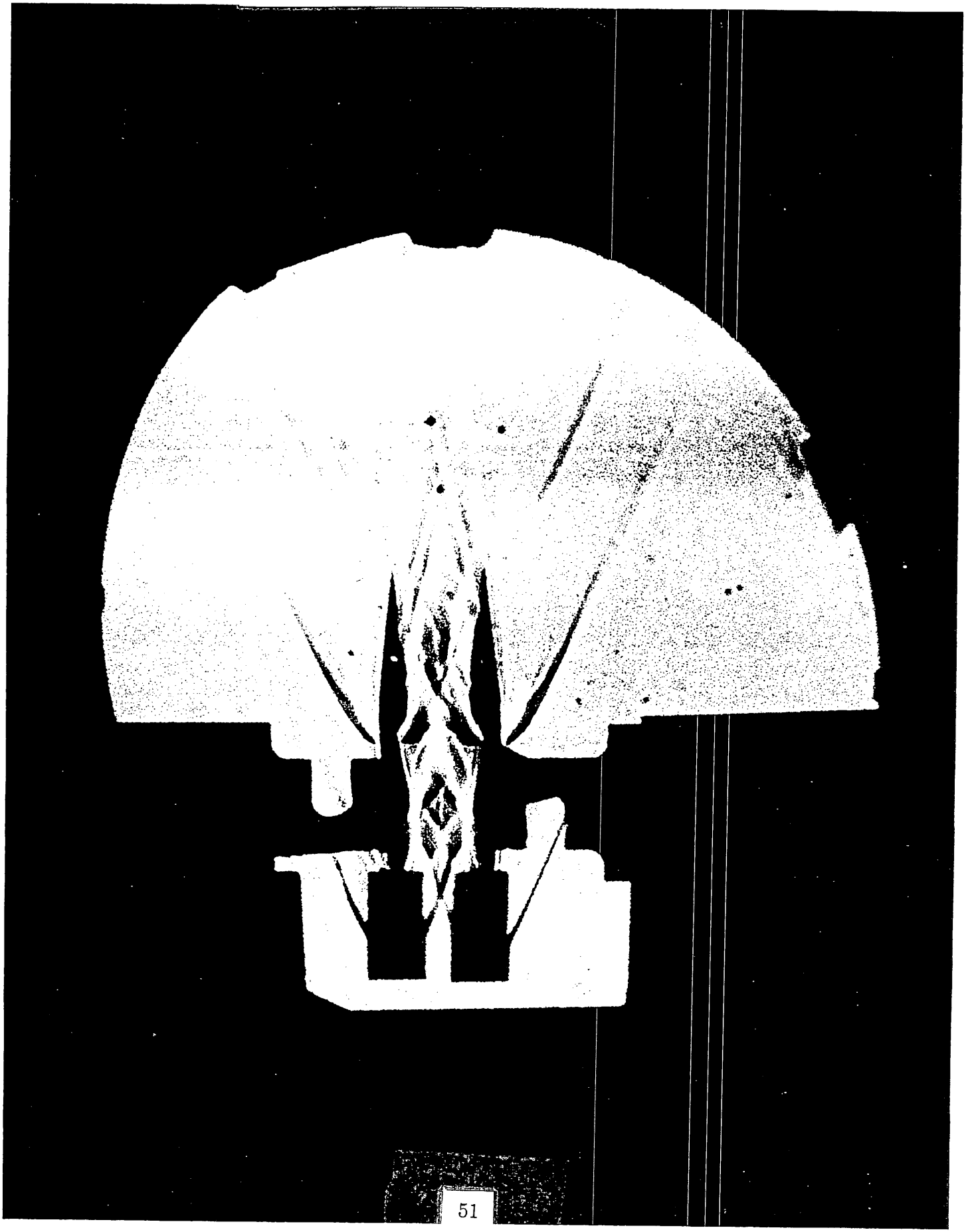

Figure 25: Schlieren of ballistic experiment H_2-air at M=6.46. Shock and flame decoupling shown.

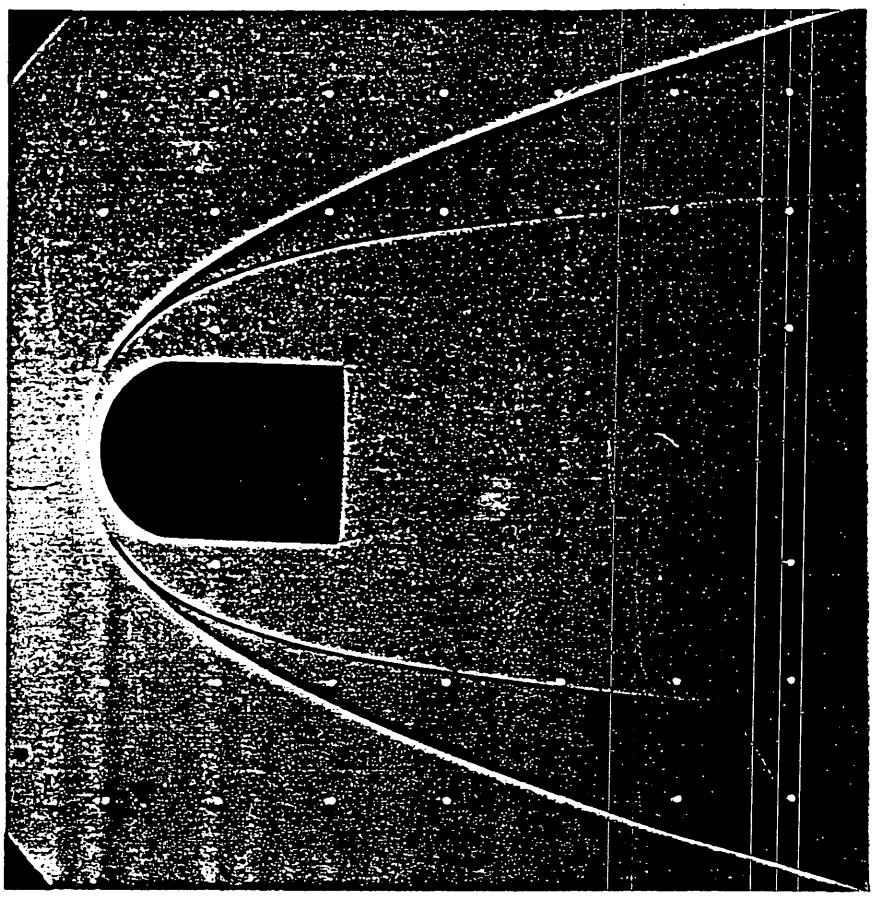

Figure 26: Computational results of Temperature contours for same case. Position of shock-flame decoupling almost identical.

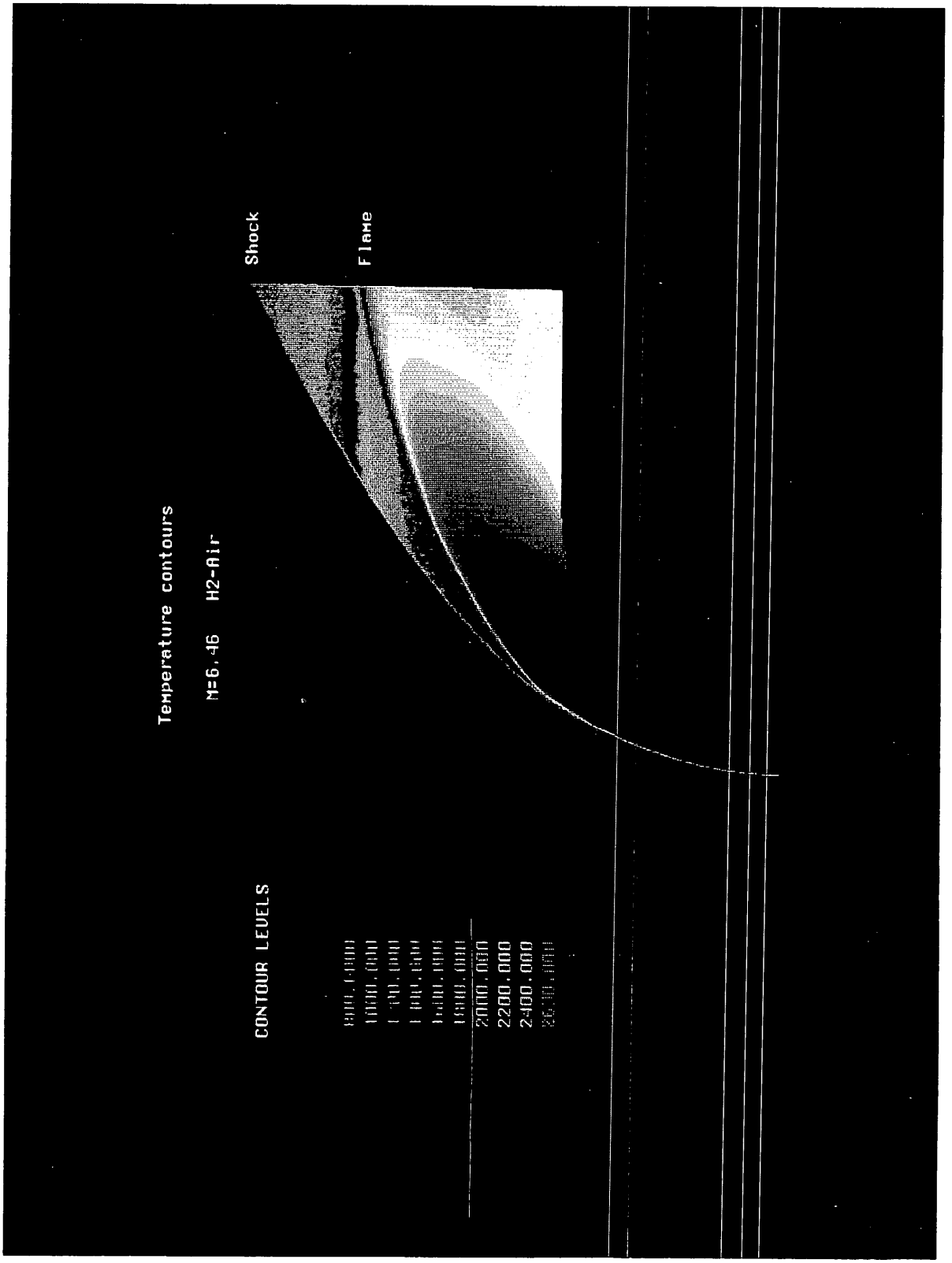

Figure 27: Schlieren of ballistic experiment for oscillating (unstable) combustion.

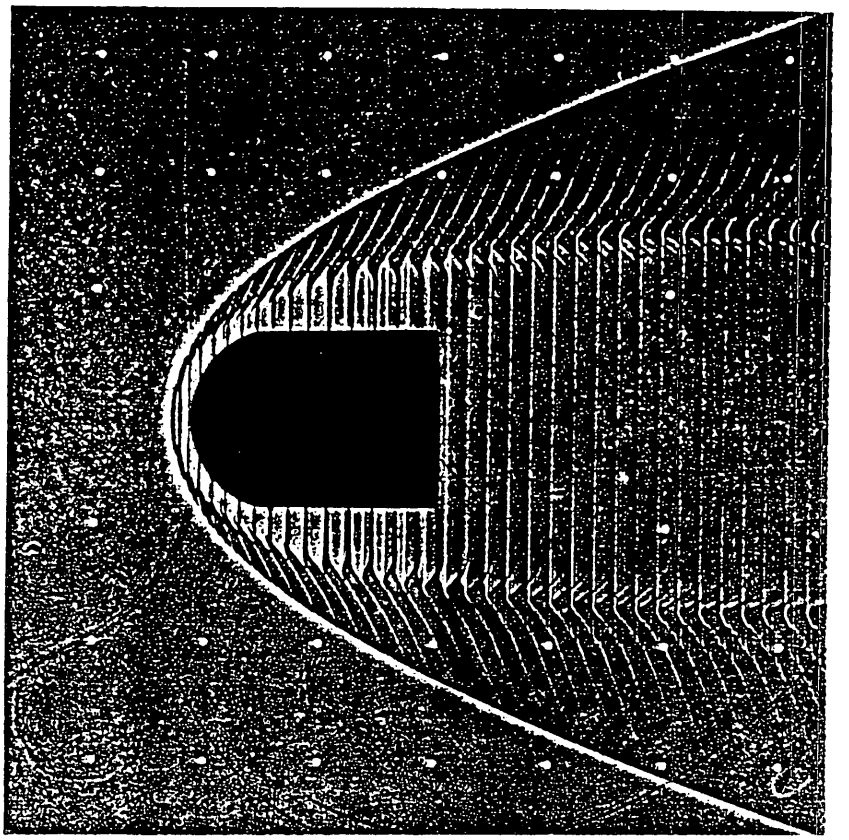

APPENDIX

ISABE 11-5

WAVE COMBUSTORS FOR TRANS-ATMOSPHERIC VEHICLES

Gene P. Menees
NASA-Ames Research Center, Moffett Field, CA

Henry G. Adelman and Jean-Luc Cambier
Eloret Institute, Palo Alto, CA

Jeffrey V. Bowles
NASA-Ames Research Center, Moffett Field, CA

9TH INTERNATIONAL SYMPOSIUM ON AIRBREATHING ENGINES
September 4-8, 1989 / Athens, Greece

WAVE COMBUSTORS FOR TRANS-ATMOSPHERIC VEHICLES

Gene P. Menees*
NASA-Ames Research Center, Moffett Field, California
Henry G. Adelman†
Jean-Luc Cambier‡
Eloret Institute, Palo Alto, California
Jeffrey V.Bowles§
NASA-Ames Research Center, Moffett Field, California

Abstract

The Wave Combustor is an airbreathing hypersonic propulsion system which utilizes shock and detonation waves to enhance fuel-air mixing and combustion in supersonic flow. In this concept, an oblique shock wave in the combustor can act as a flameholder by increasing the pressure and temperature of the air-fuel mixture and thereby decreasing the ignition delay. If the oblique shock is sufficiently strong, then the combustion front and the shock wave can couple into a detonation wave. In this case, combustion occurs almost instantateously in a thin zone behind the wave front. The result is a shorter, lighter engine compared to the scramjet. This engine, which is called the Oblique Detonation Wave Engine (ODWE), can then be utilized to provide a smaller, lighter vehicle or to provide a higher payload capability for a given vehicle weight. An analysis of the performance of a conceptual trans-atmospheric vehicle (TAV) powered by an ODWE is given here.

Nomenclature

C_T	=	thrust coefficient
I_{sp}	=	specific impulse
L/D	=	lift-to-drag ratio
LEO	=	Low Earth Orbit
l/h	=	combustor length-to-height ratio
$ODWE$	=	Oblique Detonation Wave Engine
M	=	mach Number
q	=	dynamic pressure
TAV	=	Trans-Atmospheric Vehicle
T_f	=	fuel total temperature
ϕ	=	equivalence ratio

*Research Scientist, Associate Fellow, AIAA
†Research Scientist, Member AIAA
‡Research Scientist, Member AIAA
§Research Scientist, Member, AIAA

Introduction

Investigations of wave enhanced supersonic mixing and combustion have been pursued for several decades. Detonation wave engines were reported in the 1940's[1], and studies of engines using moving and stationary detonation waves followed[2-7]. Enhancement of fuel mixing and combustion by shock waves has been investigated more recently[8,9].

The experimental and analytical program at NASA-Ames Research Center on wave enhanced mixing and combustion has been reported previously[10-12]. Experimental mixing and combustion studies are being carried out in a 20 MW arc heated wind tunnel. Analytical studies include computer predictions of fuel injection, mixing and combustion using a 2-D, viscous fluid dynamic simulation with finite rate chemistry. In addition, candidate vehicle designs are studied using design codes for aerodynamics, structures, thermal protection systems, propulsion and trajectories.

Propulsion Modeling

A propulsion system model has been constructed to provide ODWE and scramjet engine performance data for the vehicle design and trajectory codes. This propulsion model provides inlet-to-nozzle details. The inlet compression process is modeled with multiple oblique shocks, including the bow shock. The inlet operates at the bow shock-on-cowl-lip design point for all Mach numbers. This is made possible by moving the cowl forward and aft during flight. A constant area combustor is also assumed.

For the scramjet case, the inlet operates in a four shock mode which gives good performance over all flight conditions. However, for the ODWE case, the oblique detonation wave acts as a diffuser, so fewer inlet shocks are

needed. In this mode, two inlet shocks are sufficient. The shock system for both cases is shown in Figure 1.

The viscous and pressure drag forces from nose-to- tail on the underbody or engine side of the vehicle are accounted for in the two engine performance parameters, specific impulse and thrust coefficient. The thrust coefficient is defined as the thrust nomalized by the product of dynamic pressure and capture area. Engine specific impulse is obtained by dividing thrust by the fuel weight flow rate. The remaining vehicle drag not accounted for in the thrust coefficient, which includes the top, sides, cowl bottom surface and control surfaces is assigned to the vehicle aerodynamic characteristics.

For the low speed flight regime , below Mach 6, a hypothetical airbreathing engine with an average effective specific impulse of 1000 s and a thrust-to-weight ratio of 20 is used. Effective specific impulse is obtained by dividing the effective thrust (thrust minus vehicle drag) by the fuel weight flow rate. At high Mach numbers and altitudes, where the air-breathing engine thrust is diminished, a rocket engine with a thrust-to-weight ratio of 1.5 provides the final injection into orbit.

The efficiency of the propulsion system depends on various factors including the flight Mach number, dynamic pressure, forebody shape, fuel temperature and equivalence ratio. These factors are discussed in the results section.

Vehicle Modeling

Performance and sizing estimations were made using a hypersonic vehicle synthesis code for trans-atmospheric designs. This code was orginally developed at NASA-Ames to model hypersonic cruise aircraft[13] and it has since been modified to study trans-atmospheric designs. Estimates can be made of aerodynamic characteristics, aero-thermal heating, propulsion system performance and structural/subsystem weights. An automated vehicle closure algorithm iterates the trajectory analysis to close the design on both vehicle weight and volume.

The aero-thermal analysis consists of a series of performance estimates based on Mach number regime. For subsonic, transonic, and low supersonic speeds (below the critical Mach number), a set of empirical relations are used which are based on overall vehicle geometric characteristics. In the mid to high supersonic regime, real gas tangent cone/wedge models are used. Newtonian flow is assumed to determine the hypersonic pressure coefficient. Skin friction and heat transfer models are based on a reference enthalpy method[14].

Structural analysis is based on simplified beam theory, using the aero-induced loads to compute the longitudinal bending moment distribution. Longitudinal and internal pressure loads are also accounted for in the structural stresses. Additional checks on buckling, local instability and minimum gauge constraints, coupled with non-optimum fracture are then used to compute the required structural weight. The thermal protection system is sized according to the maximum temperatures and integrated heat loads over the mission. The high heating loads on the nose and wing leading edge will require active cooling systems[15].

The trajectory analysis is then used to compute the required fuel fraction for the vehicle. The equations of motion are integrated over the specified Mach number-altitude flight path to determine total fuel requirements and mission duration. Vehicle gross weight and volume are then iterated to find the closure point, that is where the required fuel fraction and the available fuel fraction are equal.

To size the vehicles, a mission was selected which carried a payload of 15,000 pounds into a Low Earth Orbit (LEO) of 120 nautical miles altitude. A horizontal takeoff in the easterly direction from Kennedy Space Center was assumed, with an on-station duration of six hours. Two ascent trajectories were studied, with dynamic pressures of 1000 and 2000 pounds per square foot (psf). The flight path was constrained to give 100 psi duct pressure at lower supersonic Mach numbers and a maximum mean surface equilibrium radiation temperature of 2000 F (1367 K) for high Mach numbers. The speed at which the airbreathing engine thrust was augmented by a rocket was optimized to minimize the gross takeoff weight. A descent trajectory was flown near peak L/D to maximize the descent cross-range capability. Fuel reserves of 2% of mission fuel were assumed for the landing maneuver.

Results

General Vehicle Design

The general vehicle configuration, shown in Figure 2, is a lifting body with aft mounted horizontal and vertical tails. Planform shape is a power-law configuration with a fore-body lower surface angle of 5.5 degrees and a nozzle chord angle of 9.5 degrees. The cross-sectional shape consists of upper and lower near elliptical sections with

major- to-minor axis ratios of 4 for the upper surface and 2 for the lower surface. The vehicle break-point (transition from fore body to aft body) is at 65% of the body length and the fatness ratio (maximum cross sectional area to planform area) is 9.7%. Engine width is 67% of the maximum width which provides adequate room for the main landing gear. The total propulsion system consists of two airbreathing engines, one for Mach numbers below 6, and a scramjet or an ODWE for the remaining part of the flight. In addition, a rocket engine is used in conjuction with the air-breathing engine for the high altitude, high Mach number portion of the trajectory. Liquid hydrogen is the fuel for all engines.

Aero-thermodynamic characteristics of the vehicle were computed using the synthesis code methods. The structural design incorporated a cool integral tank concept where the tank carries both the aero-induced bending loads as well as the internal tank pressure loads. Sufficient thermal insulation is used to maintain the tank material temperature limits and minimize the hydrogen boil-off. With a design condition of 2.0 g's at Mach 6, the unit structural weight was somewhat less than 4.0 lb/ft^2.

General Engine Performance

The results of the engine performance calculations show that specific impulse and thrust coefficients depend on dynamic pressure, combustion efficiency, fuel temperature and equivalence ratio. Certain trends can be observed. As shown in Figure 3, it is evident that higher heat recycling from the engine leads to higher injected fuel temperatures and larger values of specific impulse and thrust coefficient. We assume that the fuel is injected at a constant Mach number of 2.5. As more heat is added to increase the stagnation temperature, significant momentum can be gained from the fuel injection. However, fuel temperature is limited by the amount of heat which can be absorbed from the structure and by the temperature limits of the materials used to store and transport the fuel. In this study, we will assume that 90% of the heat loads have been absorbed by the fuel. The fuel is then heated to a limiting temperature of 1100 K (1520 F), which is representative of the current materials available for fuel storage and transport. If this temperature limit is exceeded, then an amount of fuel in excess of stoichiometric must be used. The resulting equivalence ratio versus Mach number schedule for the scramjet is shown in Figure 4 for various fuel temperature limits.

Since the ODWE combustor is shorter, a stoichiometric mixture can be maintained to a Mach number of 17.5 compared to 14 for the scramjet, for a fuel temperature of 1100 K. While heat recycle increases engine performance for stoichiometric mixtures, the effect of using excess fuel to maintain a specified temperature limit may increase the thrust coefficients but will lower the specific impulses as shown in Figure 5. It is clear that the cooling requirements seriously affect the performance of the engine at high Mach numbers.

Flight trajectories were assumed for constant dynamic pressures of 1000 and 2000 psf which bracket the range expected for airbreathing vehicles. Higher dynamic pressures, above 2000 psf, provide slightly greater specific impulses and thrust coefficients, but may impose higher heating loads on the vehicle which could increase thermal protection system weights, or exceed the 2000 F temperature limit.

Engine performance is also influenced by combustion and mixing efficiencies. Combustion efficiency is limited by the amount of fuel which can be converted to water at the conditions in the combustor. This is determined by the hydrogen-oxygen- water equilibrium constant. Combustion efficiencies at stoichiometric air-fuel ratios range from 93.5% at Mach 8 to 86.8% at Mach 20. Higher equivalence ratios provide excess fuel which lowers combustion temperatures and raises combustion efficiencies. However, while specific impulse values decrease, thrust coefficients increase due to the fact that there is momentum recovered from the hot excess fuel. Combustion efficiency can be increased if there is recombination of the dissociated products in the nozzle. Since the amount of recombination was not a subject of this study, we have assumed that it is substantial and we have assigned an overall combustion efficiency of 100% to the propulsion system.

The extent of mixing and combustion will depend on the injector design and the combustor length. We have selected a combustor length to height ratio (l/h) of 10 in this study for the scramjet and an l/h of 1.5 for the ODWE. Due to the lack of extensive mixing and combustion data, mixing and combustion efficiencies were assumed to be 100% for both engines at all equivalence ratios.

Scramjet Engine Performance

The calculated performance of the scramjet engine is shown in Figure 6 as a function of Mach number for a dynamic pressure of 2000 psf and an equivalence ratio schedule which maintains the fuel temperature below

1100 K. It can be seen that the specific impulse begins to drop at Mach 14 due to the rise in equivalence ratios necessary to maintain the 1100 K fuel temperature limit.

ODWE Performance

The ODWE performance was also calculated for dynamic pressures of 1000 psf and 2000 psf. In Figure 6 we compare the performance of both the scramjet and ODWE for the q=2000 psf case. It appears that the ODWE has a better performance than the scramjet at high Mach numbers, but has lower specific impulse below Mach 15. The reduced performance at low Mach numbers is due to the steep wave angle of an oblique Chapman-Jouguet (CJ) detonation, and therefore to higher shock losses. The wave angle can be reduced if either the Mach number is increased or the Chapman-Jouguet Mach number is decreased (i.e. the static temperature prior to the detonation wave is increased or ϕ is decreased). Therefore, the ODWE favors operation at high Mach numbers.

The ODWE also takes advantage of a shorter combustor which requires less cooling and less excess fuel at higher Mach numbers than the scramjet. It can be seen in Figure 6 that the knee in the specific impulse curve, which indicates the start of the excess fueling schedule, begins at a higher Mach number for the ODWE than for the scramjet. Since the problems of mixing and ignition delay impose a long combustor for high Mach numbers, it is clear that increasing the combustor length forces the performance of the scramjet to drop at lower Mach numbers, when the fuel must be injected in excess of stoichiometric.

For the ODWE, the benefits of a shorter combustion chamber, which results in a shorter, lighter engine will also be evident in the vehicle size and weight calculations which are discussed later.

Scramjet Vehicle Performance

A scramjet powered vehicle was modeled using the predicted engine performance data. The vehicle weight breakdowns are shown in Table 1 for the trajectory of constant dynamic pressure q=2000 psf. Since the scramjet is very inefficient below Mach 6, a hypothetical engine system with an average effective specific impulse of 1000 s was used to propel the vehicle from horizontal takeoff to Mach 6. Since the effective specific impulse takes into account the aero-dynamic drag on all surfaces (not just the inlet, combustor and nozzle), it is significantly less than the engine specific impulse. Aerodynamic heating considerations required that the dynamic pressure of the flightpath, as shown in figure 7, begins to drop below the specified value of 2000 psf at Mach 17 to about 250 psf at Mach 22. This low dynamic pressure requirement at high Mach numbers necessitates rocket power augmentation which begins at Mach 18. The amount of thrust provided by the rocket is larger than the thrust produced by the scramjet, and the rocket thrust fraction continues to increase until orbital speeds are reached.

The vehicle which flies a 2000 psf trajectory weighs 460,512 pounds and carries a 15,000 payload into orbit. The scramjet engine, low speed engine and rocket motors comprise 8.6% of the takeoff weight. For comparative purposes, a vehicle which flies a 1000 psf trajectory was also studied. This TAV is heavier at 623,000 pounds. The main reason for the increased weight is the lower mass capture per unit area of inlet, which requires a larger, heavier engine and associated structure. Also, the lower thrust-to-weight ratio results in a longer flight time to orbit which consumes a greater amount of fuel.

ODWE Vehicle Performance

The hypersonic vehicle using the ODWE has somewhat different weight characteristics as shown in Table 2. Since the ODWE offers superior performance above Mach 15, the point of rocket turn-on is delayed to Mach 19. The ODWE can operate at higher Mach numbers than the scramjet, and continues to provide a higher fraction of airbreathing thrust to orbital speeds. Therefore, less rocket thrust is needed and a lower mass fraction of LOX is consumed, 12.5% versus 15.9% for the scramjet. This represents a weight savings of 22,000 compared to the scramjet. In addition, the shorter combustor length provided by the ODWE allows a shorter, lighter engine which saves about 5,000 pounds. The ODWE represents 3.7% of the gross weight, compared to 4.4% for the baseline scramjet engine. While the fuel weight fraction is higher for the ODWE, the actual fuel weight is 14,000 pounds lower. As a result of all these factors, the ODWE configuration weighs 409,500 pounds, some 51,000 pounds less than the scramjet vehicle (for q=2000 psf), and carries the same payload of 15,000 pounds to orbit. Note that the payload weight fraction is increased from 3.3% of the takeoff weight for the scramjet to 3.7% for the ODWE.

Conclusions

The ODWE powered hypersonic vehicle shows different

performance characteristics than the scramjet powered vehicle:

1. The ODWE trades a better engine performance above Mach 15 for a lower performance below Mach 15. This trade-off still favors the ODWE overall.

2. The better performance of the ODWE at higher Mach numbers allows a delay of the rocket augmentation mode, and results in a lower mass of LOX required for orbit insertion.

3. The smaller ODWE allows another direct weight reduction of $\simeq 5,000$ lbs.

4. The overall higher performance of the ODWE results in a weight savings of 51,000 pounds and a higher payload weight fraction of approximately 12%.

Since the scramjet has better performance below Mach 15, and the ODWE above Mach 15, a combination of these two engines may be ideal. This hybrid engine would use a two-shock diffuser for the whole Mach range. At low Mach numbers, the mixing length and ignition requirements are less severe, and a relatively short combustor can be used in a scramjet mode. At higher Mach numbers, the diffusing shocks would move aft into the combustor. The engine would operate in the oblique detonation mode in the aft section of the combustor. Therefore, cooling is required only for a fraction of the combustor, and the drop in performance due to cooling requirements would still occur only at very high Mach numbers. The design of such a hybrid engine would require more sophisticated, two-dimensional analysis. Work in that direction is progressing.

Aknowledgement

The authors wish to thank Dr. D.W. Bogdanoff for providing an initial version of a one-dimensional analysis code for scramjet engine performance, which was subsequently modified for our study.

References

1. Roy M., Comptes Rendus a l'Academy des Sciences, Feb., 1946.

2. Sargent W,M. and Gross, R.A., "A Detonation Wave Hypersonic Ramjet", AFOSR TN 59-589, 1959.

3. Townend L.H., "Detonation Ramjets for Hypersonic Aircraft", RAE Technical Report 70218, November 1970.

4. Morrison R.B., "Evaluation of the Oblique Detonation Wave Hypersonic Ramjet", NASA Contractor Report 145358, January 1978.

5. Morrison R.B., "Oblique Detonation Ramjet", NASA Contractor Report 159192, January 1980.

6. Cambier J.L. and Adelman, H.G., "Preliminary Numerical Simulations of a Pulsed Detonation Wave Engine", AIAA paper 88-2960, July 1988.

7. Nichols J.A. et. al., "Intermittant Detonation as a Thrust-Producing Mechanism", *Jet Propulsion*, May, 1957, pp. 534-541.

8. Kumar A. et. al., "A Mixing Augmentation Technique for Hypervelocity Scramjets", AIAA paper 87-1882.

9. Marble F.E., Hendricks, G.J. and Zukowski, E.E.," Progress Toward Shock Enhancement of Supersonic Processes", AIAA paper 87-1880, June, 1987.

10. Cambier J.L., Adelman, H.G. and Menees, G.P., "Numerical Simulations of Oblique Detonations in Supersonic Combustion Chambers", AIAA *Journal of Propulsion and Power*, vol. 5, No. 4, July-August 1989, pp. 482-491.

11. Adelman H.G. , Cambier, J.L. , Menees, G.P. and Balboni, J.A., "Analytical and Experimental Validation of the Oblique detonation Wave Engine Concept", AIAA paper 88-0097, January 1988.

12. Cambier J.L., Adelman, H.G. and Menees, G.P., " Numerical Simulations of an Oblique Detonation Wave Engine", AIAA paper 88-0063, January 1988.

13. Gregory T.J. et. al., "Hypersonic Transport Preliminary Performance Estimates for an All-Body Configuration", AIAA paper 70-1224, October 1970.

14. Eckert, E.R.G., "Survey on Heat Transfer at High Speeds", Aeronautical Research Laboratories, University of Minnesota, ARL 189, December, 1961.

15. Tauber M.E. and Adelman, H.G., "Thermal Environments of Transatmospheric Vehicles", AIAA *Journal of Aircraft*, vol. **25**, No. 4, pp. 355-363, April 1988.

Component	Weight fraction
Empty Weight	28.0%
Structure	18.4%
Propulsion Systems	8.6%
Fixed Equipment	1.1%
LH_2	51.8%
LOX	15.9%
Payload	3.3%

Table 1: Scramjet vehicle data for fixed payload of 15,000 lbs. Fractions are relative to total take-off weight of 460,512 lbs for q=2000 psf trajectory.

Component	Weight fraction
Empty Weight	27.9%
Structure	18.8%
Propulsion Systems	8.0%
Fixed Equipment	1.1%
LH_2	54.8%
LOX	12.5%
Payload	3.7%

Table 2: ODWE vehicle data for fixed payload of 15,000 lbs. Fractions are relative to total take-off weight of 409,500 lbs for q=2000 psf trajectory.

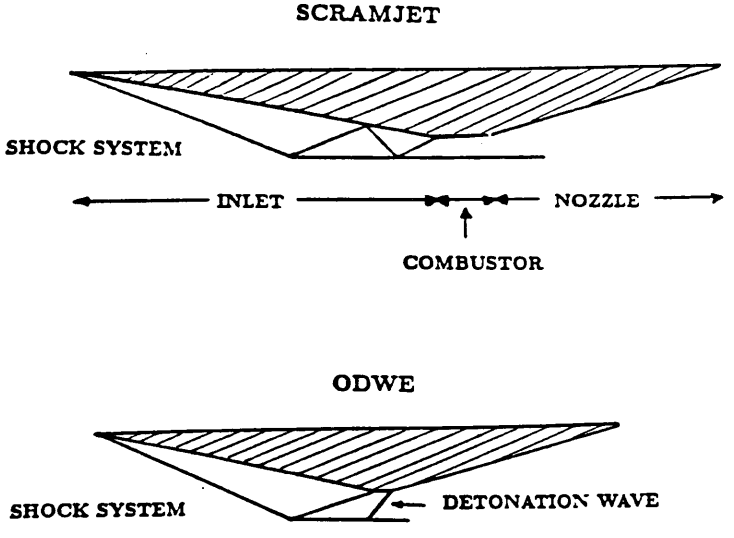

Figure 1: Schematic of shock structure for scramjet engine and ODWE, including detonation wave.

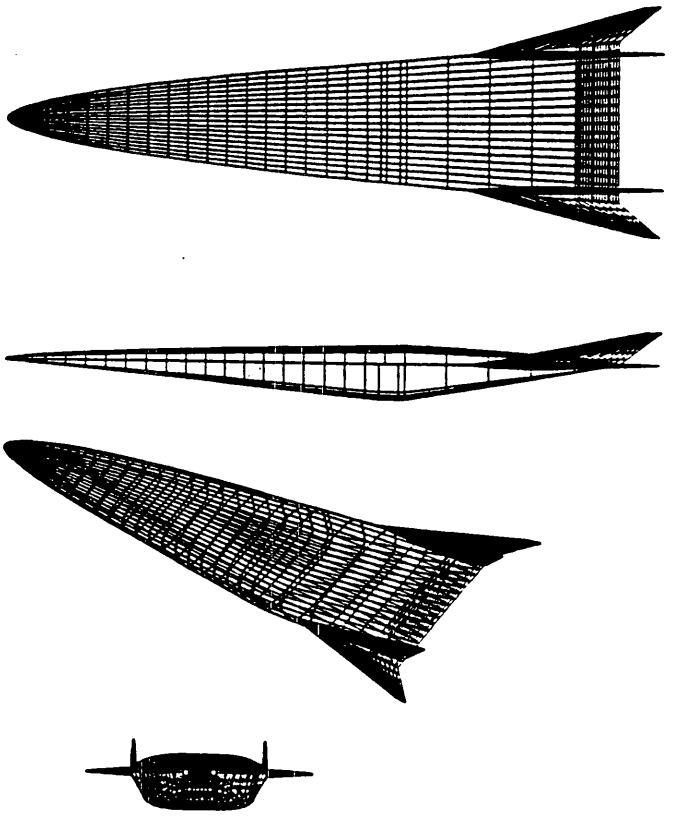

Figure 2: Schematics of generic TAV concept used in this study.

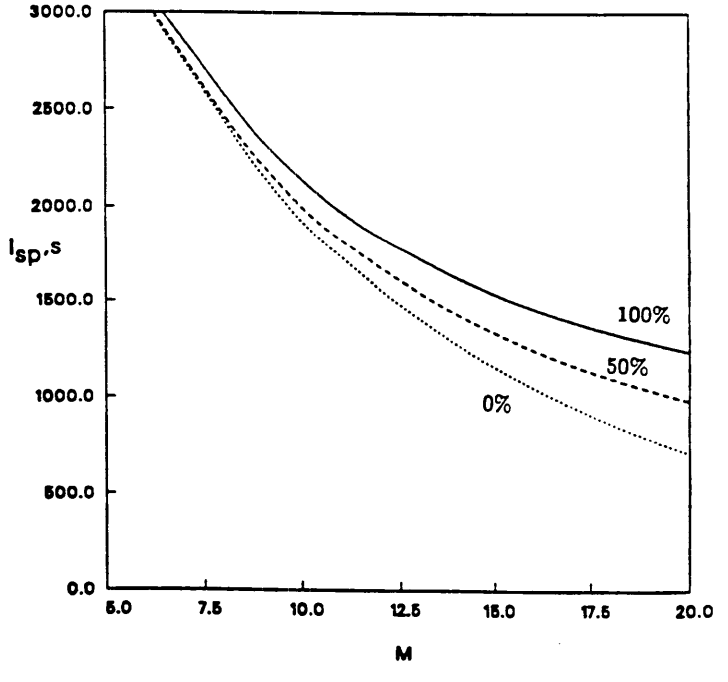

Figure 3: Specific impulse versus Mach number for scramjet engine (q=2000 psf, $\phi = 1$). Cases shown are for 0%, 50% and 100% of the heat loads absorbed into the fuel.

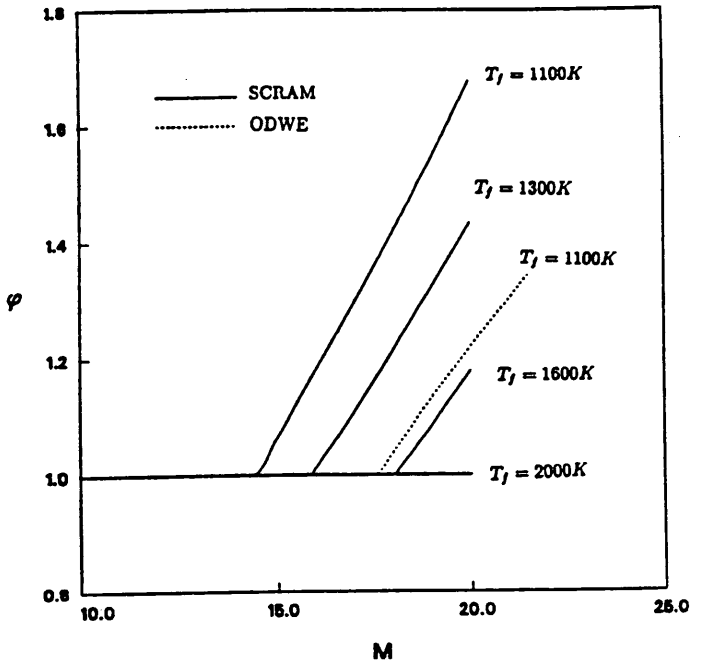

Figure 4: Equivalence ratio versus Mach number for scramjet and ODWE engines at q=2000 psf. ODWE results are shown for a fuel temperature limit of 1100 K, while scramjet results are shown for a temperature range from 1100 to 2000 K (1520 to 3140 F).

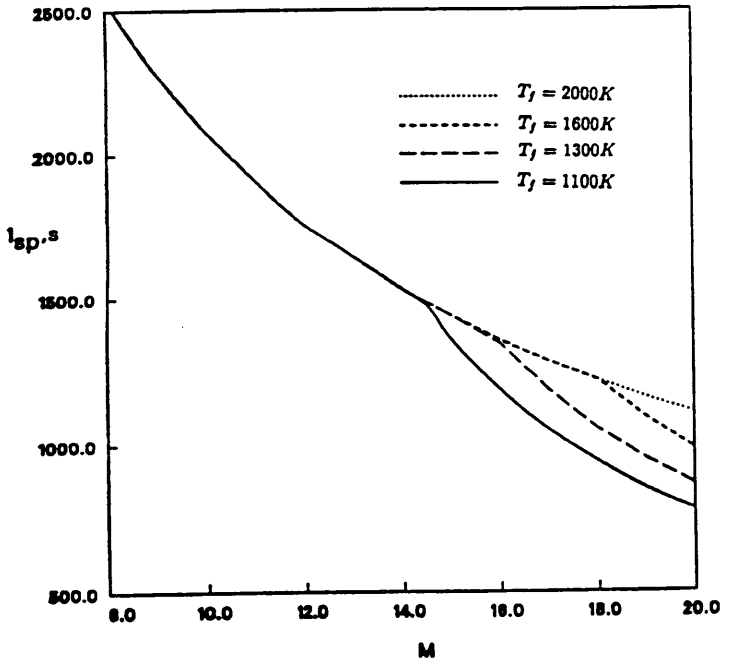

Figure 5: Specific impulse versus Mach number for scramjet engine at q=2000 psf. Results are for fuel temperature limits from 1100 to 2000 K (1520 to 3140 F).

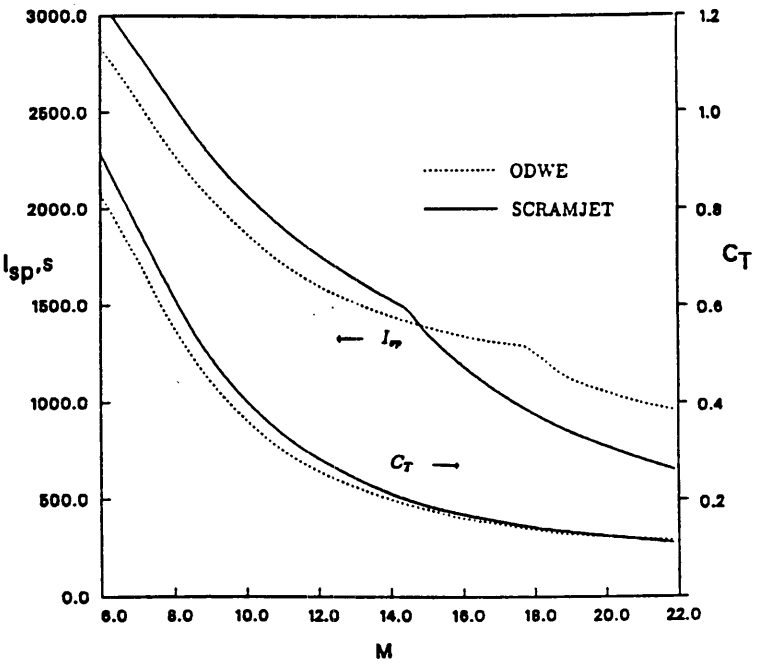

Figure 6: Comparison of scramjet and ODWE performance characteristics. Shown are I_{sp} and C_T profiles for q=2000 psf, 90% of heat loads carried by fuel and 1100 K fuel temperature limit.

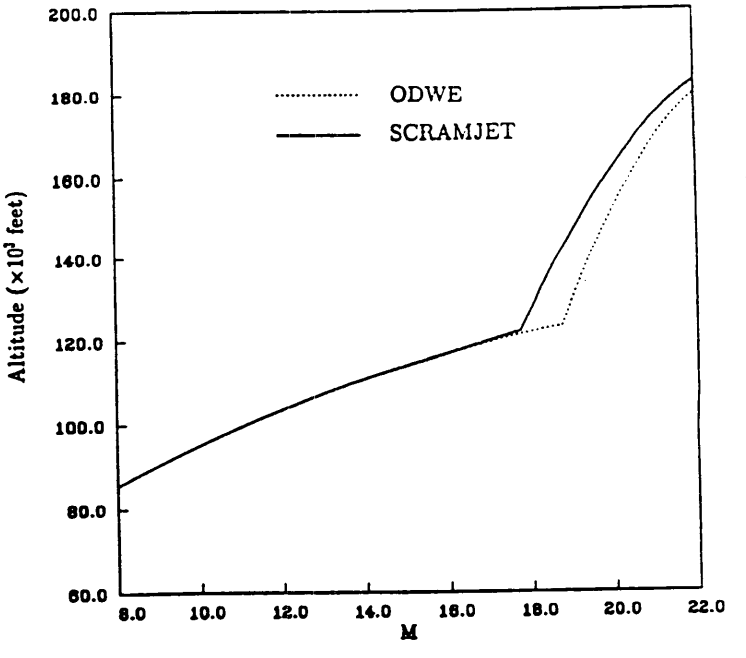

Figure 7: Comparison of flight trajectories at q=2000 psf for ODWE and scramjet vehicles.

Paper 26

Analytical and Experimental Investigations of the Oblique Detonation Wave Engine Concept

G.P. Menees, NASA-Ames Research Center, Moffett Field, CA
H.G. Adelman, Eloret Institute, Palo Alto, CA
J.L. Cambier, Eloret Institute, Palo Alto, CA

AGARD PEP 75th Symposium
Hypersonic Combined Cycle Propulsion
Madrid, Spain, May 28-June 1, 1990

ANALYTICAL AND EXPERIMENTAL INVESTIGATIONS OF THE OBLIQUE DETONATION WAVE ENGINE CONCEPT

Gene P. Menees*
NASA-Ames Research Center, Moffett Field, CA
Henry G. Adelman†
Eloret Institute, Palo Alto, CA
Jean-Luc Cambier‡
Eloret Institute, Palo Alto, CA

ABSTRACT

Wave Combustors, which include the Oblique Detonation Wave Engine (ODWE), are attractive propulsion concepts for hypersonic flight. These engines utilize oblique shock or detonation waves to rapidly mix, ignite and combust the air-fuel mixture in thin zones in the combustion chamber. Benefits of these combustion systems include shorter and lighter engines which will require less cooling and can provide thrust at higher Mach numbers than conventional scramjets. The Wave Combustor's ability to operate at lower combustor inlet pressures may allow the vehicle to operate at lower dynamic pressures which could lessen the heating loads on the airframe.

The research program at NASA-Ames includes analytical studies of the ODWE combustor using Computional Fluid Dynamics (CFD) codes which fully couple finite rate chemistry with fluid dynamics. In addition, experimental proof-of-concept studies are being carried out in an arc heated hypersonic wind tunnel. Several fuel injection designs were studied analytically and experimentally. In-stream strut fuel injectors were chosen to provide good mixing with minimal stagnation pressure losses. Measurements of flow field properties behind the oblique wave are compared to analytical predictions.

NOMENCLATURE

C_t	=	Thrust coefficient
I_{sp}	=	Specific impulse
M	=	Mach number
$ODWE$	=	Oblique Detonation Wave Engine
p	=	pressure
q	=	dynamic pressure
R_e	=	Reynolds Number
T	=	Temperature
TAV	=	Trans-atmospheric Vehicle
V	=	velocity
X	=	lateral distance from centerline of strut
Y	=	vertical distance from nozzle floor
Z	=	axial distance fron trailing edge of strut
ϕ	=	equivalence ratio

Subscripts

t	=	*total*
∞	=	free stream value

INTRODUCTION

The use of detonation waves to initiate and enhance combustion has been proposed since the 1940's[1]. Some analyses have been made using both normal and oblique waves[2,3]. Normal waves are hard to stabilize and they produce higher stagnation

*Research Scientist, Associate Fellow AIAA
†Research Scientist, Member AIAA
‡Research Scientist. Member AIAA

is evident that higher heat recycling from the engine leads to higher injected fuel temperatures and larger values of specific impulse and thrust coefficient. We assume that the fuel is injected at a constant Mach number of 2.5. As more heat is added to increase the stagnation temperature, significant momentum can be gained from the fuel injection. However, fuel temperature is limited by the amount of heat which can be absorbed from the structure and by the temperature limits of the materials used to store and transport the fuel. In this study, we will assume that 90% of the heat loads have been absorbed by the fuel. The fuel is then heated to a limiting temperature of 1100 K (1520 F), which is representative of the current materials available for fuel storage and transport. If this temperature limit is exceeded, then an amount of fuel in excess of stoichiometric must be used. The resulting equivalence ratio versus Mach number schedule for the scramjet is shown in Fig. 3 for various fuel temperature limits.

Since the ODWE combustor is shorter, a stoichiometric mixture can be maintained to a Mach number of 17.5 compared to 14 for the scramjet, for a fuel temperature of 1100 K. While heat recycle increases engine performance for stoichiometric mixtures, the effect of using excess fuel to maintain a specified temperature limit may increase the thrust coefficients but will lower the specific impulses as shown in Fig. 4. It is clear that the cooling requirements seriously affect the performance of the engine at high Mach numbers.

Scramjet Engine Performance

The calculated performance of the scramjet engine is shown in Fig. 4 as a function of Mach number for a dynamic pressure of 2000 psf and an equivalence ratio schedule which maintains the fuel temperature below 1100 K. It can be seen that the specific impulse begins to drop at Mach 14 due to the rise in equivalence ratios necessary to maintain the 1100 K fuel temperature limit.

ODWE Performance

The ODWE performance was also calculated for dynamic pressures of 1000 psf and 2000 psf. In Fig. 4 we compare the performance of both the scramjet and ODWE for the q=2000 psf case. It appears that the ODWE has better performance than the scramjet at high Mach numbers, but has lower specific impulse below Mach 15. The reduced performance at low Mach numbers is due to the steep wave angle of an oblique Chapman-Jouguet (CJ) detonation, and therefore to higher shock losses. The wave angle can be reduced if either the Mach number is increased or the Chapman-Jouguet Mach number is decreased (i.e. the static temperature prior to the detonation wave is increased or ϕ is decreased). Therefore, the ODWE favors operation at high Mach numbers.

The ODWE also takes advantage of a shorter combustor which requires less cooling and less excess fuel at higher Mach numbers than the scramjet. It can be seen in Fig. 4 that the knee in the specific impulse curve, which indicates the start of the excess fueling schedule, begins at a higher Mach number for the ODWE than for the scramjet. Since the problems of mixing and ignition delay impose a long combustor for high Mach numbers, it is clear that increasing the combustor length causes the performance of the scramjet to drop at lower Mach numbers, when fuel must be injected in excess of stoichiometric.

For the ODWE, the benefits of a shorter combustion chamber, which results in a shorter, lighter engine will also be evident in the vehicle size and weight calculations which are discussed later.

Scramjet Vehicle Performance

A scramjet powered vehicle was modeled using the predicted engine performance data for the trajectory of constant dynamic pressure q=2000 psf. Since the scramjet is very inefficient below Mach 6, a hypothetical engine system with an average effective specific impulse of 1000 seconds was used to propel the vehicle from horizontal takeoff to Mach 6. Aerodynamic heating considerations required that the dynamic pressure of the flightpath begins to drop below the specified value of 2000 psf at Mach 17 to about 250 psf at Mach 22. This low dynamic pressure requirement at high Mach numbers necessitates rocket power augmentation which begins at Mach 18. The amount of thrust provided by the rocket is larger than the thrust produced by the scramjet, and the rocket thrust fraction continues to increase until orbital speeds are reached.

The scramjet powered vehicle which flies a 2000 psf trajectory weighs 460,512 pounds and carries a 15,000 pound payload into orbit. The scramjet engine, low speed engine and rocket motors comprise 8.6% of the takeoff weight. For comparative purposes, a vehicle which flies a 1000 psf trajectory was also studied. This TAV is heavier at 623,000 pounds. The main reason for the increased weight is the lower mass capture per unit area of inlet, which requires a larger, heavier engine and associated structure. Also, the lower thrust-to-weight ratio results in a longer flight time to orbit which consumes a greater amount of fuel.

ODWE Vehicle Performance

The hypersonic vehicle using the ODWE has somewhat different weight characteristics. Since the ODWE offers superior performance above Mach 15, the point of rocket turn-on is delayed to Mach 19. The ODWE can operate at higher Mach numbers than the scramjet, and continues to provide a higher fraction of airbreathing thrust to orbital speeds. Therefore, less rocket thrust is

and temperatures are raised by factors of 2.4 and 1.3 respectively. These higher pressures and temperatures will shorten the ignition distance behind the oblique wave. The pressure field due to combustion should influence the oblique shock wave and create a detonation. In reality, the hydrogen injection will create shock waves which will cause higher stagnation losses than predicted by this analysis along with higher static pressures and temperatures.
While the increased pressures will shorten ignition delays behind the oblique wave, raising the temperatures may create pre-ignition problems prior to the wave. One consideration for injector design and location is premature ignition of the fuel. A study was made of the effects of introducing fuel at various locations inside the wind tunnel nozzle. The results indicated that fuel must be introduced at a location in the nozzle somewhere downstream of the point where the area ratio is 10. However, extensive modifications would be required to inject fuel in the existing nozzle. This result led to the study of strut type injectors which would be located at the exit of the nozzle.

Injection Simulations

In order to verify some of the simplified analyses of fuel injection and combustion behavior, a more sophisticated computer simulation was employed. This code is described in detail elsewhere[13,14]. Many different simulations were performed to validate the fluid dynamic and chemical kinetics portions of this code. Once the code was validated, it was used to guide the experimental program. The first simulation consisted of wall injection through an orifice normal to the air stream. This configuration, which could model injection from a flat plate resulted in an oblique shock ahead of the injected fuel. Unfortunately, the penetration of the fuel jet was poor. A similar result has been observed experimentally, where fuel jet penetrations appeared to peak at a value of about five times the orifice diameter[15].

In an effort to improve the fuel penetration, a projection or finger was added downstream of the fuel orifice. In this case, fuel was forced over the projection further into the air stream. However, a normal shock was also formed upstream of the injector which reduced the flow velocities to subsonic values. Since a detonation can only exist in supersonic flows, this geometry would preclude the establishment of an oblique detonation wave downstream of the injector. A third configuration was examined where the finger was modified to include a ramp on the upstream side. Fuel penetration remained good and the fuel injection shock became oblique. Most of the flow remained supersonic except for a small recirculation zone behind the leward side of the projection. While this configuration appeared to provide improved penetration and supersonic flow downstream of the injection point, this design would have to be installed on a wall where the high temperatures in the boundary layer region could prematurely ignite the fuel. In addition, the boundary layer might decrease the fuel penetration. For these reasons, it was decided to examine strut type fuel injectors located outside the nozzle. Here fuel could be injected by multiple struts into the core flow region where viscous effects are reduced.

In order provide a better model of the detonation process, a 2-dimensional combustion code was also developed. This code uses the same Total Variation Diminishing (TVD) algorithm as the injection model to capture strong shocks without smearing or oscillations. Temperature oscillations could incorrectly predict premature ignition and invalidate the detonation conditions. Finite rate chemistry is incorporated in order to model the heat release of the detonation process. The chemistry is fully coupled to the fluid dynamics so that heat release will couple to the shock front and show the correct rotation of the detonation wave. The fluid dynamics and chemical kinetics parts of this code were verified using many existing data sets and conditions[13].

Simulation of ODWE Experiment

The focus of this work was the simulation of the flow field in the strut region. This was done first with an Euler (inviscid) computation to obtain the position of the reflected shocks. The computations were done for free stream Mach numbers of 4.5 and 5.4. Two values of the vertical separation between the struts were studied (0.67 inches and 0.75 inches). It was apparent from the results that multiple shock interactions occured between the struts, as well as shock impingement on the flat surfaces of the struts. It was clear that in the case of high stagnation enthalpy, extreme care should be taken in avoiding locally high temperatures. In order to model the strut injection and mixing, a series of computations were made with greater refinements, which included blunting the leading edge of the struts and providing a high grid density. The full Navier-Stokes equations were solved for an assumed laminar case. The conditions were $M_\infty = 5.4$, $T_\infty = 42.2K$, $p_\infty = 0.0128$ atm, $Re_\infty \simeq 2\text{x}10^5$ per inch. The total length of the strut is approximately 5 inches and transition to turbulence should occur somewhere at the end of the strut. However, because of the leading edge compressive ramp (7^o) and the porous transpiration plate in the first half of the flat strut section, transition could be expected sooner. There is, however, no definite way to predict the transition with precision and there were no measurements to determine the properties of the boundary layer on the strut. In addition, when fuel injection takes place, the flow obviously becomes turbulent and the algebraic (Baldwin-Lomax) model is then unable to model the correct physics. Ideally a 2-equation model should be used at this point. The development and validation of such a model which uses the turbulent kinetic energy equation is one of the high priority development areas.

An example of the injection patterns for two struts is shown in Fig. 5. This design indicated hot spots on the center strut which caused the fuel to ignite immediately after injection. In fact, it was necessary to inject nitrogen at the tip of the strut to cool the mixture and decrease the oxygen content of the boundary layer[14]. The strut design is discussed in more detail in the next section.

Test Body

The oblique waves will be created by a water cooled wedge located approximately one foot downstream of the struts in the test section. Optical access is provided by 12 inch windows on either side of the test section and a schlieren system will provide photographic records of the wave angle with and without fuel. Pressure and temperature transducers on the wedge will be used to assess the state of combustion behind the oblique wave.

Mixing Studies

A series of mixing studies were carried out in the hypersonic wind tunnel. The first set of tests were made with two injection struts spaced from 0.5 in to 0.75 inches apart. the extent of fuel mixing was measured by an on-line mass spectrometer. Gas samples were obtained by a probe which was mounted on a traversing table that allowed motion in all three dimensions. Some results of the fuel-air determinations are shown in Fig. 12 for two locations, 0.5 inches and 12 inches behind the strut trailing edge. While mixing is poor at 0.5 inches, it is significantly improved at 12 inches. The further location was representative of the proposed position of the wedge for the detonation tests. Note that the fuel distribution at 0.5 inches resembles the simulated case of Fig. 5 with relatively unmixed jets. The experiment verified the concerns about thermal failure at the areas of shock impingement on the struts. Further mixing tests with multiple struts were carried out only with cold flow to avoid overheating while hot flow tests were run with a single strut.

Oblique Detonation Wave Studies

After the mixing studies were completed, the wedge test body was installed in the wind tunnel. While the original plan was to locate the wedge 12 inches downstream of the struts, this required the fabrication of new doors for the wind tunnel test section to place the windows in the proper location for viewing. Unfortunately, there was insufficient time to fabricate these doors, so the wedge was located in the field of view with the struts. Only 1.0 inches separated the trailing edge of the strut and the front edge of the strut. While this placed the strut in a relatively unmixed region, it was thought that combustion could occur behind the oblique bow shock of the wedge.

Tests were run with both helium and hydrogen injection to determine the effects on the wedge shock. The effects of fuel injection can be seen by comparing Figs. 13 and 14 for the cases of no injection and injection, respectively. It was observed that the injection of either combustible or inert gases caused a similar displacement of the bow shock. This was due to the low molecular weights and high speeds of sounds of hydrogen and helium. The effect is to lower the Mach number of the flow and cause the oblique wave to be more normal. During one test run, an increase in pressure was observed on the wedge with hydrogen injection, indicating combustion. However, in the limited time remaining for the tests, this phenomenon was not repeated.

CONCLUDING REMARKS

An experimental and analytical program has been undertaken to study the characteristics of stable oblique detonation waves in a NASA-Ames arc-jet wind tunnel. The analytical models have been used extensively to aid in the experimental design and to ensure a successful experiment.

The existance of stable oblique detonation waves has been predicted previously for premixed hydrogen-air in supersonic flows. However, complete mixing of the fuel and air streams is not possible within reasonable distances in supersonic combustors. Therefore, it is necessary to introduce the fuel in a manner that provides good mixing in short distances with minimal losses. Several injector designs were examined analytically and a strut type was chosen for its ability to introduce the fuel in the nozzle free jet. The mixing characteristics and the effects of incomplete mixing on the detonation wave are still being studied.

The simulation of the strut flow field in the ODWE experiment provided great detail on the shock-shock interactions and shock-boundary layer interactions. Notably, the flow structure near the injector is particularly detailed (shock, Mach disk). The results agree reasonably well with the experimental schlieren records.

A mission analysis study compared the performance of vehicles powered by a scramjet or an ODWE. The results showed that the ODWE had better overall performance than the scramjet. The increased performance allowed the ODWE powered vehicle to weigh less than the scramjet powered vehicle for the same payload weight.

REFERENCES

[1] Roy,M., Comptes rendus a l'Academy des Sciences, February, 1946.

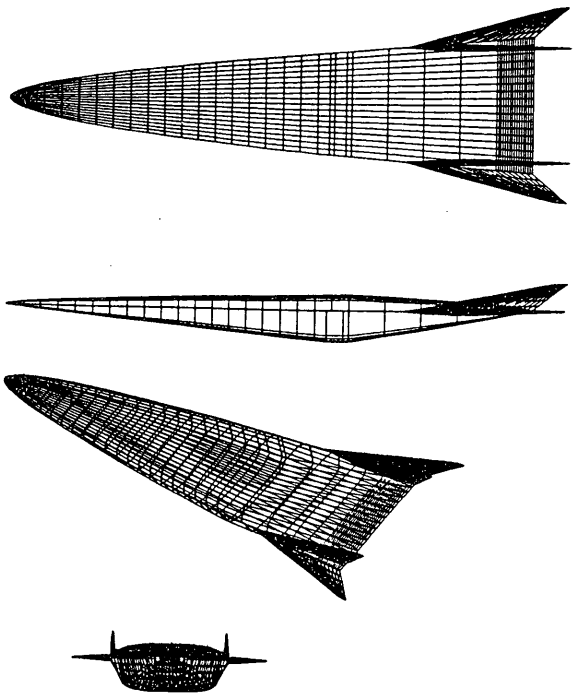

Fig. 1. Schematic of generic hypersonic trans-atmospheric vehicle used in mission analysis study.

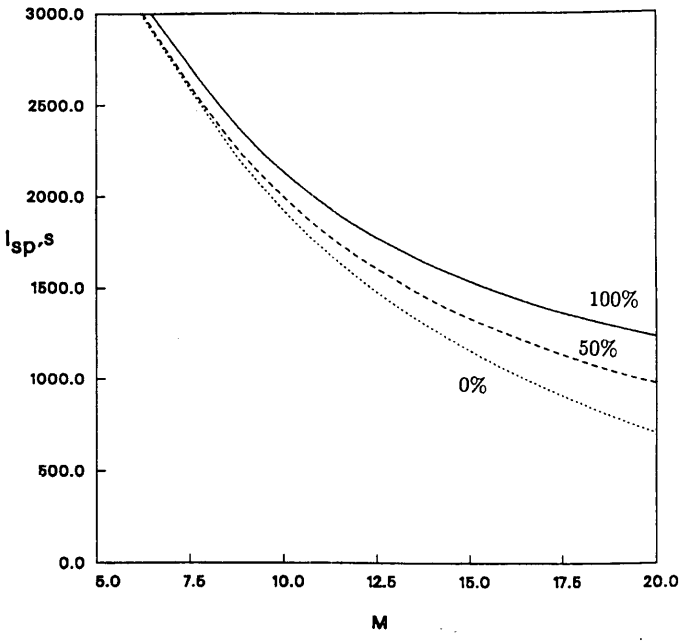

Fig. 2. Specific impulse versus Mach number for scramjet engine (q=2000 psf, ϕ=1). Cases shown are for 0%, 50% and 100% of the heat load absorbed into the fuel.

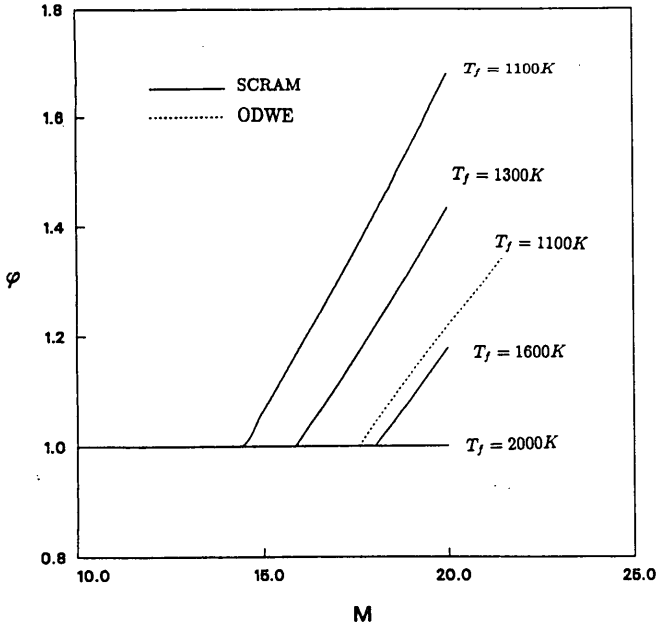

Fig. 3. Equivalence ratio versus Mach number for scramjet and ODWE engines at q=2000 psf. ODWE results are shown for a fuel temperature limit of 1100 K while scramjet results are shown for a range from 1100 to 2000 K (1520 to 3140 F).

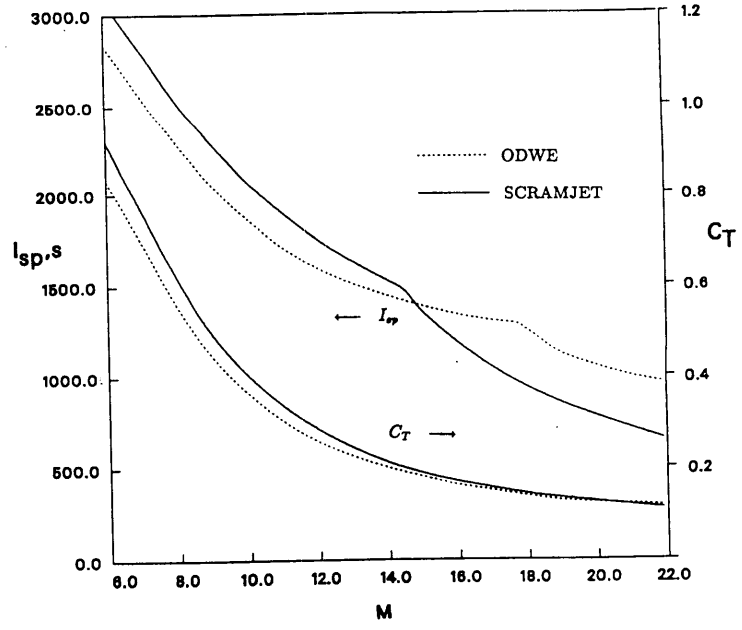

Fig. 4. Comparison of scramjet and ODWE performance characteristics. Shown are I_{sp} and C_T profiles for q=2000 psf, 90% of heat loads carried by fuel and 1100 K fuel temperature limit.

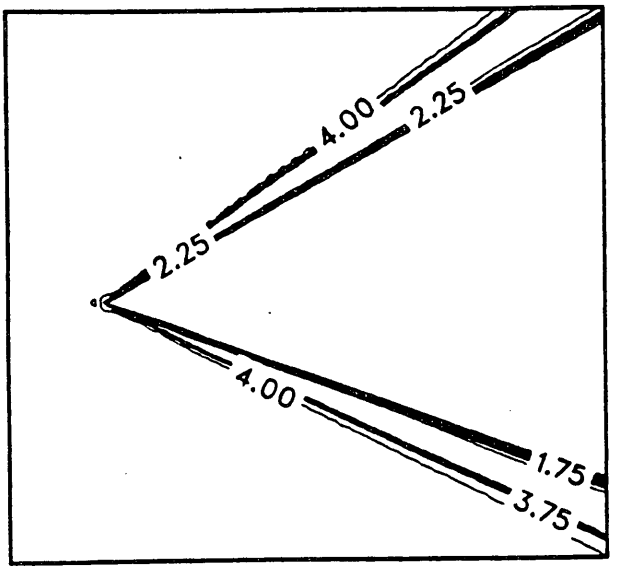

Fig. 7. Mach number contours for non-reacting stoichiometric air-fuel mixture flowing over a wedge at Mach 4.2.

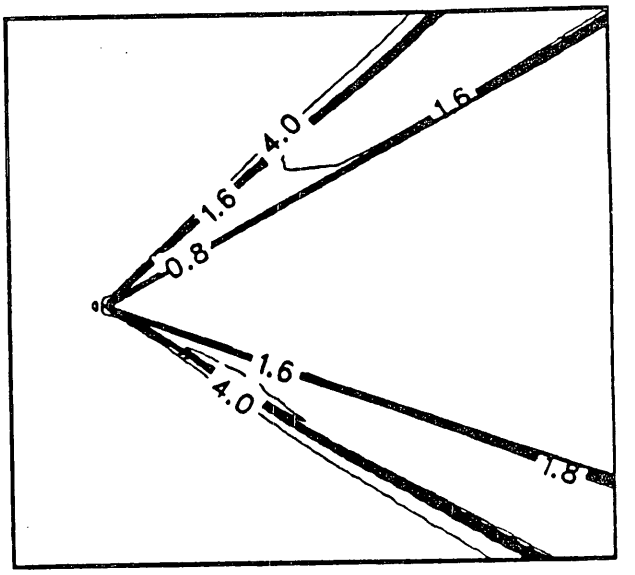

Fig. 8. Mach number contours for reacting stoichiometric air-fuel mixture flowing over wedge at Mach 4.2. The rotation of the wave with combustion indicates a detonation.

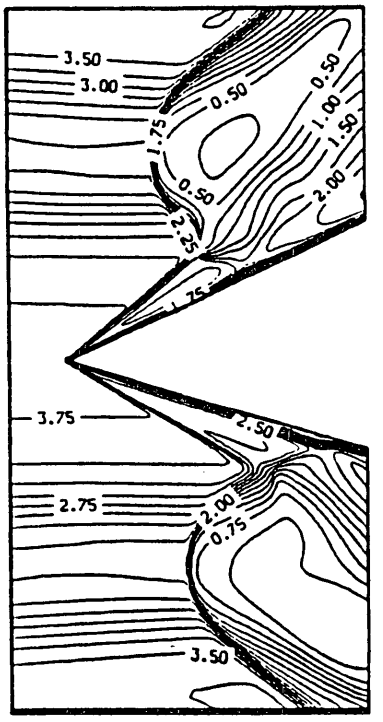

Fig. 9. Mach number contours for relatively unmixed fuel jet flowing over wedge.

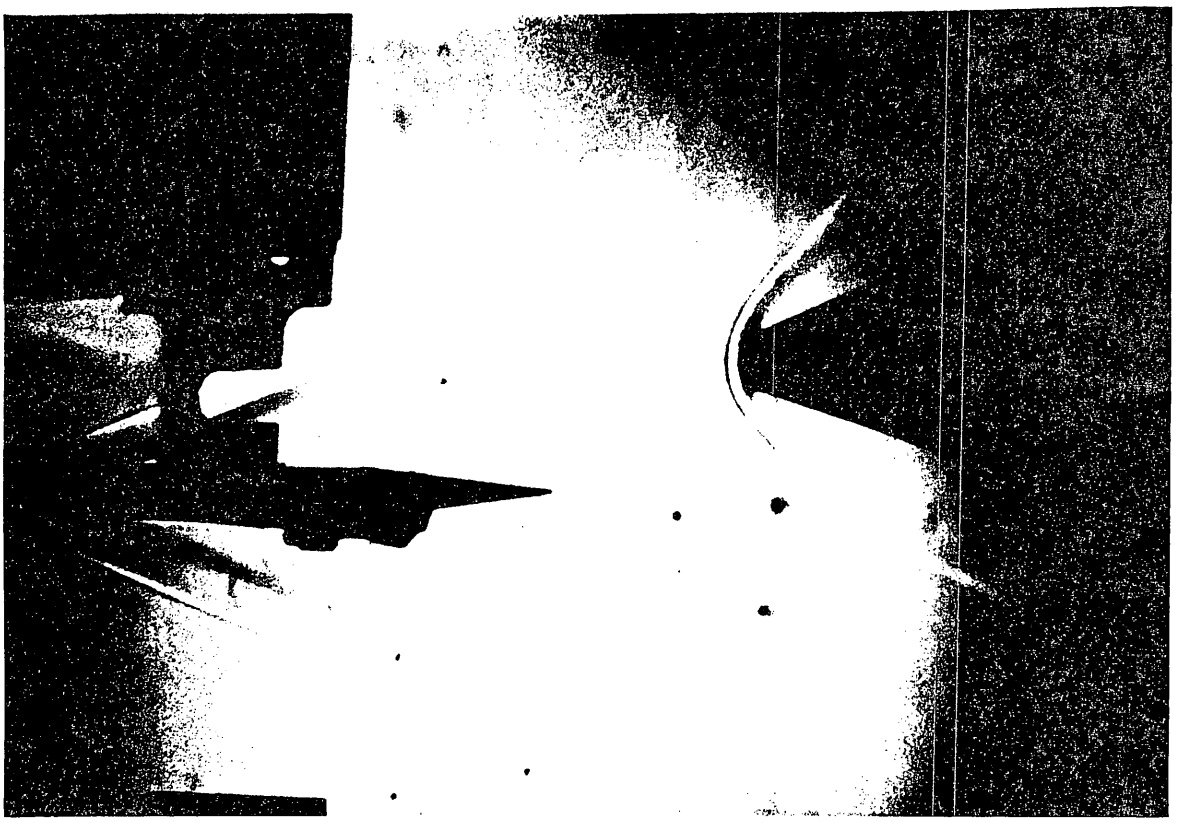

Fig. 13. Schlieren photograph of a shock wave created by a wedge in Mach 4.5 flow. A single strut fuel injector is positioned slightly below the wedge centerline. No fuel is injected in this case.

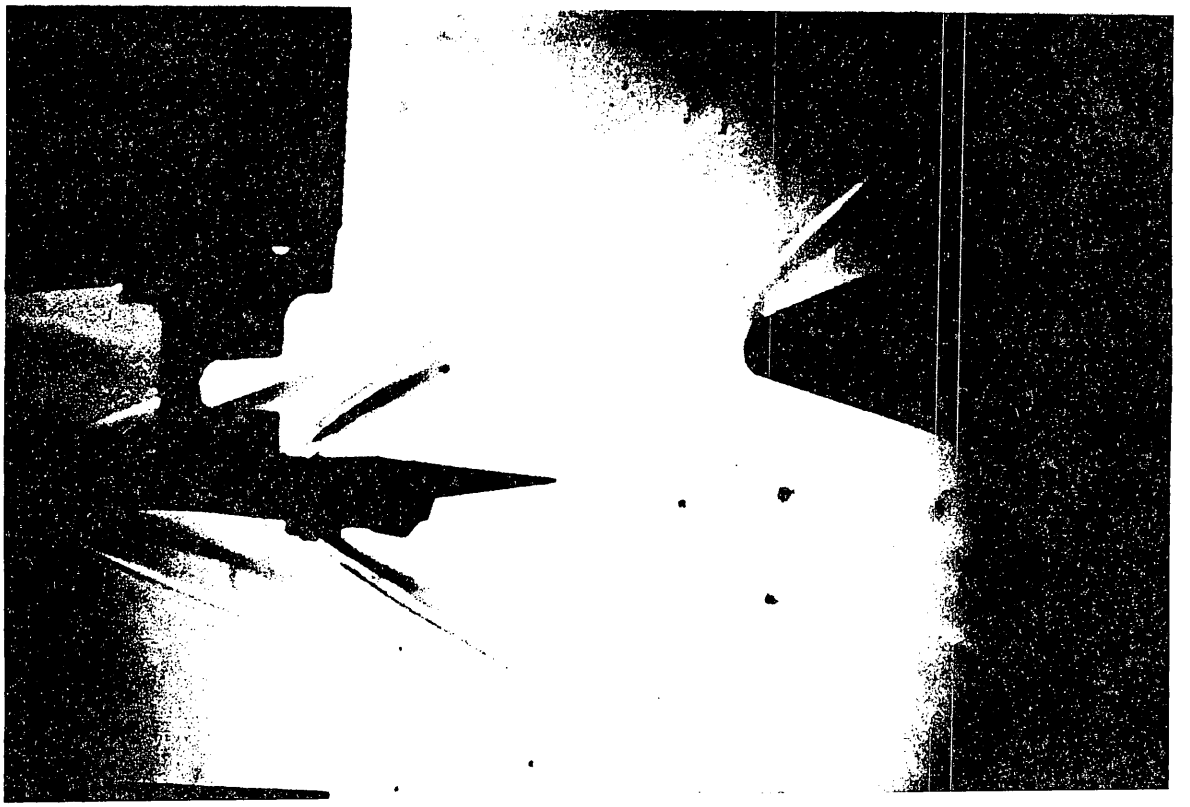

Fig.14. Schlieren photograph of an oblique wave created by a wedge in Mach 4.5 flow. Fuel is injected from a single strut. Note the displacement of the lower portion of the wave compared to the previous figure.